REPORT DOCUMENTATION PAGE

Form Approved
OMB No. 0704-0188

1. AGENCY USE ONLY *(Leave blank)*	2. REPORT DATE	3. REPORT TYPE AND DATES COVERED
	15 Apr 98	

4. TITLE AND SUBTITLE
CHARACTERIZATION OF MOLECULAR CRYSTALLINE THIN FILMS ON SUBSTRATES

5. FUNDING NUMBERS

6. AUTHOR(S)
Jeff Tyron Stricker

7. PERFORMING ORGANIZATION NAME(S) AND ADDRESS(ES)
University of Minnesota

8. PERFORMING ORGANIZATION REPORT NUMBER

9. SPONSORING/MONITORING AGENCY NAME(S) AND ADDRESS(ES)
THE DEPARTMENT OF THE AIR FORCE
AFIT/CIA, BLDG 125
2950 P STREET
WPAFB OH 45433

10. SPONSORING/MONITORING AGENCY REPORT NUMBER
98-004

11. SUPPLEMENTARY NOTES

12a. DISTRIBUTION AVAILABILITY STATEMENT
Unlimited distribution
In Accordance With AFI 35-205/AFIT Sup 1

12b. DISTRIBUTION CODE

13. ABSTRACT *(Maximum 200 words)*

14. SUBJECT TERMS	15. NUMBER OF PAGES
	99
	16. PRICE CODE

17. SECURITY CLASSIFICATION OF REPORT	18. SECURITY CLASSIFICATION OF THIS PAGE	19. SECURITY CLASSIFICATION OF ABSTRACT	20. LIMITATION OF ABSTRACT

Standard Form 298 (Rev. 2-89) (EG)
Prescribed by ANSI Std. 239.18
Designed using Perform Pro, WHS/DIOR, Oct 94

OVERVIEW

In the past few decades, there has been significant progress in developing an understanding of the role that non-covalent interactions have on the self-assembly and structural order of molecular crystals. This understanding has led to the development of crystal engineering, which is a promising approach to manipulate solid-state structures at the molecular level. Modification of the topochemical nature of the constituent molecules can enhance the ability to manipulate the solid-state properties of single crystals. Controlling the structures at this level may lead to new materials with chemical and physical properties that are desired in practical applications.

Crystalline guanidinium sulfonate (GS) materials are currently being synthesized in our laboratory through crystal engineering techniques because of their robust structure. The GS compounds have layered structures that result from the stacking of hydrogen bonded sheets consisting of topologically complementary guanidinium [$C(NH_2)_3^+$] and organosulfonate [$R\text{-}SO_3^{1-}$] or organodisulfonate [$O_2S\text{-}R\text{-}SO_2^{2-}$] ions. The robustness of this system has been demonstrated by the systematic incorporation of different compounds into GS crystals without disrupting the layered structure.

The objective of this thesis is to demonstrate the growth of GS crystals as thin films on substrates. Two-dimensional growth of these crystals are expected to occur because of their tendency to self-assemble into two-dimensional layers with strong intralayer hydrogen-bonding. Additionally, a low surface energy is expected for the hydrogen-

bonded planes since weak van der Waals interactions exist between adjacent layers. The growth of these monolayers will also depend on favorable interactions between the low energy surface of the hydrogen-bonded layer and the exposed surface of the substrate. The development of thin film growth methods based on self-assembled systems such as GS under ambient conditions may obviate more expensive film growth methods such as chemical vapor deposition and molecular beam epitaxy. Furthermore, the GS films may be tailored with properties desired in applications such as chemical sensors, wave guides, electrical conductors, and non-linear optical applications.

The first half of Chapter 1 provides a background on the guanidinium sulfonates, including crystal engineering, hydrogen-bonding, and the typical structures for both the guanidinium monosulfonates and guanidinium disulfonates. The latter half of the chapter describes the possible application of the GS crystals as thin films. Chapter 2 provides the additional background needed for this research, which will include a discussion of nucleation and growth of thin crystalline films, and epitaxy.

Chapter 3 describes the 2-D growth of guanidinium methanesulfonate (GMS) and guanidinium dithionate (GD) on various substrates. Atomic force microscopy (AFM) and wide angle X-ray diffraction were used to characterize growth features observed on the substrates. The results indicated preferred growth of these crystals with an orientation of their (001) plane parallel to the substrate, and that the wettability of the substrate has a direct influence on the 2-D growth of the crystals.

Chapter 4 presents possible epitaxial growth of GMS on both muscovite and highly oriented pyrolitic graphite. Epitaxial matches will be presented with lattice resolution obtained from the surfaces of the materials and through calculations made by computer simulation. Chapter 5 indicates the growth mode of these thin films on muscovite to be the Volmer-Weber mode. This deduction will be presented by comparing growth features observed on substrates to data obtained from monitoring growth by real time *in situ* AFM.

Finally, a concluding chapter will summarize the results presented in this thesis and suggest future research related to the growth of GS thin films.

UNIVERSITY OF MINNESOTA

This is to certify that I have examined this copy of a master's thesis by

Jeff Tyron Stricker

and found that it is complete and satisfactory in all respects,
and that any and all revisions required by the final
examining committee have been made.

Michael D. Ward

Name of Faculty Adviser

Signature of Faculty Adviser

March 17, 1998

Date

GRADUATE SCHOOL

CHARACTERIZATION OF MOLECULAR CRYSTALLINE THIN FILMS ON SUBSTRATES

A THESIS
SUBMITTED TO THE FACULTY OF THE GRADUATE SCHOOL
OF THE UNIVERSITY OF MINNESOTA
BY

JEFF TYRON STRICKER

IN PARTIAL FULFILLMENT OF THE REQUIREMENTS
FOR THE DEGREE OF
MASTER OF SCIENCE

MARCH 1998

PREFACE AND ACKNOWLEDGMENTS

I was born in Minneapolis, MN and raised in Apple Valley, MN until I graduated from Apple Valley High School in June of 1992. After two weeks of summer vacation, I ventured off to Colorado Springs, CO to attend basic training at the United States Air Force Academy. Four years later, I graduated from the academy with a bachelor's degree of Materials Science and many friendships that I will cherish for a lifetime. I started graduate school in September of 1996 and carried out this masters research at the University of Minnesota Chemical Engineering and Materials Science Department under the advisory of Professor Michael D. Ward. During this experience I have learned great deal about Materials Science and a lot more about the college environment, of which I was always envied from my civilian friends while attending the academy. I hope to internalize the lessons that I have I learned during my experiences here at Minnesota and apply them in my role as an officer in the United States Air Force. My next assignment will be served at Wright-Patterson AFB, OH.

I would like to thank my advisor Professor Mike Ward for allowing me to work in his group. He provided an extensive amount of scientific guidance, which at times required him to have a lot of patience. I would also like to thank the members of the Ward group for creating a unique working environment and for all the support they provided during my research. I would especially like to thank Tory Russell and Jen Swift for putting up with my endless list of questions. Now they will only have to deal with Dave Plaut's endless list of questions. I wish luck to Dave as he continues his pursuit in academia. My appreciation also goes to Yohaan John for all the editing he did with my thesis. Additionally, I am grateful for the assistance of Eric Granstrom while I was working on the AFM, and keeping me up to date on the Vikings.

My thanks goes to my roommates, Adam Pivovar, Chris Goralski, and Bryan Pivovar, for their advice they gave me throughout my research. Additionally, I would like to thank Adam for instigating martini time when I needed it.

Finally, I thank my parents, brother and family for their constant interest and support over the years.

CONTENTS

OVERVIEW

In the past few decades, there has been significant progress in developing an understanding of the role that non-covalent interactions have on the self-assembly and structural order of molecular crystals. This understanding has led to the development of crystal engineering, which is a promising approach to manipulate solid-state structures at the molecular level. Modification of the topochemical nature of the constituent molecules can enhance the ability to manipulate the solid-state properties of single crystals. Controlling the structures at this level may lead to new materials with chemical and physical properties that are desired in practical applications.

Crystalline guanidinium sulfonate (GS) materials are currently being synthesized in our laboratory through crystal engineering techniques because of their robust structure. The GS compounds have layered structures that result from the stacking of hydrogen bonded sheets consisting of topologically complementary guanidinium [$C(NH_2)_3^+$] and organosulfonate [$R\text{-}SO_3^{1-}$] or organodisulfonate [$O_2S\text{-}R\text{-}SO_2^{2-}$] ions. The robustness of this system has been demonstrated by the systematic incorporation of different compounds into GS crystals without disrupting the layered structure.

The objective of this thesis is to demonstrate the growth of GS crystals as thin films on substrates. Two-dimensional growth of these crystals are expected to occur because of their tendency to self-assemble into two-dimensional layers with strong intralayer hydrogen-bonding. Additionally, a low surface energy is expected for the hydrogen-

bonded planes since weak van der Waals interactions exist between adjacent layers. The growth of these monolayers will also depend on favorable interactions between the low energy surface of the hydrogen-bonded layer and the exposed surface of the substrate. The development of thin film growth methods based on self-assembled systems such as GS under ambient conditions may obviate more expensive film growth methods such as chemical vapor deposition and molecular beam epitaxy. Furthermore, the GS films may be tailored with properties desired in applications such as chemical sensors, wave guides, electrical conductors, and non-linear optical applications.

The first half of Chapter 1 provides a background on the guanidinium sulfonates, including crystal engineering, hydrogen-bonding, and the typical structures for both the guanidinium monosulfonates and guanidinium disulfonates. The latter half of the chapter describes the possible application of the GS crystals as thin films. Chapter 2 provides the additional background needed for this research, which will include a discussion of nucleation and growth of thin crystalline films, and epitaxy.

Chapter 3 describes the 2-D growth of guanidinium methanesulfonate (GMS) and guanidinium dithionate (GD) on various substrates. Atomic force microscopy (AFM) and wide angle X-ray diffraction were used to characterize growth features observed on the substrates. The results indicated preferred growth of these crystals with an orientation of their (001) plane parallel to the substrate, and that the wettability of the substrate has a direct influence on the 2-D growth of the crystals.

Chapter 4 presents possible epitaxial growth of GMS on both muscovite and highly oriented pyrolitic graphite. Epitaxial matches will be presented with lattice resolution obtained from the surfaces of the materials and through calculations made by computer simulation. Chapter 5 indicates the growth mode of these thin films on muscovite to be the Volmer-Weber mode. This deduction will be presented by comparing growth features observed on substrates to data obtained from monitoring growth by real time *in situ* AFM.

Finally, a concluding chapter will summarize the results presented in this thesis and suggest future research related to the growth of GS thin films.

1

BACKGROUND

1.1 CRYSTAL ENGINEERING

The pioneering work of Schmidt on topochemical reactions of crystalline cinnamic acids[1] suggested a relationship between the molecular assembly and the solid state reactivity of organic crystalline materials. The topochemically governed reactivity of these materials suggested possible control of the crystal structure by manipulating molecular interactions. Further research has since then increased the understanding of the role of molecular interactions in directing the self-assembly of highly ordered crystalline aggregates.[2, 3, 4] Such examples are the dimeric or linear hydrogen-bonding motifs in the formation of carboxylic acids[5] or π–π interactions[6] in the solid state packing of planar aromatic rings. This field of research has been described as crystal engineering, which is

[1]Schmidt, G. M. J. *Pure Appl. Chem.*, 27 (1971) 647.
[2]Desiraju, G. R. Angew. *Chem. Ed Engl.* 1995, 34, 2311-2327.
[3]M. C. Etter, *Acc. Chem. Res.* 23, (1990), 120 - 126; M.C. Etter, J. C. MacDonald, and J. Bernstein, *Acta Crystallagr.*, Sect. B,46 ,(1990), 256.
[4]S. Subramanian and Michael J. Zaworotko, *Coord. Chem. Rev.*, 137 (1994) 357-401.
[5]Frankenbach, G. M. and M. C. Etter. *Chem. Mater.*, 4, (1992), 272.
[6]Zhdanov, G. S. Crystal Physics. Academic Press: New York, 1965.

defined as "the understanding of intermolecular interactions in the context of crystal packing and in the utilization of such understanding in the design of new solids with desired physical and chemical properties".[7] Molecular interactions include all non-covalent forces such as van der Waals interactions, hydrogen-bonds, and Coulombic forces. The solid-state structures of organic materials represent the free energy minima of all non-covalent interactions. As a result of this understanding, crystal engineering is very promising for the synthesis of new useful solid-state organic materials with tailored physical and chemical properties.

There are three stages in crystal engineering for the synthesis of a functional material.[4] Previous research like the systematic characterization of the H-bonding interactions by Etter initiated the first stage by outlining some of the building blocks commonly found in crystal structures.[3] These building blocks are robust supramolecular units with specific functional groups, which self-assemble through molecular interactions into ordered crystal structures.[2] The statistical analysis of these building blocks has been accelerated with the development of the Cambridge Crystallographic Database.[8] This database enhances the ability to investigate a large number of structures to help decipher the more favorable interactions that may occur within a new crystal system. Understanding the influence of interactions on molecule arrangements in new organic crystal structures is the second stage of crystal engineering. The predictability of these structures is evident when studying a large number of molecules, with various functional groups, that show tendencies to self-assemble into recurring topological arrangements.[9] For example, successful engineering of one-dimensional networks such as the molecular tapes and strands, two-dimensional networks such as hydrogen-bonded sheets, and three-

---

[7]Desiraju, G. R. Crystal Engineering: The Design of Organic Solids, Elsevier: Amsterdam, 1989.
[8]Allen, F. H. and O. Kennard. *Chem Des Auto News* 8(1) (1993), 31-37.
[9]Russell, V. A.; Ward, M. D. *Chem Mater.* 8, (1996), 1654.; Russell, V.A.; Etter, M. C.; Ward, M. D. *J. Am. Chem. Soc.* 116, (1994), 1941.; Russell, V.A. Doctoral Thesis, University of Minnesota, 1995; Pivovar, A. M. Dossier, University of Minnesota, 1997.

dimensional networks such as diamonoid structures have been achieved.[4] The final stage is the elucidation of the relationship between the structure and the bulk physical or chemical properties of the newly synthesized crystals. Crystal engineering may be used to create new materials with desirable properties.

1.2 HYDROGEN BONDING

The concept of the H-bond was first proposed by Latimer and Rodebush[10] in 1920, although its definition is still debated.[11, 12] Typically, the H-bond is considered to be a weak electrostatic interaction between two highly electronegative atoms (a hydrogen bond donor, D, and the hydrogen bond acceptor, A) mediated by a positively charged hydrogen atom (D-H•••A). The H-bond length is generally shorter than the sum of the van der Waals radii of the two electronegative atoms ($d_{D\bullet\bullet\bullet A} \leq d_{vdW(D)} + d_{vdW(A)}$), but this requirement has been argued by Jeffrey and Saenger as being too restrictive.[13] Their argument states this definition fails to acknowledge the electrostatic nature of the H-bond (with a r^{-1} dependence), which will continue to have an influence at distances larger than the van der Waals criterion. They suggested the definition of the H-bond would be more accurate if based on the binding energies because it would account for interactions involving weak proton donors such as the C-H group or weak acceptors such as the π-electron cloud of aromatic rings. The classification of these longer range interactions as H-bonds is still debated.

The electronegative donor and acceptor atoms on molecules involved in H-bonding create electron density gradients within their respective molecules. Associated with these

---

[10]Latimer W. M. and W. H. Rodebush, *J. Am. Chem. Soc.*, , 42, (1920), 1419.
[11]Aakeroy, Christer B. and Kenneth R. Seddon, *Chem. Soc. Rev.* (1993), 397-407.
[12] F. Albert Cotton, Lee M. Daniels, Glenn. T. Jordan IV, and Carlos A. Murillo, *Chem. Commun.*, (1997), 1673-1674.
[13]Jeffrey, G. A. and W. Saenger, Hydrogen Bonding in Biological Structures. Springer: Berling, 1991.

gradients are local dipole moments, which align the H-bonded molecules in such a way that the electropositive region of molecules are near the electronegative regions of other molecules. Additionally, the strength of the H-bond should increase as more electronegative D and A atoms induce stronger dipole moments. Figure (1.1) illustrates the ideal linear (180°) alignment of the dipole moments of two molecules with the electron densities concentrated near the D-H bond and atom A. H-bonds commonly deviate from a linear geometry due to the presence of other non-covalent forces.

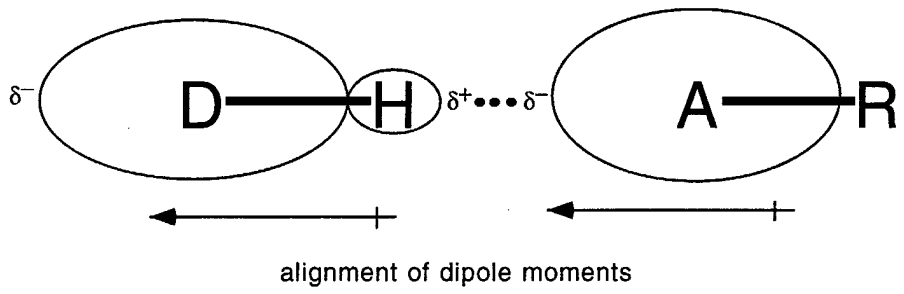

Figure 1.1 Diagram illustrating the areas of electron density and the tendency of the dipole moments to align. The sizes of the oval shapes correlate with the electron density.

The strength and directionality of the hydrogen (H) bond drive the self-assembly and supramolecular bonding in many organic crystals.[14] H-bonding interactions play a primary role in the 2-D growth of the GS crystals, which will be demonstrated in the following section. The typical strength of the H-bond can range from 10-65 kJ mol^{-1}, and 40-190 kJ mol^{-1} if one of the components is ionic in character.[13] Thus, the H-bond is significantly stronger than other intermolecular interactions, surpassing even that of weaker covalent bonds.[15] Despite this strength, the H-bond is flexible and highly polar and

[14]Desiraju, G. R., *Angew. Chem. Int. Ed. Engl.*, 34, (1995), 2311-2327.
[15]Th. Zeegers-Huyskens and P. Huyskens, in Intermolecular Forces-An Introduction to Modern Methods and Results. ed. P. L. Huyskens, W. A. P. Luck, and T. Zeegers -Huyskens, Springer-Verlag: Berling, 1991, 1; Yamdagni R. and P. Kebarle, J. *Am. Chem. Soc.* 93, (1971), 7139.

commonly deviates from its expected linearity. In some cases, multiple bonds may even form with a single atom.

1.3 GUANIDINIUM SULFONATE CRYSTALS

Crystal engineering principles utilizing H-bonding interactions have been successfully applied in previous studies of guanidinium organosulfonates. Although the discovery of some guanidinium sulfonates were made in the 1940's,[16] the characterization and manipulation of their structures was achieved only recently.[17] The exploration of this family of structures is continuing and their properties may be useful in thin film applications because of their layered motifs. This section will briefly describe the structural composition of the GS crystals in order to provide an understanding of their potential use in thin film applications.

1.3.1 GUANIDINIUM ORGANOSULFONATES

The main constituents in guanidinium organosulfonates (GS) are the topologically complementary guanidinium [$C(NH_2)_3^+$] and organosulfonate [$R\text{-}SO_3^-$] ions. The H-bonding interactions occur between the six proton donors of the guanidinium and the six lone electron pairs of the oxygen, which are the H-bond acceptors. Upon self-assembly these interactions result in a layered structure with a hexagonal or quasi-hexagonal symmetry in each layer. Although altering the structure in the third dimension influences the 2-D structure of the layers, the robust H-bonded network allows for tailoring of new

[16]Karrer, P.; Epprecht, A. Helv. *Chem. acta.* 24, (1941), 310; Price, C. C.; Reitsema, R. H. *J. Org. Chem.* 12, (1947), 269.
[17]Russell, V. A. Doctoral Thesis, University of Minnesota. 1995.

GS crystals with similar layering motifs. Therefore, crystal engineering of the GS structure is possible in the third dimension.

1.3.1.1 GUANIDINIUM MONOSULFONATES

The first crystal to be studied in this research was guanidinium methanesulfonate (GMS) because it has the simplest structure amongst guanidinium monosulfonates and is easy to synthesize. The guanidinium and organosulfonate ions self-assemble with each other through H-bonding to form the cyclic dimer motif. The H-bonding interaction of these ions continue to form extended H-bonded ribbons, which in turn are cross-linked through similar H-bonding interactions to form 2-D layers with a quasi-hexagonal motif. Figure (1.2) illustrates the formation of the GS sheet. The length of the linear N•••O bond is 2.93 Å, which is less than the sum of the van der Waals radii (3.07Å) of N and O.[2] The third dimension of the GMS structure consists of stacking these sheets on top of each other with interactions among sulfonated R-groups between the sheets. These interactions within the third dimension will have an influence on the crystal structure.

The robustness of the H-bonded sheets in the GS system allows for substitution of different R-groups on the sulfonate, which enables crystal engineering of this system in the third dimension. The robustness of the GS layered structure has been observed with the GS system's tendency to structurally adapt for steric hindrance caused by the incorporation of different sulfonated R-groups.[17, 18] The 2-D structure of the H-bonded sheets adapts to the steric requirements of the sulfonated R-groups. Examples of the system adaptability that have been observed are the shifted ribbon motif and the puckering of the sheets with substantial deviation of the interribbon dihedral angle (θ_{IR}) from 180° (Figure 1.2B). The

[18]Russell, V. A.; Evans, C. C.; Wenjie, L., and M. D. Ward. *Science.* vol. 276, (1997), 575-579.

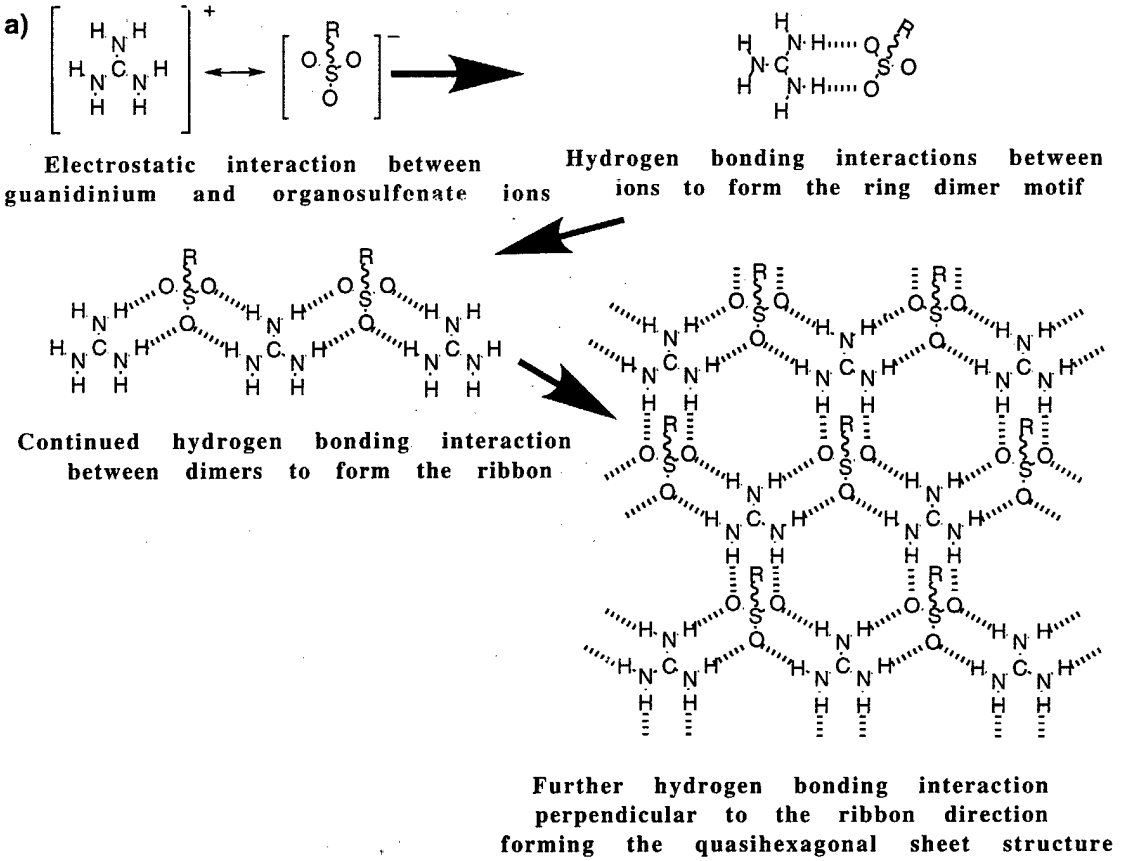

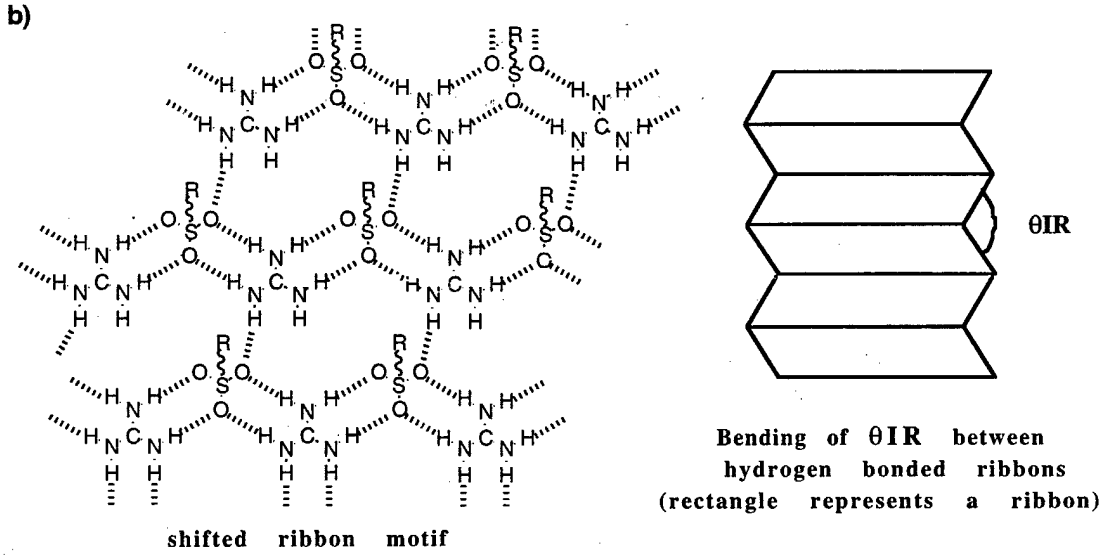

FIGURE 1.2. a) Diagram for the self-assembly of the guanidinium and sulfonate ions into sheets through H-bonding interactions. The step by step process includes the direct interaction between ions, continued interaction along ribbons, which combine to form the 2-D sheets. b) Illustration of the H-bonded sheet's ability to adapt for hindrance encountered with the incorporation of various sulfonate identities.

structural adaptability of the H-bonded sheets stems from the flexibility of the H-bonding interactions, which act as a stress relief mechanism in response to steric hindrance caused by sulfonates with different R-groups. The flexibility within the 2-D structure may be a benefit in the growth of the GS crystalline films on substrates, which may tolerate strain induced at the interface and provide strain relief within its structure.

The GS crystals also accommodate steric hindrance by exploring different layering motifs. The two types of layering motifs for the guanidinium monosulfonates are the single-layer and bilayer "sandwich" motif, which are indicated in Figure (1.3). The bilayer "sandwich" motif consists of H-bonded layers with the sulfonated R-groups positioned on only one side of the sheet. Two sheets then combine to form a bilayer with the sulfonated R-groups interdigitating within one another like the teeth of a zipper. The bilayer sandwich motif finally forms upon stacking of these bilayers. The R-groups interact primarily by dispersive forces whereas dispersive and ionic interactions exist between the H-bonded sheets. The single layer stacking motif also demonstrates the same zipper effect, but the R-groups alternate sides of the H-bonded sheet as a result from steric hindrance due to larger sulfonated R-groups. The single layer motif will not be of concern for this thesis.

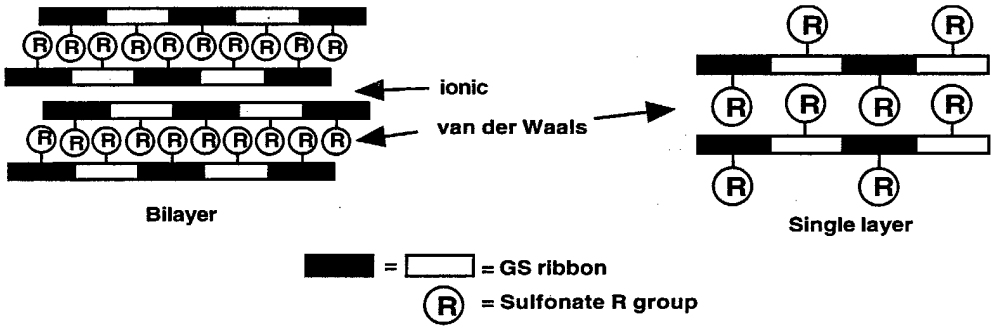

FIGURE 1.3. The two layering motifs for the guanidinium monosulfonates. a) Bilayer motif demonstrates the zipper effect through van der Waals interaction. b) Single layer motif demonstrates the same effect, but the R-groups alternate sides of the H-bonded sheet to account for steric hindrance.

1.3.1.2 GUANIDINIUM DISULFONATES

The other crystal system explored in this research was guanidinium dithionate (GD), which has the simplest structure of guanidinium disulfonates. The structure of this system also consists of stacking bilayers as seen with the bilayer structure of GMS. The difference in the GD system is that the two H-bonded sheets are covalently linked together by sulfonated R-groups to create the guanidinium organodisulfonates. These covalent links act as pillars between the H-bonded sheets resulting in channels within the crystal structure. Larger separations between layers form with the alkane and arene disulfonates, which usually result in the enclathration of a guest upon crystal formation to prevent the structure from self-collapse. There have been many examples of pillars, such as naphthyl and biphenyl, and many more guests that have been successfully incorporated into the guanidinium disulfonate system.[18] The 2-D structure of the H-bonded sheet is essentially the same as that described for the guanidinium monosulfonate system.

There are also two different types of layering motifs for the guanidinium disulfonate system as there were for the guanidinium monosulfonates (Figure 1.4). The first motif is the bilayer "sandwich" motif. This motif consists of stacked bilayers, each bilayer consisting of two H-bonded sheets connected by the disulfonated pillars. The interactions between the layered sheets are primarily ionic in nature. The other layering motif for this system is the brick motif. This motif is similar to the interdigitated single-layer stacking motif for the guanidinium monosulfonates in that the R-groups alternate sides of the H-bonded sheet as a result of steric hindrance caused by larger R-groups. The difference is that the R-groups are covalently bonded to two sulfonates in different, but parallel H-bonded sheets. The brick motif will not be of concern for this thesis.

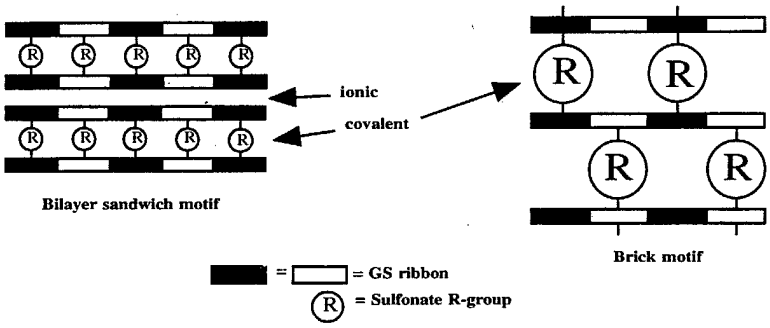

FIGURE 1.4. The stacking motifs for the guanidinium disulfonates. Bilayer sandwich motif consists of stacking layers each with two H-bonded sheets connected by the pillars. The brick layer motif forms to accommodate for steric hindrances caused by larger pillars or guests.

1.3.2 USE OF THE GS SYSTEM AS THIN FILMS

The layered structure of the GS system suggests opportunities for the growth of these crystals as thin films on substrates. These crystals are expected to grow on substrates with the H-bonded planes oriented parallel to the surface. This orientation is expected because of favorable growth within the H-bonded layers. These planes should have a low surface energy because of strong H-bonds. The growth of the H-bonded sheets are expected to occur on substrates exposing similar low energy surfaces. Two of the substrates used in this research were HOPG and muscovite since they both cleave to expose flat surfaces. The ability to cleave these materials indicates the exposed surfaces are of planes with strong bonding, thus low surface energies. The 2-D growth of GS thin films will be governed by favorable interfacial interactions with the substrate.

The properties of organic materials can include nonlinear optical behavior, ferromagnetism, electrical conductivity, and chemical reactivity.[19] These properties have been used in many thin film applications such as chemical sensors,[20] photovoltaic cells,[21]

---

[19]1- Nonlinear Optical Properties of Organic Molecules and Crystals. vol. 1, Chemla, D. S.; Zyss, J., Eds.; AcademicPress: Orlando Florida, 1987; Linear Chain Compounds. vols. 1 - 3., Ed. J. S. Miller, Plenum, New York, 1982 - 1983.

[20]Brousseau, L. C.; and T. E. Mallouk. *Anal. Chem.* 69 (4) , (1997), 679 - 687.

[21]Tang, C. W. *Appl. Phys. Lett.* 48 (2), (1986), 183-5.

capacitors,[22] transistors,[23] and microwave or optical guides.[25, 26, 27] The continued development of new GS crystals may incorporate these properties into their structure, which will increase their potential use in thin film applications. This section will discuss the unique structural features of the GS system and how they could be used in certain thin film applications.

1.3.2.1 UNIQUE STRUCTURAL FEATURES OF THE GS SYSTEM

The sulfonated R-groups and the quasi-hexagonal 2-D network within the GS crystal structure may be beneficial for the use of these crystals in thin film applications. Substitution of sulfonated R-groups allows for engineering of the GS structure in the third dimension. Additionally, the incorporation of guests into the channels of the disulfonates enhances the ability to synthesize new GS structures. The incorporation of different compounds into the GS structure will introduce different properties to the crystal. Another possible advantage of the porous structure may be the ability to intercalate specific external reactants into void spaces that are engineered with geometrical and reactive specificity.

Anisotropic properties are expected in the GS thin films because their properties are created by the differing pillars and guests, which lie along the H-bonded ribbons. Our laboratory is investigating the introduction of metallic components into the GS structure and reactions within the channels that can produce stereoregular polymers. Figure (1.5) illustrates the unique structural features of the GS crystals that can be manipulated to obtain desired properties.

---

[22]Kepley, L. J.; Sackett, D. D.; Bell, C. M. and T. E. Mallouk, *Thin Solid Films*, 208, (1992), 132 - 6.
[23]Roberts, G. G.; Pande, K. P. and W. A. Barlow, *IEE J. Solid-State Electronic Devices*. 2, (1978), 169.

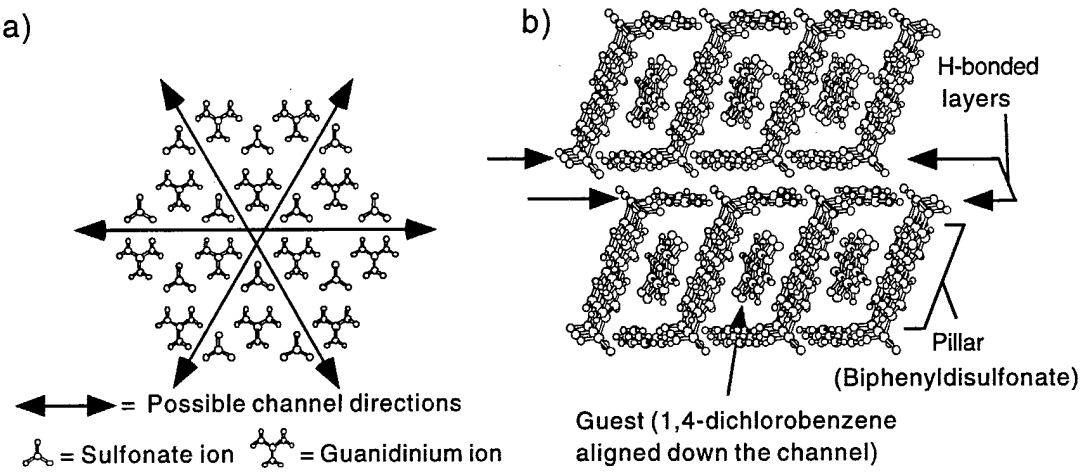

FIGURE 1.5. Illustration demonstrating unique characteristics of the GS crystal structure. a) Example of the anisotropic order within the H-bonding sheet as viewed from the (001) plane of guanidinium dithionate. This figure indicates the channel directions before modification caused by steric hindrances of the pillar or guest. b) Parallel view along the H-bonded layers of guanidinium biphenyldisulfonate•1,4-dichlorobenzene, which demonstrate the ability to introduce different pillars and guests into the crystal structure. The guest occupies the void space of the host lattice, which align down the channels parallel to the ribbons.

1.3.2.2 ADVANTAGES IN THIN FILM APPLICATIONS

The objective of this research is to determine whether GS crystals will grow as self-assembled ultrathin films on substrates. Attaining this goal will demonstrate the ability of GS crystals to grow as layers without structural dependence on interactions in the third dimension. Often, the structure of a bulk material is different from that of a thin film, as reconstruction may occur to lower the high surface energies resulting from dangling bonds or lone electron pairs.[24] Surface reconstruction is not expected to occur during growth of GS thin films because the H-bonded layers contain strong H-bonds, and hence, exhibit low surface energies. Therefore, the GS thin films are expected to form a 2-D structure similar to that found in the (001) plane of the bulk crystal. Additionally, self-assembled growth of GS films under ambient conditions may reduce the need for more complicated methods of growing thin films. This growth method is preferred over methods like molecular beam

24 Kittell, C.; Introduction to Solid State Physics. 7th Ed. John Wiley and Sons, New York, 1996.

epitaxy or chemical vapor deposition, which can be expensive since they require using apparatuses to accommodate for thermally reactive components and non-equilibrium conditions. Also, the non-covalent nature of GS films allows for self-repair during assembly. If GS thin films can be made, the GS system will allow for facile introduction of functional groups and promises precise tuning of properties.

The potential to stack different GS crystals to create multilayered heterostructures is of interest because alternating stacks of different thin films may be useful in thin film applications. The multilayered growth of thin film materials has been limited because of required lattice-matched heterojunctions. Epitaxial growth, commonly required for the layered growth of thin crystalline films on ordered substrates, will be discussed in Chapter 2. The absence of a lattice match can result in interfacial stress that can instigate lattice defects, which can degrade the optical and electronic properties of the material. Consequently, this requirement has stimulated efforts to grow multilayers of organic materials due to their flexibility. Multilayered growth may be achieved by using different GS films since they are expected to have favorable Coulombic interactions and structural matching at their interfaces.

The directionality and possible multilayer formation of modified GS crystals may be useful in optical and X-ray waveguide applications.[25, 26, 27] Multilayer devices that behave as microwave producers and guides have been constructed. The submicrowave X-ray is produced when the wave propagates along the horizontal plane of the dielectric layer and reflects back and forth between the interfaces, causing one of the wave components to resonate with an amplitude equal to the thickness of the layer. The ability of the waveguide

---

[25] Camley, R. E. and D. L. Mills, *J. Appl. Phys.* 82 (6), (1997), 3058 - 67.

26 Lagomarsino, S.; Jark, W.; Di Fonzo S.; Cedola, A.; Engstrom, P.; and C. Riekel. *J. Appl. Phys.* 79 (8), (1996), 4471 - 3.

27 Carniglia, C. K.; Black, J. P.; Watkins, S. E.; and B. J. Pond. *Applied Optics.* 32 (28) , (1993), 2204 - 10.

to direct propagation through the dielectric material stems from the coupling of the magnetic spin waves in the ferromagnetic material with the microwave or optical beam. The manipulation of the GS system may produce thin films with ferromagnetic or insulating properties that can be used for this multilayer device. A ferromagnetic film could be designed with the incorporation of metal centers (Fe, Co, or Ni) within the layers, whereas insulating films could be synthesized by the enclathration of non-conducting molecules with a controllable dielectric constant. GS multilayers may also be used as optical wave guides. The optical wave guides need to consist of a crystalline material with a dielectric character that allows initial penetration of the wave and acts as a medium for its propagation. The stacking sequence would entail a layer with a high refractive index bound by layers with a low refractive index.[27]

The porosity of the GS layers might permit the formation of devices based on the principles of diffusion and intercalation. Layered organic materials have been used as thin film gas sensors. An example is the intercalation of ammonia (NH_3) into a Cu biphenyl(phosphonate) thin film and detection with a quartz crystal microbalance.[20] The GS system may be used for such an application because of its ability to be tailored to meet the demands of this device. The sensors need to be constructed from a durable material with rapid response time, reversibility for repeated use, and voids that are chemically and geometrically specific to certain analytes.[20]

The porous GS network may also enable the synthesis of materials that are conducting or semiconducting. This may be achieved by appropriate modification of the guests and pillars, or intercalating reactants into the layered structure. A conductor is described as a material with overlapping or partially filled energy levels that allow for the free movement of electrons. An insulator, however, restricts the flow of electrons as its energy levels are filled and a large band gap (between the highest occupied molecular orbital and the lowest unoccupied molecular orbital) exists under ambient conditions ($E_g >$

4 eV). A semiconductor is characterized by a band gap of approximately 0.01-4 eV. These energy levels are depicted in Figure (1.8). The smaller band gap allows for conduction to occur if electrons are thermally excited into conduction band, which leave holes in the valence band. Doping the semiconductor with donor and acceptor ions can also increase the conductivity. A p-type semiconductor is created by acceptor ions withdrawing electrons from the valence band to form holes. A n-type semiconductor is created if a donor ion contributes an electron to the conduction band.

Similar p and n-type properties can be obtained from the intercalation of a reactant into a layered material. These reactants can cause the oxidation or reduction of the layers to change the electronic properties of the material. A common example used to describe the ability to alter the conductivity of a layered material is the intercalation of bromine in between the layers of highly oriented pyrolitic graphite (HOPG) to form conducting layers through oxidation.[28] Figure (1.6) demonstrates the oxidation of the layers within HOPG, which create p-type characteristics.

28 Keller, S. W.; and T. E. Mallouk. *J. Chem. Ed.* 7 (10), (1993), 850 - 860.

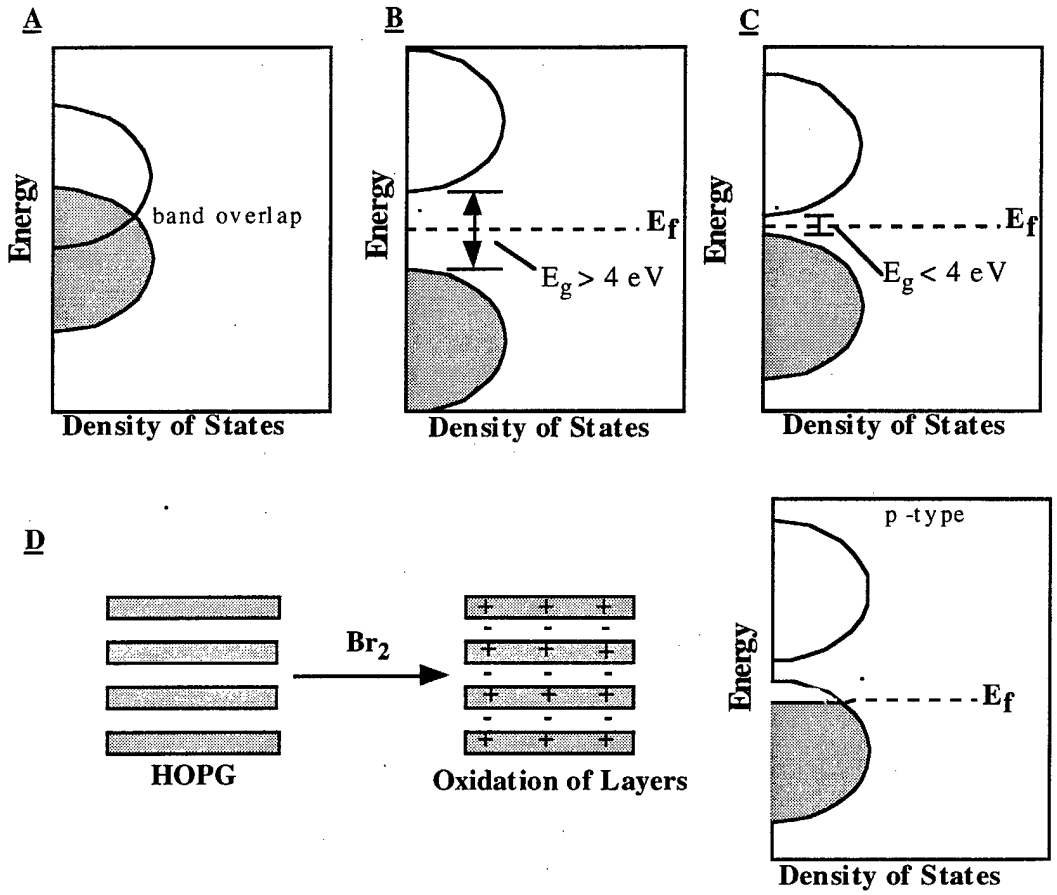

FIGURE 1.6.[28] Illustration of energy level diagrams with respective Energy gaps (E_g) between orbitals for A)conductor, B) insulator and C) semiconductor. D) Demonstrating how intercalation can introduce ions within layered materials to dope the energy bands with electrons or holes. The example demonstrated is the oxidation of layers in HOPG as Br^- ions intercalate between them to dope the lower band with holes (p - type). The fermi energy level (E_f) is state of energy where the probability of electron occupancy is half.

The multilayered growth of thin film semiconducting materials has been limited because of required lattice-matched heterojunctions. With the incorporation of GS films and/or other organic films into multilayer films, a greater diversity of properties can be obtained from doped semiconductor junctions. Heterostructures of other layered organic materials have been suspected to form p-n, n-n or p-p junctions.[29] These semiconductor junctions lead to applications such as diodes, transistors, capacitors, photovoltaic cells, and

[29]So, F. F. and S. R. Forrest, *J. Appl. Phys.* 64 (1), (1998), 399 - 409, So, F. F. and S. R. Forrest, *J. Appl. Phys.* 63 (2), (1988), 442 - 6.

light emitting diodes (LED).[24] With an increased diversity of heterostructures from the GS multilayers, a better understanding of the properties at the interfaces between organic thin films may be achieved. A particular area of interest is with the activity of excitons (paired hole and electrons) in multiple quantum well (MQW) structures.[30]

1.4 CONCLUSION

This chapter has presented the background on the GS system and why this research intends to grow these layered crystals as thin films. The large number of crystals within the GS system are a product of efforts made in crystal engineering, which will continue to produce new GS crystals. Continued development of the GS system will increase the potential use of these crystals in many applications. This thesis intends to demonstrate the tendency of the GS crystals to grow as thin films. The next chapter will review the fundamentals for nucleation and growth of crystals and thin films.

---

[30]/So, F. F.; Forrest, S. S.; Shi, Y. Q.; and W. H. Steier. *Appl. Phys. Lett.* 56, (1990) 674-676; So, F. F. and S. S. Forrest, *Phys. Rev. Lett.* 66 (20), (1991), 2649 - 52.

2

NUCLEATION AND GROWTH

Studies of nucleation and growth of crystalline films at the nanometer scale are necessary for the understanding and control of film structure and orientation. Control of nucleation and growth is important because macroscopic properties such as the conductive or optical behavior can be altered by subtle changes in structure. Several factors influencing nucleation and growth will be described for both crystals and thin films. Although crystal growth can originate from the vapor phase or the melt,[1] the growth of the GS crystals have only been attempted from solution. The factors that will be discussed are the adsorption of the material to the surface of the substrate and its subsequent 2-D growth. The advent of scanning probe microscopy has enabled investigation of this phenomenon at the near-molecular level. In particular, atomic force microscopy (AFM) has been used in this research to study the 2-D growth of the GS system.

[1] Aquilano, D. Crystal Growth in Science and Technology Eds. Arend, H. and J. Hullinger, Plenum Press: New York, 1989, 49-67.

2.1 CRYSTAL NUCLEATION

Crystallization is the solidification of an ordered material from either solution, vapor or melt, which is initiated by deviation from thermodynamic equilibrium. The initiation of crystal growth from solution occurs by formation of a nucleus upon supersaturation of solute within a solvent. The nucleation within the system arises with the lowering of the Gibbs free energy of the system as described by the equation: $\Delta G = \Delta H - T\Delta S$ where ΔG is the change in Gibbs free energy, ΔH is the change in enthalpy, T is the temperature of the system, and ΔS is the change in entropy. After nucleation a precipitate is formed in the solution to produce a highly ordered crystal. Two methods for achieving supersaturation are by evaporating or by cooling the solution. Upon evaporation, the number of solute-solvent interactions decreases, thereby increasing the number of solute-solute interactions by which the crystalline material is formed.

2.1.1 HOMOGENEOUS NUCLEATION AND GROWTH

The first step in crystallization is the agglomeration of the molecules by diffusion through the solution to initiate nucleation. Three dimensional nucleation of a crystal from solution is described by the following equations:[2]

$$\Delta G(r) = -(4\pi/3)r^3[k_B T \ln(\sigma + 1)]/\nu + 4\pi r^2\gamma \qquad \textbf{(2.1)}$$

$$r^* = 2\nu\gamma/[k_B T \ln(\sigma + 1)] \qquad \textbf{(2.2)}$$

$$\Delta G_c(r^*) = 16\pi\nu^2 g^2/[3k_B{}^2T^2\ln^2(\sigma + 1)] \qquad \textbf{(2.3)}$$

where k_B is the Boltzmann constant, T is the temperature of the system, σ is the relative supersaturation, γ is the interfacial surface free energy and ν is the molar volume of the cluster. The critical radius (r^*) is the required size of the cluster needed to form a stable

[2]Zhang, Z. and M. G. Legally, Science, vol. 276, (1997), 377 - 83.

nucleus and is used to give equation (2.3), which describes the energy barrier to nucleation. The size of the energy barrier is determined by the conflicting effects of the volume free energy (G_V) and the surface free energy on the total free energy. Figure (2.1) illustrates this competition. The volume free energy is the difference in energy between the crystal and the solution. This value is always negative and so it promotes growth. The surface free energy is the energy at the interface and has the opposite effect to promote dissociation. The first part of equation (2.1) represents the volume free energy and the latter part represents the surface free energy. As the cluster grows the volume free energy becomes dominant with a lower surface to volume ratio to initiate nucleation. The surface energy inhibits the growth often requiring undercooling of the solution below the supersaturation temperature.

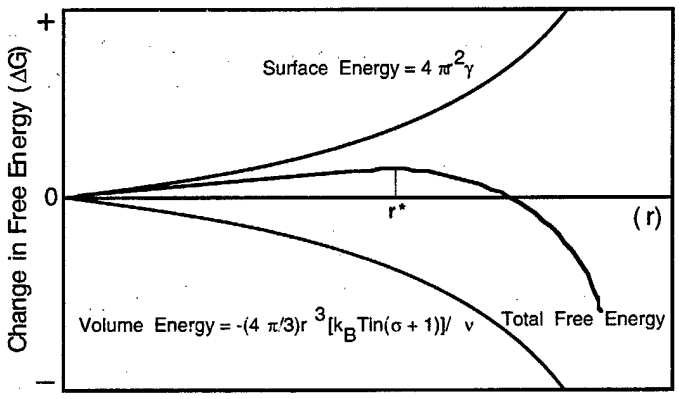

FIGURE 2.1. A function of the total free energy vs. radius of cluster with competing effects from the volume free energy and the surface free energy. The values for the critical radii and the energy barrier are each labeled on the appropriate axis.

2.1.2 CRYSTAL GROWTH

After nucleation, the next stage is the growth of the crystal. The first step of this process is the movement of the particles (ions or nuclei) to the surface of the crystal

through diffusion and mass transfer.[3] Once adsorbed to the surface the particles diffuse to sites offering the lowest energy with a diffusion coefficient of $D = a^2 k_S$, in which a describes the hopping distance from site to site and $k_S = \exp[-V_S/ k_B T]$, where V_S is the potential barrier between sites.[2] The growth rate of the crystal's surface is estimated to be equal to the mass transfer rate and the surface diffusion rate.[3] This approximation assumes no overgrowth with adequate surface diffusion on the crystal and is directly related to the mass transfer rate since the hopping distance is decreased with more adatoms on the surface.

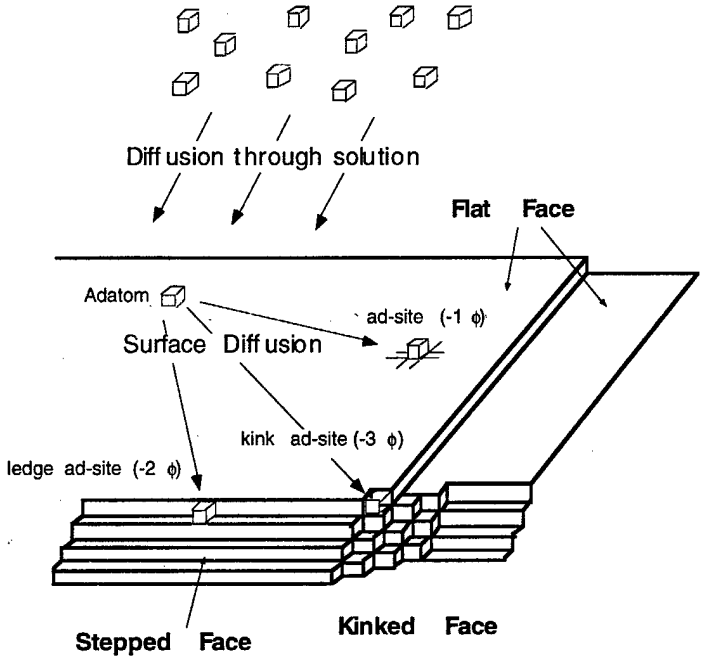

FIGURE 2.2. [1] Sites available on a facet of a crystal along with their potential energies in parenthesis.

Once the particle is on the crystal's surface, it diffuses under ideal circumstances (enough time to travel without getting trapped by rapid nucleation) to a site offering the

[3] Wilcox, W. R. Crystal Growth in Science and Technology Eds. Arend, H. and J. Hullinger, Plenum Press: New York, 1989, 119-132.

lowest potential.[1] Figure (2.2) illustrates the type of sites available on the facets of a crystal along with their potential energy. In the model, the particle is thought of as a cube with six faces exposed to the solution. The change in the number of exposed faces correlates with the change in the potential of the particle. The number in parentheses indicate the change in the number of exposed faces of the particle at different surface sites. The three types of faces found on the crystal's surface are the flat (F), stepped (S), and kinked (K) faces. The K and S faces indicated in Figure (2.2) have two or three exposed faces. These sites lower the potential of the particle more than the sites on the F face, which only occupy one face (adatom). Therefore, the growth of the crystal will preferably be layered at one of its facets, as the sites on the K and S faces are more likely to be occupied before those on the F faces. Past work has demonstrated that the growth of certain facets can be limited by interactions with terminating groups in the solution to cause preferential growth on other facets.[4] Although this technique may be useful with the GS system in the future, this research will focus on promoting the layered growth of their (001) planes with favorable Coulombic interactions between these planes and certain substrates.

2.1.3 HETEROGENEOUS NUCLEATION

Homogeneous nucleation, which depends on supersaturation, almost never occurs. Heterogeneous nucleation relies on surfaces to lower the Gibbs free energy of nucleation. These surfaces allow the cluster to reach r* at a smaller volume, and less undercooling, by lowering the amount of interfacial area with the solution (illustrated in Figure 2.3). The Gibbs equation for this nucleation is essentially the same except interfacial interactions with the substrate need to be accounted for in the expression of the energy

[4] Weissbuch, I.; Popovitz-Biro, R.; Lahav, M. and L. Leiserowitz. *Acta Cryst.* B51, (1995), 115 - 148.

barrier described in equation (2.3). The adjusted expression is

$$\Delta G_c(r^*) = 16\pi v^2\gamma^2/[3k_B{}^2T^2\ln^2(\sigma + 1)]\bullet 1/4(2 + \cos\theta)(1 - \cos\theta) \qquad \textbf{(2.5)}$$

where θ is the contact angle of the nucleus upon wetting the surface (Figure 2.3). The value of this angle measures the wettability of the nucleus and is determined by the surface energies of the three medium (surface, nucleus, and solution). A larger angle ($\theta >$ 90°) occurs when the interfacial interactions between the surface and solution are more favorable than those with the surface and nuclei. The growth of a monolayer on a surface is described by complete wetting of the surface (θ = 0°). Therefore, the critical free energy from equation (2.5) can be altered to describe 2-D nucleation as

$$\Delta G_c(r^*) = 8\pi v^2\gamma^2/[3k_B{}^2T^2\ln^2(\sigma + 1)] \qquad \textbf{(2.6)}$$

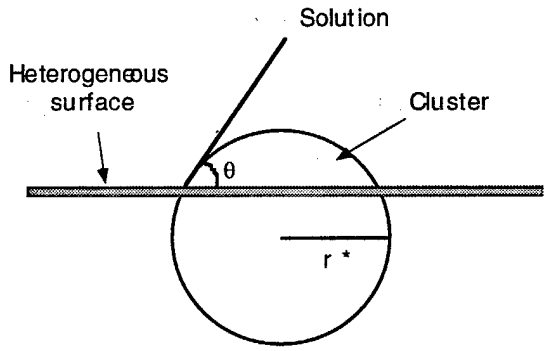

FIGURE 2.3 The formation of a spherical cap upon heterogeneous nucleation. This formation lowers the surface energy with the solution to decrease the size of the critical radii. Theta is the contact angle between the nucleus and the flat surface. This measures the wettability of the nucleus with the surface.

2.2 GROWTH OF THIN CRYSTALLINE FILMS

The combination of the preferred nucleation on a surface and layered growth of bulk GS crystals indicates potential for their growth as thin films. The steps for the formation of thin crystalline films are 1) diffusion of the particles through the solution to the substrate, (2) adsorption (and desorption) of the particle on the substrate, (3) nucleation, and (4) diffusion of clusters along the surface to active sites. The diffusion within the solution and along the surface have already been discussed for the growth of bulk crystals and are identical for thin films. Therefore adsorption and modes of growth will now be discussed.

2.2.1 ADSORPTION

Adsorption of the particle (adsorbate) to the surface (adsorbent) is described by the concentration of solute in solution with the Langmuir adsorption isotherm.[5]

$$X_2 = (K_{ads}C)/(K_{ads}C + 1) \qquad \textbf{(2.7)}$$

K_{ads} is the equilibrium constant for adsorption reactivity and is directly related to the attraction of the solute to the substrate as compared to the solution. X_2 and C are measurable quantities representing the fraction of the surface occupied by the adsorbed solute molecules and the concentration of the solution, respectively. This equation is created by equating the chemical potentials of the solute in solution and of the solute on the surface. Additionally, it also assumes a homogeneous surface with non-interacting adsorbates and is only applicable for the formation of the first monolayer.

Adsorption can range from a weak attraction, physisorption, to a strong attraction, chemisorption. An adsorption energy (ΔG_{ads}) of 60 kJ/mole ($\approx$ .06 eV/atom) is generally

---

[5]Stokes, R. J. and D. F. Evans. Fundamentals of Interfacial Engineering. Wiley-VCH, New York, 1997.

used to define these two ranges of adsorption. Physisorption is further defined as being reversible upon removal of the adsorbate from the substrate, while chemisorption alters the adsorbate chemically. Both types of adsorption begin with the physisorption of a monolayer, but chemisorption continues with a chemical reaction to form covalent or ionic bonds between the adsorbate and the substrate.

2.2.2 GROWTH MODES FOR THIN FILMS

The final stage of thin film formation is growth and can be characterized by three basic modes. Although these modes typically refer to film growth from vapor deposition, they will suffice for growth from solution since the only difference is the interaction of a different medium (solution) with the substrate. The three modes of growth are Volmer-Weber, Frank-van der Merwe, and Stranski-Krastanov (demonstrated in figure 2.4).[6]

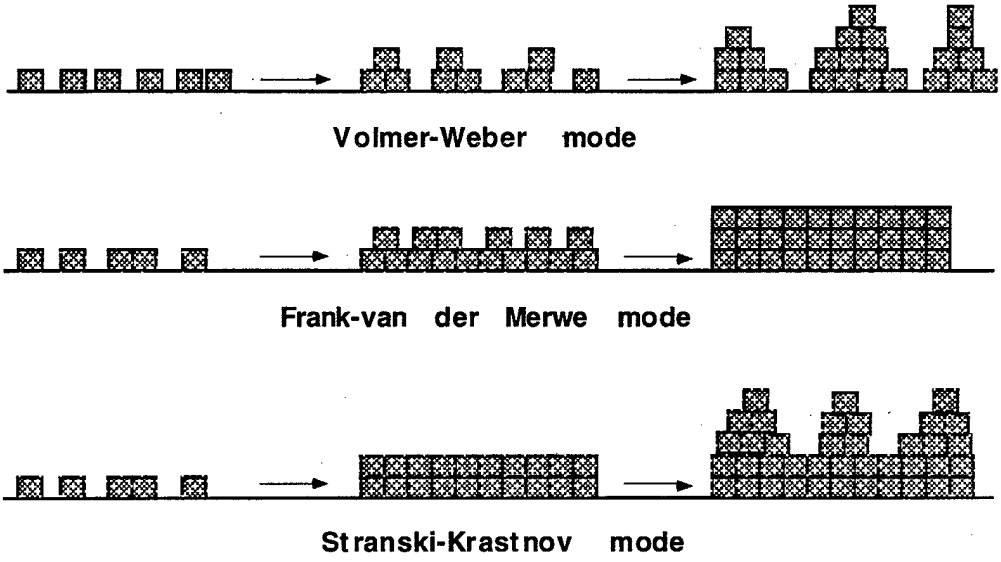

FIGURE 2.4.[6] Illustration of the three modes of growth observed for thin films.

[6]Bauer E. G.; Dodson, B. W.; Ehrlich, D. J.; Feldman, L. C.; Flynn C. P, et al . *J. Mater. Res.* 5, (1990), 852-94.

The Volmer-Weber growth is described as the nucleation of clusters on the surface followed by 3-D growth into islands. The island growth commences as the clusters have a more favorable interaction with the solution than with the substrate, which causes it to form a contact angle greater than 0° with the surface. Continued growth of these clusters into thin films is achieved by coalescence and ripening. Coalescence occurs when the clusters have a contact angle greater than 90° because of their weak interaction with substrate. This weak interaction allows the clusters to migrate and combine with others to obtain a lower surface to volume ratio. Ripening involves larger clusters growing at the expense of smaller ones. The contact angles of these clusters are near 90° causing the smaller clusters to have a higher surface energy relative to the larger clusters. These smaller particles therefore migrate to the larger clusters to obtain lower surface energies. The Frank-van der Merwe mode occurs when the clusters wet the substrate as their interfacial interaction with the substrate is lower in energy than its interaction with the solution. The result is a layer-by-layer growth as demonstrated in Figure (2.4). This mode of growth is the same as described for the layered crystal growth and is commonly seen with epitaxial growth. Stranski-Krastanov growth also begins with the formation of one or two layers, but transitions into island growth (demonstrated in Figure 2.4) due to a short range attraction with the substrate.

2.3 EPITAXY

The 2-D layered growth of thin films on substrates by the Frank-van der Merwe mode is often displayed in epitaxial growth. Epitaxy involves two crystalline materials as one rests upon (epi) the surface of the other and grows with an arrangement (taxis) relative to that surface. This type of growth requires the growing material to wet the substrate, which depends on the surface energy of the materials as previously discussed.

For this to occur the surface energy of the initial material has to be greater than the sum of the surface energy of the overlayer and the interface energy. This requirement usually limits the growth of alternating layers to form heterostructures because the reversal growth of the initial material on the overlayer would have a higher surface energy.[7]

2.3.1 HOMOEPITAXY

The best case for epitaxy is the growth of an ordered material on itself, or homoepitaxy. This thesis is concerned with the growth of the GS thin films on various substrates, that is, heteroepitaxy. The weak interlayer interactions within these layered organic materials makes them good candidates for thin film growth on flat or layered ordered substrates, while maintaining properties similar to the bulk structure.[8, 9] Additionally, the flexibility of the H-bonding interactions within the sheets may enable them to adapt their 2-D structure to obtain a lattice match with the substrate. The lattice matching lowers the surface energy as the overlayer tends to imitate the lattice of the substrate. The lowest energy is obtained from a direct lattice match between two materials, as in homoepitaxy. Deviation from a direct lattice match creates strain at the interface and is called a misfit. The % misfit is the difference between lattice constants of the overlayer (b) and the substrate (a) and is defined as $\varepsilon = [(b - a)/a]100$. Large lattice misfit strain at the interface can cause the growth to switch to the Stranski-Krastanov mode or it can instigate lattice defects that could degrade the structure-dependent properties of the film.[5]

---

[7]Palmstrom, C. *J. Annu. Rev. Mater. Sci.* . 25, (1995), 389 - 415.

[8]Scaringe, P. Electron Crystallography of Organic Molecules. Eds. J. R. Fryer and D. L. Dorset, Kluwer: Boston, 1991, 85; Perlstein, *J. Am. Chem. Soc.* 116 (11), (1994), 420.

[9]A. C. Hillier, M. D. Ward, "Epitaxial interactions between molecular overlayers and ordered substrates," *Phys. Rev. B*, 54, (1996), 14037- 51.

2.3.2 EPITAXIAL GROWTH OF ORGANIC THIN FILMS

Direct one-to-one epitaxial matches of the lattice parameters are unlikely for the growth of organic materials on inorganic substrates. The unit cells of the organic materials are larger and have lower symmetry than typical inorganic materials. The orientation for the epitaxial growth of organic films usually occurs at a large scale than a direct lattice match. Figure (2.7) demonstrates an example of this orientation with parameters of $\mathbf{b_1}$, $\mathbf{b_2}$ and β for the overlayer and $\mathbf{a_1}$, $\mathbf{a_2}$ and α for the substrate with θ as the azimuthal angle between $\mathbf{a_1}$ and $\mathbf{b_1}$.

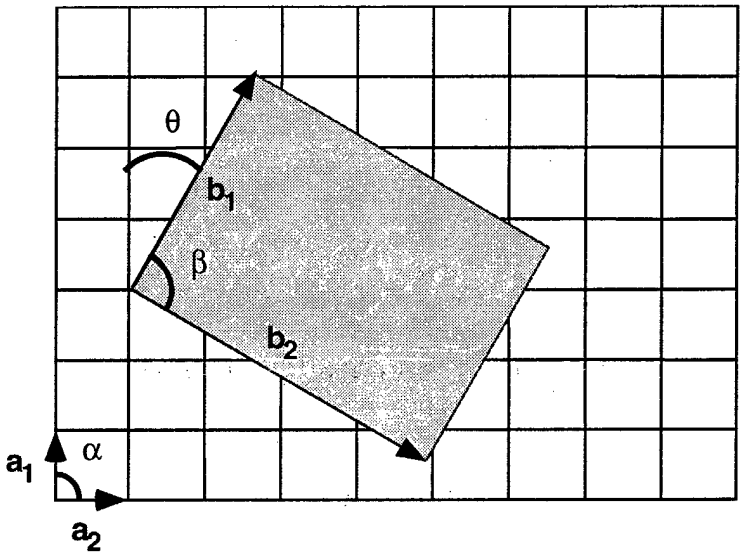

FIGURE 2.5. An example of an overlayer with lattice parameters b_1, b_2 and β oriented with respect to the substrate with parameters a_1, a_2 and α, by an angle of theta.

Organic materials have the ability to tolerate strain up to 15%[5] because they are bonded by weak non-covalent forces as compared to inorganic materials, which can only tolerate up to 5%.[5] Consequently, there has been interest in the epitaxial growth of differing organic crystals as larger strain energies are required to generate lattice defects. Previous literature have reported organic overlayers growing with long range order with

respect to ordered substrates and termed it as 'quasiepitaxy'.[10] A definite relationship was determined in our laboratory to exist between the lattice structures of two materials for this mode of epitaxy. This relationship was determined from monitoring growth of bis-(ethylenedithio) tetrathiafulvalene triiodide ($(ET)_2I_3$) *in situ* on highly oriented pyrolitic graphite (HOPG).[11] The mode of epitaxy for this growth was determined to be coincidence, which exists when only a fraction of the lattice sites in a non-primitive overlayer supercell coincide with substrate sites. Therefore, the three modes of epitaxy are commensurism, coincidence and incommensurism.[12] Commensurism is the direct lattice match between materials as discussed previously, and incommensurism has no lattice-match. The degree of epitaxy for coincidence is lower than with a commensurate match, but can still lower the interfacial energy enough to promote 2-D growth. The degree of epitaxy increases with a smaller sized supercell in the overlayer.

2.3.3 SIMULATION OF EPITAXIAL GROWTH

To determine the mode of epitaxy an analytical model has been developed in our laboratory. This model is used in a computer simulation program called EPICALC and is available on the internet at http://www.cems.umn.edu/research/ward/software.html.[13] This program has been reliable in finding predetermined epitaxial matches with a dimensionless potential energy (V/V_o) function and a transformation matrix, **C**, which relates the orientation of the overlayer to the substrate with Equation (2.8).

---

[10]Fenter, P.; Burrows, P. E.; Eisenberger, P. and S. R. Forrest *J. Crys. Growth*, 152 (1995) 65-72; So, F. F.; Forrest, S. R.; Shi, Y. Q. and W. H. Steier, *Appl. Phys. Lett.* 56 (7), (1990), 674 - 6.

[11]A. C. Hillier, J. B. Maxson, M. D. Ward, "Electrocrystallization of an ordered organic monolayer: selective epitaxial growth of β-(ET)2I3 on graphite," *Chem. Mat.*, 6, (1994), 2222.

[12]A. C. Hillier, M. D. Ward, "Epitaxial interactions between molecular overlayers and ordered substrates," *Phys. Rev. B*, 54, (1996), 14037- 51.

[13]A.C. Hillier, "Assembly of Molecular Lattices on Crystalline Substrates," Ph. D. Thesis, University of Minnesota, 1995.

$$\begin{bmatrix} b_1 \\ b_2 \end{bmatrix} = [\mathbf{C}] \begin{bmatrix} a_1 \\ a_2 \end{bmatrix} = \begin{bmatrix} p_x p_y \\ q_x q_y \end{bmatrix} \begin{bmatrix} a_1 \\ a_2 \end{bmatrix} \qquad \textbf{(2.8)}$$

Matrix elements p_x, p_y, q_x, and q_y are related to the materials lattice constants and the azimuthal angle with the following equations.

$$p_x = b_1 \sin(\alpha - \theta)/a_1 \sin(\alpha) \qquad \textbf{(2.9)}$$

$$p_y = b_2 \sin(\beta + \theta)/a_2 \sin(\alpha) \qquad \textbf{(2.10)}$$

$$q_x = b_2 \sin(\alpha - \theta - \beta)/a_1 \sin(\alpha) \qquad \textbf{(2.11)}$$

$$q_y = b_1 \sin(\theta)/a_2 \sin(\alpha) \qquad \textbf{(2.12)}$$

The program uses equation (2.14) to determine the degree of an epitaxial match by referencing the overlayer sites to the substrate sites along the interface at a certain azimuthal angle.

$$V/V_o = \left\{ 2(2M+1)(2N+1) - \frac{\sin[(2M+1)\pi p_x]\sin[(2N+1)\pi q_x]}{\sin(\pi p_x)\sin(\pi q_x)} - \frac{\sin[(2M+1)\pi q_y]\sin[(2N+1)\pi p_y]}{\sin(\pi q_y)\sin(\pi p_y)} \right\} \times \left(\frac{1}{2(2M+1)(2N+1)} \right) \qquad \textbf{(2.14)}$$

where MxN corresponds to the size of the overlayer used for the calculations. The program then calculates the same dimensionless potential at integral steps of the azimuthal angle to find a global minimum describing a possible epitaxial match. V/V_o = 1 for a incommensurate match and decreases to 0.5 for a coincidence match. $V/V_o = 0$ for a commensurate match. The program then repeats calculations for integral values of lattice parameters for the substrate and the overlayer. Only the overlayer parameters will be varied for the growth of GS thin films on HOPG or mica.

3

GROWTH OF GUANIDINIUM METHANESULFONATE AND GUANIDINIUM DITHIONATE AS THIN FILMS

This research focuses on the growth of guanidinium methanesulfonate (GMS) and guanidinium dithionate (GD) as thin films on various substrates. These two crystals were chosen from the GS system because they had the simplest structures and were easy to prepare. If successfully grown, these films can then act as templates for the 2-D growth of more complicated structures within the GS system or at least increase the understanding of the system's growth as thin films. GMS has a monoclinic lattice structure with lattice parameters of a = 12.778 Å, b = 7.342 Å, c = 9.998 Å, $\alpha = 90°$, $\beta = 126.96°$ and $\gamma = 90°$, and GD has a hexagonal lattice structure with lattice parameters of $a = b$ = 7.504 Å, c = 12.129 Å, $\alpha = 90°$, $\beta = 90°$ and $\gamma = 120°$. The lattice parameters within the H-bonded layers are a, b, and γ for both crystals. This section will describe general growth characteristics of these crystals and relate them to their 2-D growth on various substrates.

3.1 EXPERIMENTAL

GMS CRYSTALS (155.17 g/mole). The synthesis of guanidinium methanesulfonate ($C_2H_9N_3O_3S$) was achieved by precipitating the crystals through slow

evaporation of solutions consisting of equimolar quantities of guanidinium hydrochloride (Aldrich, 99%, 95.53g/mole) and methanesulfonic acid (Aldrich, 99%, 96.1 g/mole, 1.481 g/mL) in a solvent of either water, methanol, or a mixture of both. The crystals were characterized by IR (nicollet OMNIC spectrometer), and NMR (Varian Inova 300 MHz NMR equipped autosampler, in DMSO-d_6) spectroscopy and compared to previously reported data. Once the crystals were formed, they were removed from solution and allowed to dry under ambient conditions.

GD CRYSTALS (280.27 g/mole). The synthesis of guanidinium dithionate ($C_2H_{12}N_6O_6S$) was achieved through the precipitation of the crystals from slow evaporation of solutions consisting of 2:1 molar ratio of guanidinium hydrochloride (95.53 g/mole) and sodium dithionate (Pfaltz and Bauer inc., 97%, 242 g/mole) in water. These crystals were also grown by cooling a supersaturated solution. Again these crystals were characterized by IR, and NMR spectroscopy and compared to previously reported data.

GROWTH OF FILMS. The solutions used for growing thin films were prepared by mixing in know amounts of previously grown GD and GMS crystals into MeOH or H_2O. Initial attempts at growing GS films consisted of depositing these solutions at known concentrations on glass. Further attempts at thin film growth was proceeded by using TEFLON* encapsulated o-rings (Ace Glass Inc., Vineland, NJ), which contained solutions with known concentration of previously grown GD or GMS crystals in MeOH, H_2O, or a mixture of both. The substrates used consisted of a microscope cover glass, muscovite, HOPG, silicon wafer, and silane treated muscovite. The muscovite (Mica New York Corp., New York) and HOPG (grade ZYH, Advanced Ceramics Corp., Lakewood, Ohio) were always freshly cleaved with an adhesive tape to obtain flat and pure surfaces. The silane treated muscovite was synthesized by submerging freshly cleaved muscovite into a solution of 10% 3-aminopropyltriethoxysilane and 90% MeOH. After thirty minutes the material was removed and immediately rinsed with MeOH.

The contact angle of H_2O and MeOH with the surface of the silane treated muscovite were measured with a goniometer (Gaertner Scientific Corp., Chicago). The surface was also imaged by AFM to check its degree of flatness.

The o-ring method involved clamping from top to bottom, as displayed in Figure (3.1), a washer, PARAFILM, o-ring, substrate, AFM puck, and another washer. The washer allowed an opening for the insertion of a know amount of solution onto the substrate. The syringe was also used to pierce the PARAFILM with small holes for slow evaporation. The desired thickness (t) for an ideal spread of the thin film on the substrate was calculated from the concentration of solution, area within the o-ring ($6.36 \cdot 10^{-5}$ m^2) and density of the crystals (ρ = density of crystal (ρ = 1.574 g/cm^3 for GD and 1.375 g/cm^3).

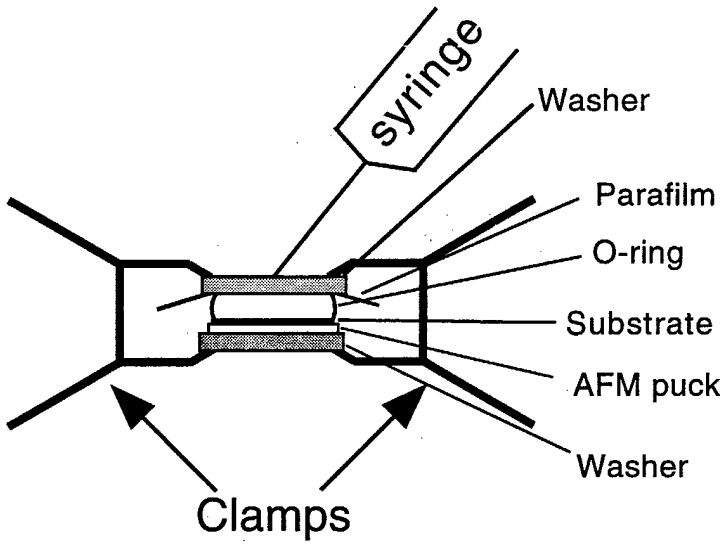

FIGURE 3.1. Demonstration of how the o-ring was used to contain the solution on the substrate and induce slow evaporation of the solution.

CHARACTERIZATION OF FILMS. Characterization of films grown on substrates was performed with atomic force microscopy (AFM) and wide angle X-ray diffraction. Details for both of these methods are available in Appendix A and B,

respectively. Initially the samples were viewed by the AFM in contact mode without success when using a fluid cell containing either saturated or non saturated solutions. AFM imaging was then attempted in air by using a scanner with a scan size of $(175\mu m)^2$ to locate and characterize areas of interest on the sample. Lattice images were obtained using a scanner with a scan size of $(15\mu m)^2$.

3.2 SUBSTRATES

Muscovite and HOPG are highly ordered layered materials often used as substrates for the growth of thin films because they cleave to expose low energy surfaces. Both of these layered materials expose 2-D hexagonally structured surfaces upon cleavage, suggesting possible use as epitaxial templates for the GS system. The lattice parameters for the substrates are listed in Table (3.1).

Material	*a* (Å)	*b* (Å)	*c* (Å)	α(°)	β(°)	γ(°)
Muscovite	5.203	8.995	20.030	90	94.47	90
HOPG	2.46	2.46	6.8	90	90	120

TABLE 3.1. The lattice parameters for both mica and HOPG. Both materials have layered structure with hexagonally ordered surfaces.

Muscovite $[(KAl_{2(oct)}Al_{(tet)}Si_3O_{10}(OH)_2]$, a common form of mica, is a layered silicate crystal with each layer consisting of two parallel sheets. Figure (3.2) is a view of the (001) plane illustrating the arrangement of silicate (SiO_4) tetrahedra within the sheet into hexagonal rings. The sheets within the layer are bonded between OH^- and Al^{3+} ions at octahedral sites and the layers are bonded by K^+ ions in the center of hexagonal rings of O^{2-} ions on the (001) plane. Cleavage occurs along the K^+ ions leaving the surface electrically neutral when half of the surface K^+ sites are occupied. The K^+ ions are

expected to dissociate from the surface once exposed to the solution and are even displaced by the AFM tip while scanning in air due to their low activation energy for diffusion (0.5eV).[1] Figure (3.3) is the AFM image with lattice resolution of the mica surface revealing the hexagonal lattice structure. Figure (3.2A) indicates the relationship between the periodicity observed in the AFM and the hexagonal structure on the surface of the (001) plane of mica. The lattice constants typically were $a = 5.3 \pm 0.3$ Å and $b = 9.2 \pm 0.3$ Å. Cleavage of the material often exposed atomically flat surfaces up to scales of $(175\ \mu m)^2$. The steps observed were usually very large (>100 nm), which allowed distinction from the thin films discussed later in the section.

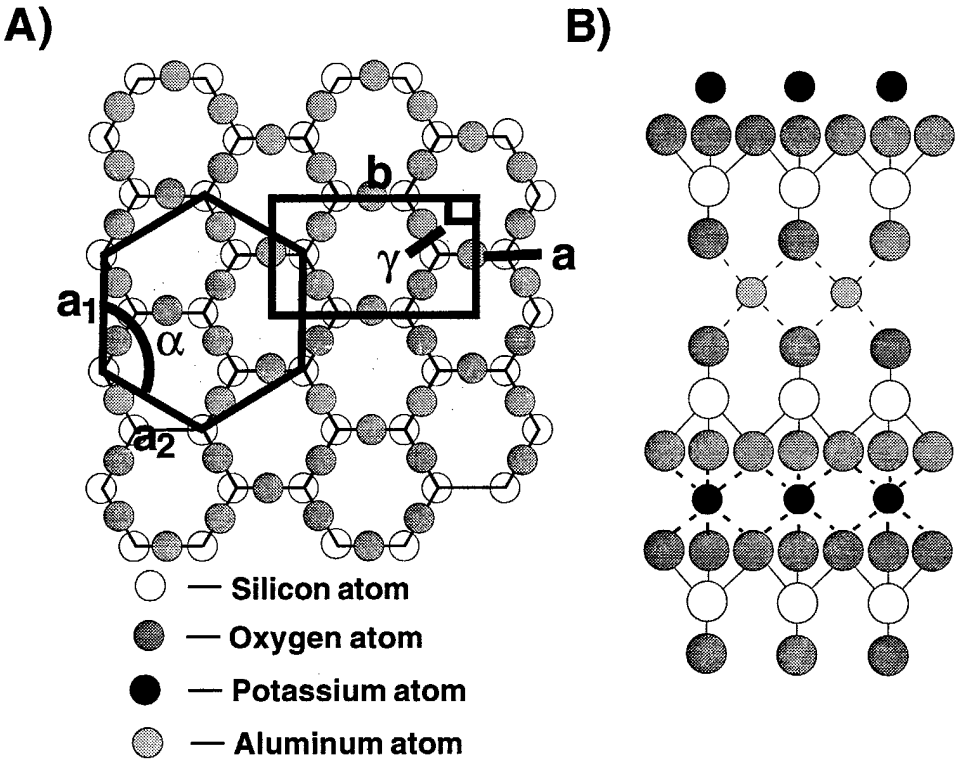

FIGURE 3.2.[2] Perpendicular (A) and parallel (B) views of the (001) plane of muscovite. The hexagonal periodicity observed by AFM is related to the surface of the (001) plane.

[1]Purton, J. A.; Allan, N. L., and J. D. Blundy. *J. Mater. Chem.*, 7(9), (1997), 1947 - 1951.
[2]Zaslavskii, B. I.; Shantarovich, V. P. and M. S. Metsic, Physica Scripta. 34, (1986), 248 - 251.

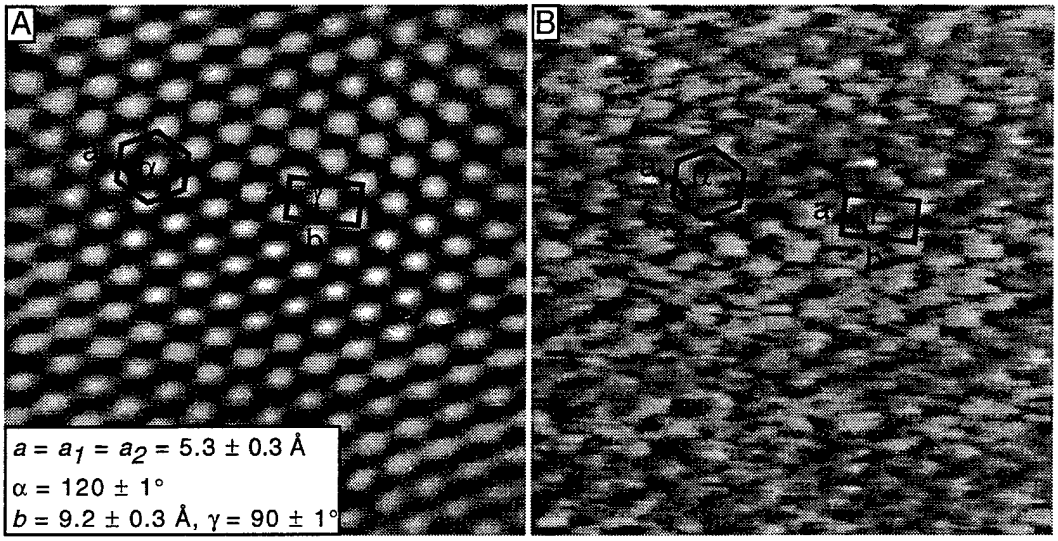

FIGURE 3.3. AFM images of muscovite. Image A is a Fourier-filtered version of the original deflection image (B) displaying a lattice image with measured parameters correlating to those for the (001) plane of mica. The lattice resolution of mica tends to indicate a 2-D hexagonal structure.

HOPG also has a layered structure, which exposes a surface with a hexagonal lattice structure when cleaved. Viewing under the AFM typically revealed hexagonal periodicities of 2.5 ± 0.2 Å in all three directions as seen in Figure (3.4). Figure (3.5) relates the hexagonal periodicity in the lattice image of HOPG to the 2-D structure within its (001) plane.

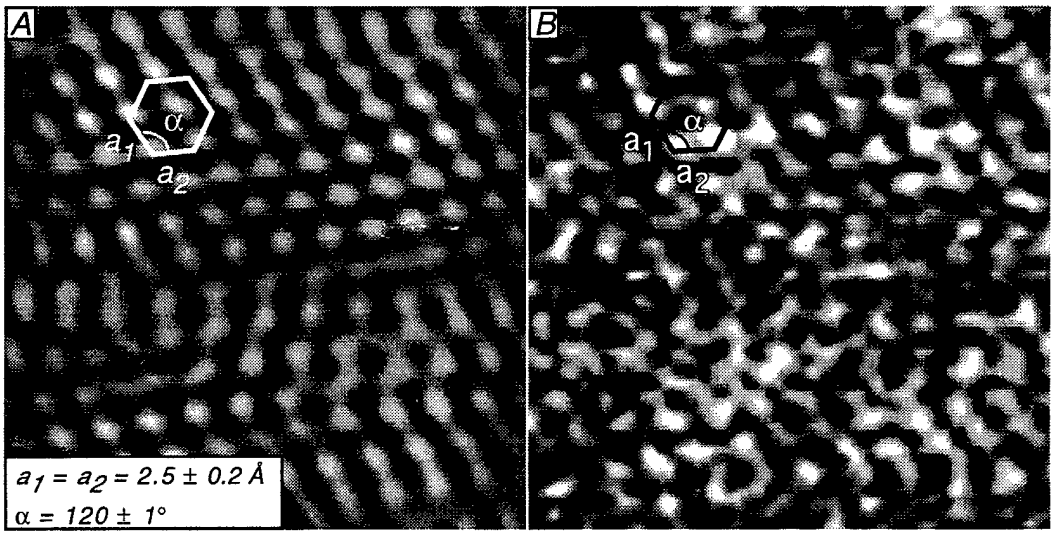

FIGURE 3.4. Fourier-filtered (A) and original deflection image (B) with lattice resolution obtained on a freshly cleaved surface of HOPG. Periodicities of the hexagonal structure are typically 2.5 ± 0.2 Å.

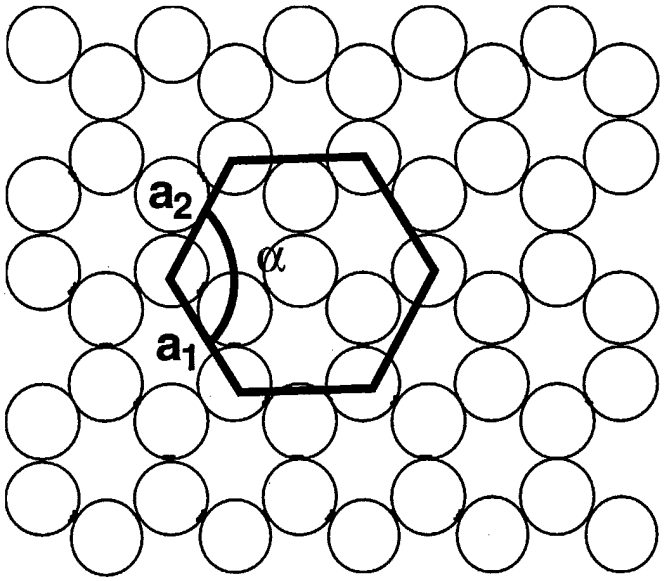

Figure 3.5. Perpendicular view of the (001) plane of HOPG. The hexagonal periodicity observed by AFM is related to the surface of the (001) plane.

3.3 GROWTH

The trends of growth for the GS crystals were studied by varying the nucleation rate, solution content and substrate. The rate of nucleation was observed to have a direct effect on the extent of 2-D crystal growth versus growth in thickness. Rapidly cooling a supersaturated solution afforded the fastest nucleation rate, which formed small hexagonal crystals possessing relatively equal height (≈ 1-2 mm) to width (≈ 1-2 mm) ratios . On the other hand, supersaturating the solution by evaporation of the solvent induced a slower nucleation rate, which produced plate-like crystals.

Figure (3.6) is an image of a GD sheet grown on the bottom of a petri dish from H_2O by slow evaporation. The growth of GD sheets entailed filling the petri dish with just enough solution to cover the bottom, and then covering the dish with PARAFILM (pierced with holes) to slow the evaporation of the solvent. The solution evaporated in fifteen days resulting in the growth of sheet-like crystals covering over half of the glass surface. A

sheet with a surface area of approximately 1 cm^2 was cleaved from the glass surface of the petri dish with a razor blade and then analyzed by AFM and wide angle X-ray diffraction (Figure 3.7A). The thickness of this sheet was measured with an optical microscope to be 10 ± 5 μm .

The X-ray data obtained from the sheet's surface suggested exposure of the H-bonded planes for GD with peaks at values of 2θ correlating to the (00l) (l = 2, 4, 6) planes of the crystal. The X-ray pattern for the GD sheet is given in Figure (3.13A) as a reference for future discussion of other samples. The values of 2θ for the peaks are indicated with angles of 14.60°, 29.54°, 44.83° and 61.08°, which agree with the expected values of 14.59°, 29.42°, 44.78, and 61.04° for the (00l) (l = 2, 4, 6, 8) planes of GD. The peaks are labeled in the diagram for the respective planes. Values of 2θ were calculated for the planes of the crystal as demonstrated in Appendix B.

Figure (3.6B) indicates the outer edges of an uncleaved GD sheet where thicknesses were measured by AFM. The thicknesses at the outer edges ranged from 800 nm to 2.2 μm . Figure (3.7) is an image of the upper surface of the sheet that was cleaved (A) and when it was viewed in acetonitrile by AFM (B). Figure (3.8) displays the Fourier-filtered (A) and the original AFM deflection image (B) with lattice resolution obtained from the upper surface of the sheet.

The observed triangular facets, step heights and lattice periodicity observed in the AFM images of the sheet agree with the hexagonally layered structure of GD. The step heights were 6.4 ± 0.5 Å (Figure 3.7B), which correlate with the bilayer thickness (6.06 Å)[3] of GD. These steps also indicate the formation of triangular facets, which are usually observed for hexagonally layered crystals. The triangular facets are due to the tendency of molecules to occupy sites of lower potential at the edges of the facet as compared to less stable sites at the corners (2 nearest neighbors versus 1).[4] The hexagonal structure

[3]Russell, V. A. Doctoral Thesis, University of Minnesota, 1995.
[4]Zhang, Z. and M. G. Lagally. *Science*, 276, (1997), 377 - 383.

observed in the lattice images of Figure (3.8) has lattice parameters of $a = b = 7.7 \pm 0.3$ Å, and $\gamma = 120 \pm 1°$, which also agrees to the X-ray results for GD ($a = b = 7.504$ Å, and $\gamma = 120$ °). Figure (3.9) relates these observed periodicities and step heights to perpendicular and parallel views of the (001) plane for a model of GD.

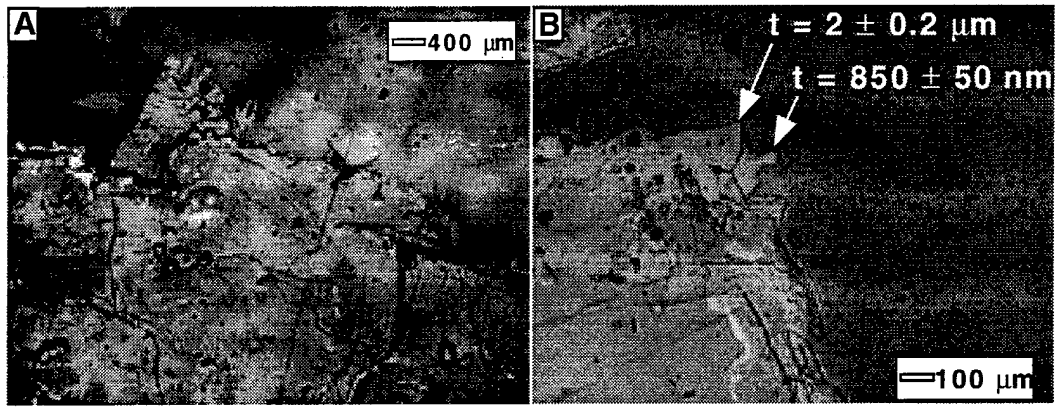

FIGURE 3.6. Optical image at 2.5X (A) and 10X (B) magnification displaying the growth of the sheet-like crystals on the glass surface. The indicated locations are where thicknesses were measured by AFM.

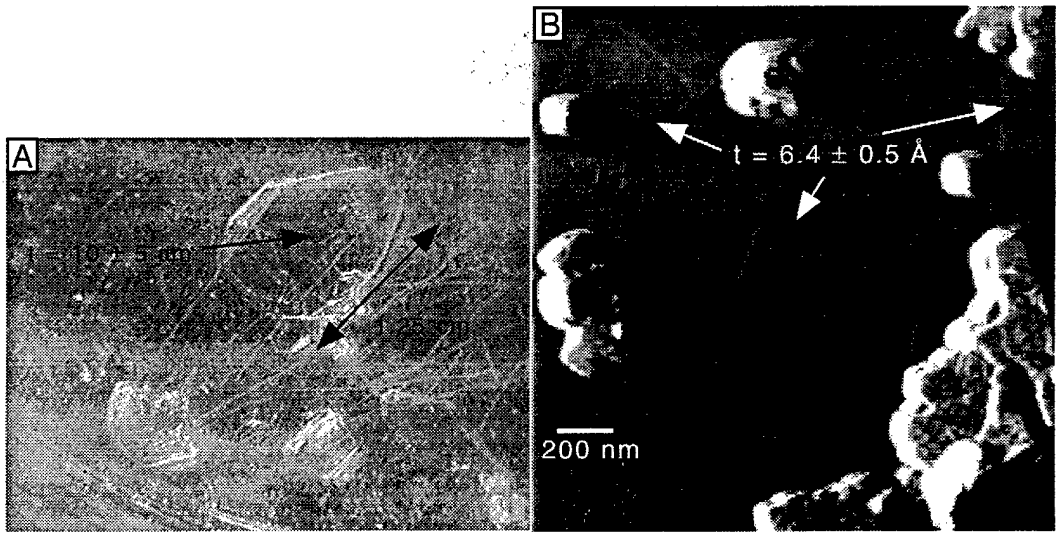

FIGURE 3.7. A) Optical image of the GD sheet after it was cleaved off the glass surface. B) AFM image of its surface displaying the hexagonal facets with step heights of 6.4 ± 0.5 Å.

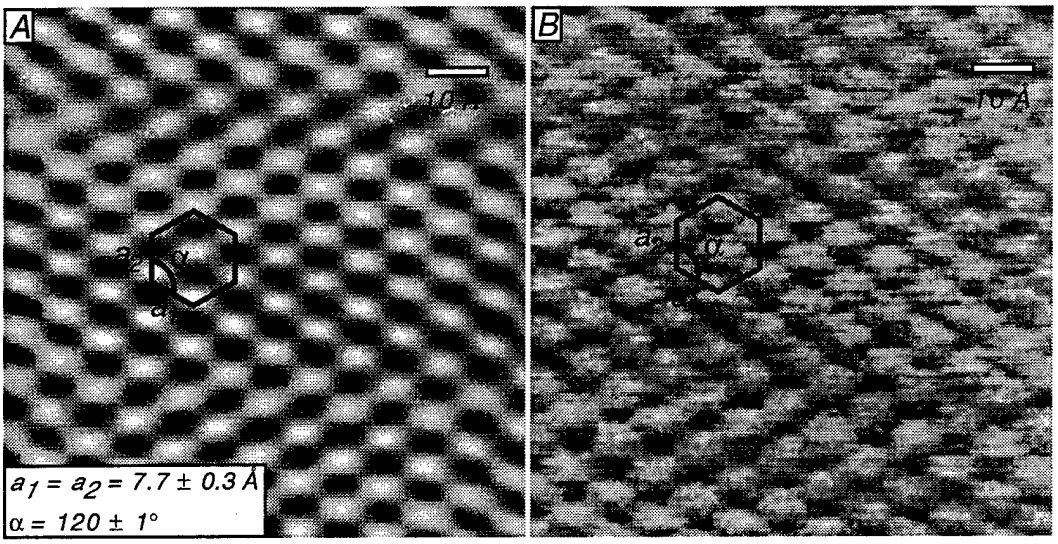

FIGURE 3.8. Fourier-filtered (A) and the original deflection image (B) with lattice resolution obtained from the surface of the GD sheet displayed in Figure (3.2).

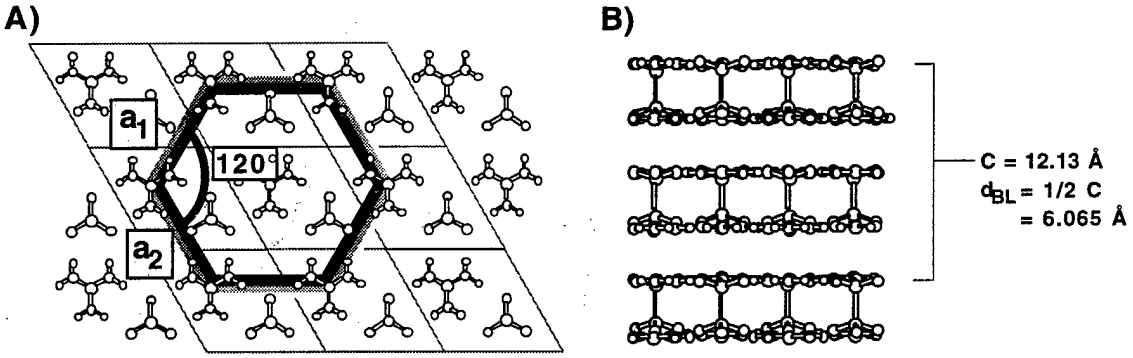

FIGURE 3.9. Perpendicular (A) and parallel (B) views of the (001) plane in GD. Model A relates the structure within the H-bonded plane to the hexagonal periodicity in Figure (3.3). The lighter grid background indicates the 2-D unit cells of the (001) surface, with lengths of 7.504 Å. Model B indicates the lattice constant (C) perpendicular to the H-bonded plane and the expected step height of 6.065 Å.

Figure (3.10) demonstrates a similar layering structure for a sheet of GMS grown from MeOH. Images of the GMS sheet were acquired from an optical microscope at 50X magnification (3.10A), and when viewed in air by AFM (3.10B). The optical image implies the formation of hexagonal facets within the layered structure. The step heights within the AFM image were approximately 8.2 ± 0.3 Å, which correlates with the bilayer thickness of GMS. The lattice image obtained from the surface of the sheet agrees with the quasihexagonal lattice structure of the H-bonded sheet. The 2-D lattice parameters of the

surface were determined to be $a_1 = 12.7 \pm .3$ Å, $a_2 = 7.5 \pm 0.3$ Å, and $\alpha = 90 \pm 1°$ (Figure 3.11). These lattice parameters agree with the expected values of $a = 12.778$ Å, $b = 7.342$ Å and $\gamma = 120°$ for GMS. Figure (3.12) illustrates perpendicular (A) and parallel views (B) of the (001) plane in a model of GMS. The expected step height is demonstrated in Figure (3.12B) to be 7.99 Å.

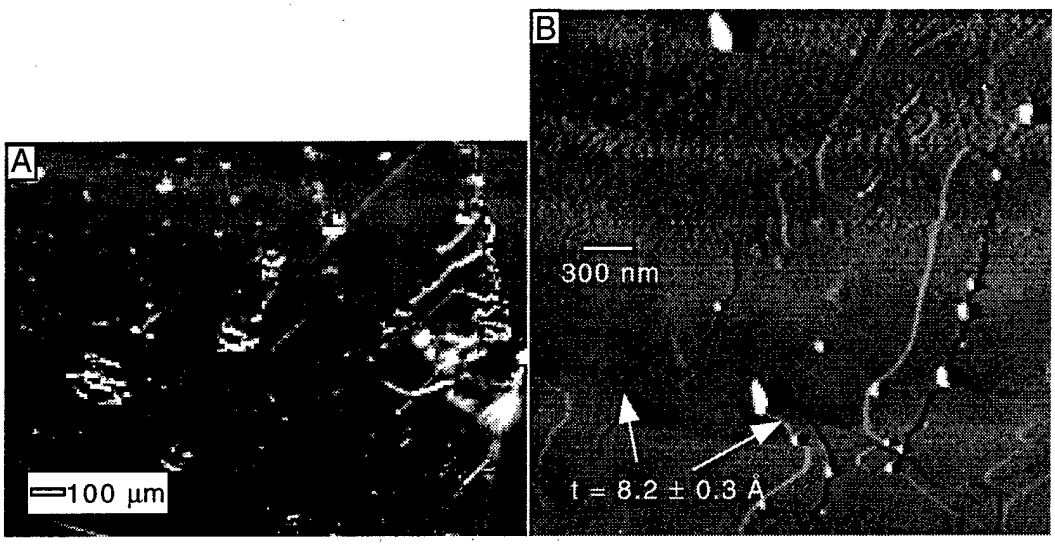

FIGURE 3.10. A) Surface of the GMS sheet as viewed in a optical microscope at 50X magnification. Notice the layered structure with quasi-hexagonal facets. B) The same surface when viewed by AFM. The dimensions of the image are $(2.75\ \mu m)^2$. The layers are indicated with step heights of 8.2 ± 0.3 Å.

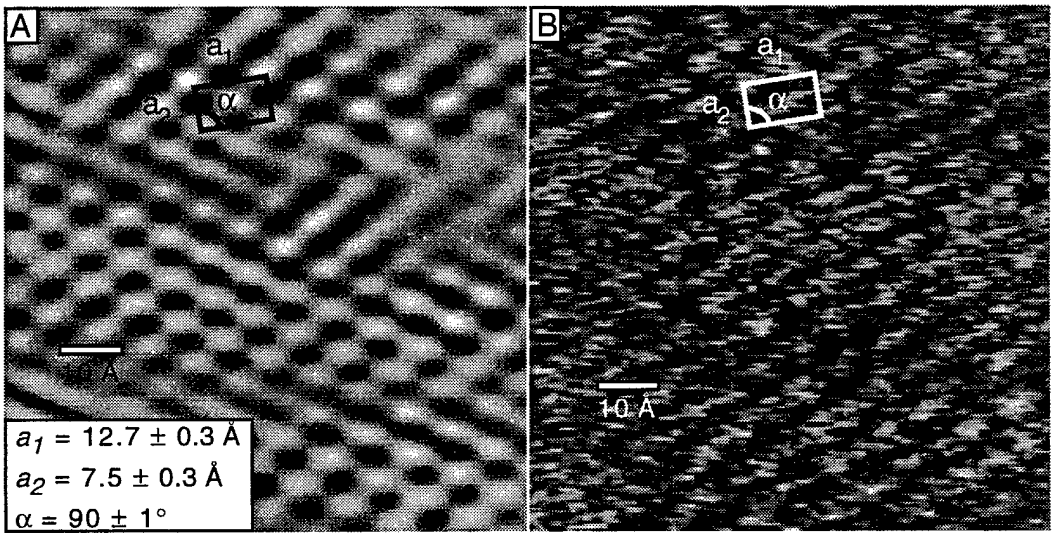

FIGURE 3.11. The Fourier-filtered (A) and the original deflection (B) image with lattice resolution obtained by AFM from the surface of the GMS crystal indicated in Figure (3.4).

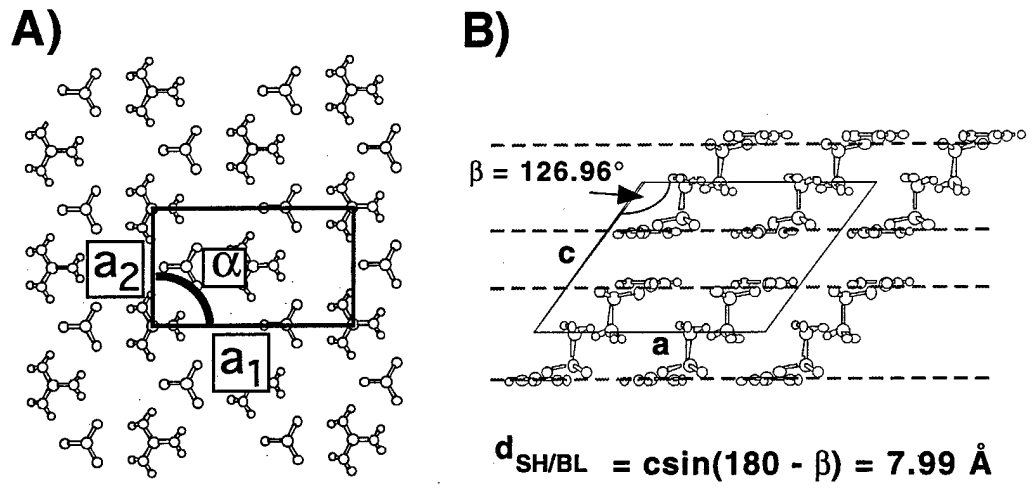

FIGURE 3.12. Perpendicular and parallel views of the (001) plane for GMS. The step height is calculated to be 7.99Å.

Occasionally, sheet-like crystals of GMS and GD grew on the glass walls of the flask to suggest 2-D nucleation and growth of these crystals on heterogeneous surfaces. To determine the orientation of the crystal growth, GD was grown on both glass and mica by submerging these substrates into solutions at 0° and 90° angles to the horizontal and then allowing the solutions to completely evaporate. Upon complete evaporation sheet-like crystals were attached to the surfaces of the substrates positioned at both angles. Figure (3.13) contains X-ray patterns for samples of GD on glass, and muscovite along with X-ray patterns for GD and muscovite. The observed peaks suggest preferred growth of GD with an orientation of the (00l) planes parallel to the surfaces of both glass and muscovite. The peaks are labeled with their correlating (00l) planes for both GD and muscovite. The broad maxima within the X-ray data for the glass samples represent the short range order within glass.[5] The layered growth of GD on these surfaces is indicative of the lowest energy growth mode within the H-bonded sheets. The orientation of this growth results from the stronger H-bonds contained within the sheets and the weaker van der Waals

[5]Cullity, B. D. Elements of X-ray Diffraction. 2nd Ed., Addison-Wesley, Menlo Park, 1978.

interactions within the interlayers. Therefore, these H-bonded planes contain the lowest surface energy to commence growth by van der Waals interaction between the H-bonded plane of the crystal and the surface of the substrate.

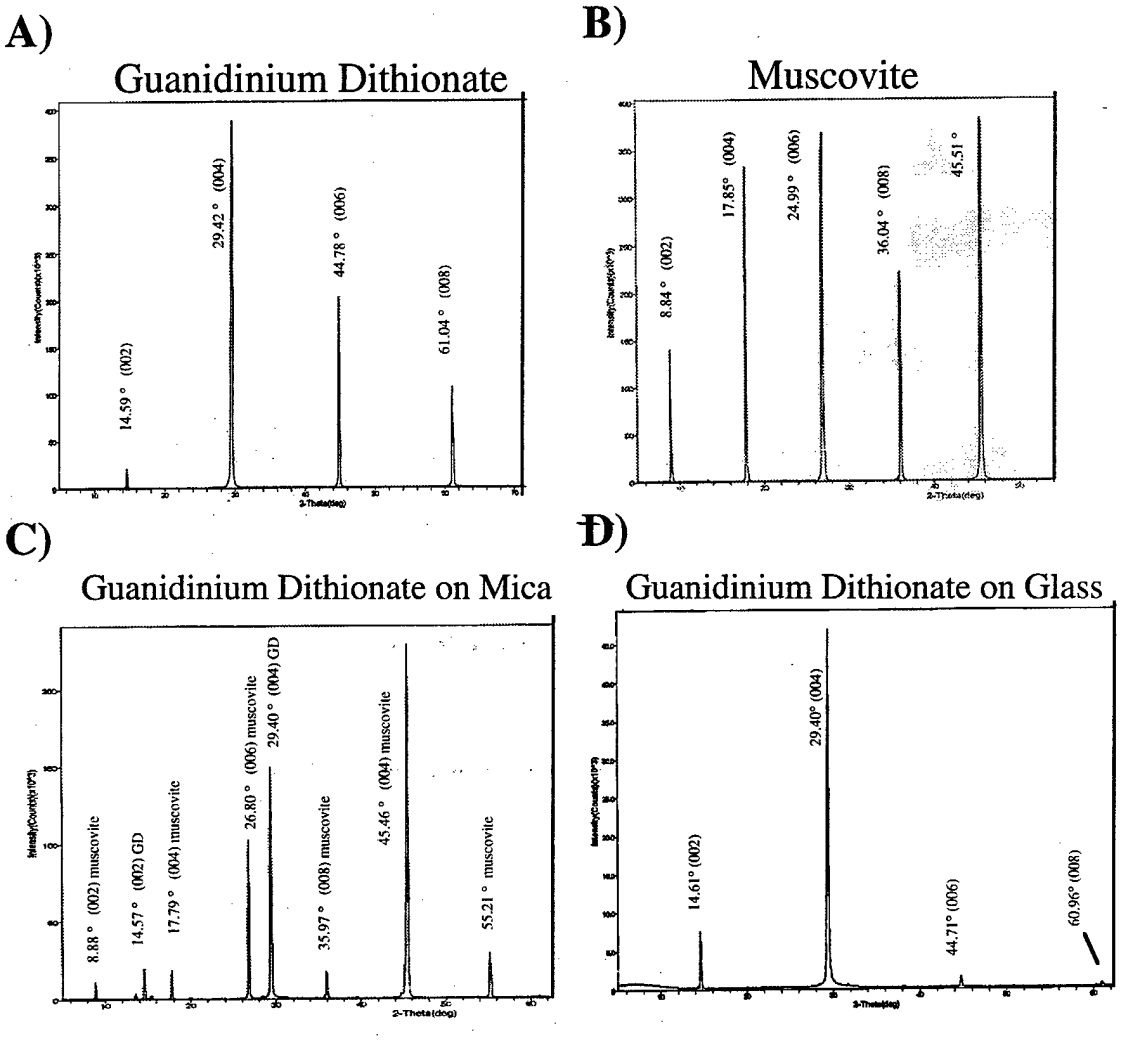

FIGURE 3.13. X-ray diagrams indicating growth of the H-bonded planes of GD on glass and mica. A) Sheet of GD B) Muscovite C) GD on muscovite D) GD on glass.

3.3 2-D GROWTH AS THIN FILMS ON SUBSTRATES

Although the previous results demonstrated the tendency for these crystals to grow 2-D on flat surfaces, characterization of ultra thin crystals will help determine the influence

the substrate has on the growth and resulting structure of the crystal. Often the properties of a thin film are different from the bulk material due to surface restructuring or adsorption interactions with the substrate.[6] The dependence of these interactions can be determined by analyzing the influence of different substrates, solution contents, and evaporation rates on the growth and resulting structure of the crystal.

3.3.1 CRYSTAL GROWTH ON GLASS

The characteristics of crystal growth were determined by studying the surface of the sample at the nanoscale with AFM. Wide angle X-ray diffraction was also used to determine the presence of the crystals and the orientation of their growth relative to the substrate. The first experiment involved depositing a known amount of dilute solution onto a glass cover slide and letting it evaporate. The concentration of GMS in MeOH was varied from 1.16 M x 10^{-4} M to 6.44 x 10^{-3} M solutions.

The two samples worthy of note were with 1.13 x 10^{-3} M (1) and 6.44 x 10^{-3} M GMS solutions in MeOH (2). Both samples formed flat hexagonal crystals as indicated in Figure (3.14) under an optical microscope. The X-ray and AFM data taken from these samples suggest the formation of an additional structure besides that of GMS. Figures (3.15) and (3.16) are the AFM and X-ray results for the respective samples. The AFM images for Sample (1) display the formation of small islands with thickness of 20 ± 5 Å found around the larger crystals. The complementary X-ray data for Sample (1) contains a pair of peaks at angles of $2\theta = 22.26^\circ$ and 22.58°. The plane-spacing (d) for these angles were 4.07 Å and 4.01 Å, which is a 1.5 % difference. These angles are close to the angle of 22.23° (d = 3.99 Å) for the (002) plane of GMS. The additional peak was not due to

[6]Ohring, M. The Materials Science of Thin Films. Academic Press, New York, 1992.

lack of filtering out $K\beta_1$ (1.3922 Å) as this wavelength is expected to produce a peak at 20.07°. The additional peak may be due to another face of the crystal.

Peak doublets have been observed to occur for the growth of pentacene as thin films on SiO_2.[7] One peak represented the single-crystal phase of pentacene while the other peak represented the thin film phase. The thin-film phase for pentacene was a metastable phase caused by the inability of the admolecules to reposition themselves to a lower free energy before they were trapped by other deposited molecules. A different structure for the GMS thin film could also be metastable phase. The molecules may have been trapped by overgrowth and/or by interactions with either the substrate or the solutions. The pair of peaks may suggest the presence of another polymorph for the GMS caused by the substrate or impurities within the system. Although the small difference in plane-spacing between the observed peaks may indicate a slight difference in crystal structure, an explanation for the additional peak could not determined from the current data.

The AFM image for Sample (2) indicates similar growth as thin (40 ± 5 Å) amorphous islands were found immediately around thicker (250 ± 50 nm) hexagonally faceted crystals. The similar location of the islands may suggest that the thinner islands are precursors to the larger crystalline islands. Lattice imaging was attempted on each type of island growth, but could not be obtained. The X-ray data for this sample did not indicate the split peaks as strong single peaks were present for the (00l) planes (l = 1, 2, 3, and 4) of GMS. An additional peak at $2\theta = 19.32°$ was observed suggesting another exposed face of the crystal, but it does not match with any expected angle for the bulk phase.

---

[7]Dimitrakopoulos, C. D.; Brown, A. R. and A. Pomp. *J. Appl. Phys.* 80 (4), (1996), 2501 - 3.

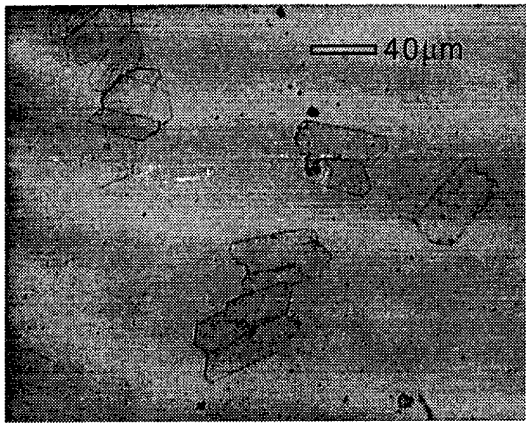

FIGURE 3.14. Optical image of Sample (1) at 50X magnification. Both samples formed these quasihexagonal crystals on the glass with thicknesses of 250 ± 50 nm.

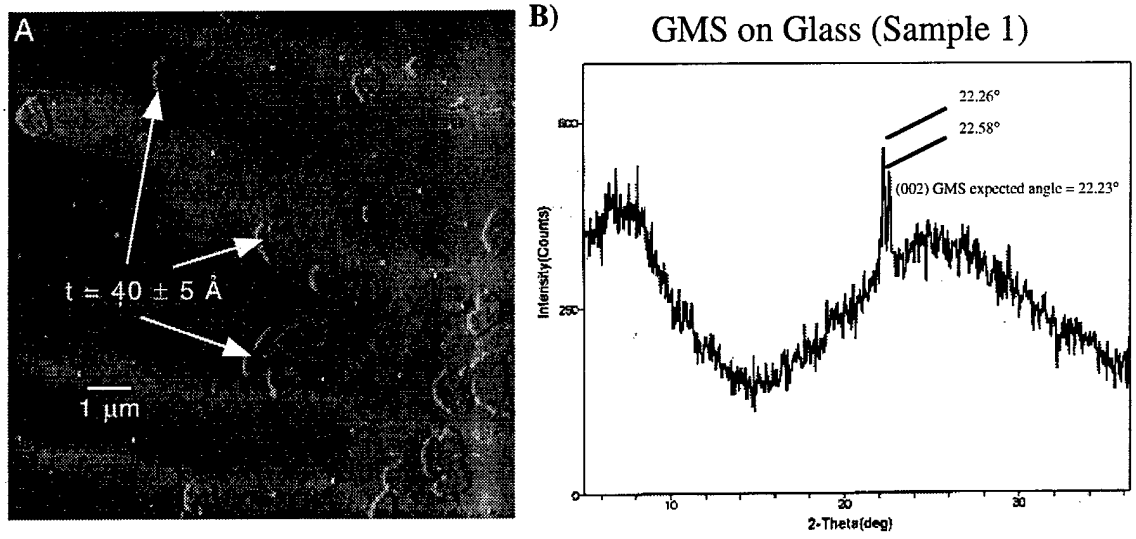

FIGURE 3.15. A) Surface of Sample (1) as viewed by AFM displaying the growth of small islands with thicknesses of 40 ± 5 Å. These islands were found around larger hexagonally faceted crystals. B) X-ray diffraction pattern for Sample (1) with a peak doublet near an angle for the expected peak ($2\theta = 22.23)^{\circ}$ for the (002) plane.

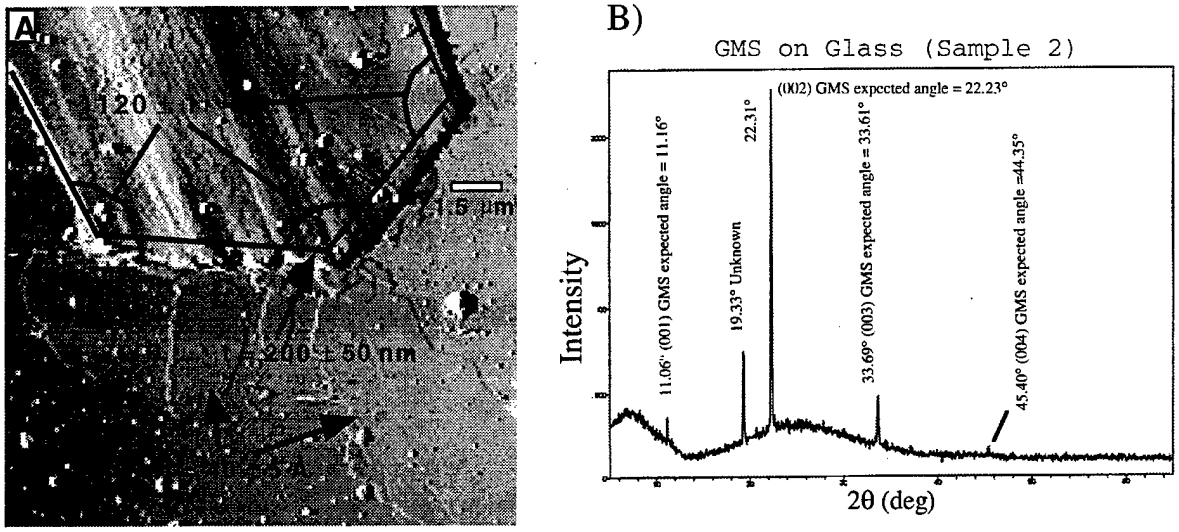

FIGURE 3.16. A) Surface of Sample (2) as viewed by AFM indicating a larger hexagonal crystal surrounded by thinner 2-D growth, which have less of a defined shape. B) X-ray diffraction pattern with peaks at angles of 2θ indicating the H-bonded planes of the crystal. An additional peak occurs at 2θ = 19.33° for an unknown reason.

Similar results were observed for the growth of GD on glass as a 7.14 M x 10^{-4} M GD solution in H_2O was evaporated on glass. Figure (3.17A) is an AFM image of the glass surface when viewed at a scan size of $(5\ \mu m)^2$. This image displays a few of the many small islands observed just outside a cluster of bulk crystals formed on the glass. The thickness of these islands were 20 ± 5 Å. These islands could be precursor films to larger GD crystals, but cannot be determined from this data.

The X-ray diffraction pattern for this sample is displayed in Figure (3.17B), which reveals the (002) and (004) planes of GD parallel to the substrate. The peaks for these planes are indicated in pairs at 2θ = 14.15° (d = 6.25 Å) and 14.55° (d = 6.08 Å), and 2θ = 28.65° (d = 3.11 Å) and 29.41° (d = 3.03 Å). The expected values for the (002) and (004) planes were calculated to be 14.59° (d = 6.06 Å) and 29.42° (d = 3.03 Å), respectively. These peaks are not due to $K\beta_1$ since the expected values of 2θ for these planes would then be 13.18° and 26.54°, respectively. The additional peak at 28.65° may indicate exposure of either the (201) or the (021) planes of GD since they are both expected

to generate a peak at an angle of 28.4°. The exposure of either the (021) or the (201) crystal faces implies that the H-bonded sheets of the GD were tilted with respect the surface of the substrate. The small difference in plane-spacing between the peaks of each pair may also be a result of a slight difference in crystal structure. The different crystal structure could be a metastable phase for the thin film or an additional polymorph due to impurities. These additional peaks were also observed for a bulk crystal of GD, which may indicate an additional polymorph. An explanation for the additional peaks could not be determined from the current data. Peaks were often observed in pairs for the growth of GD and GMS on glass, mica, and silicon wafer.

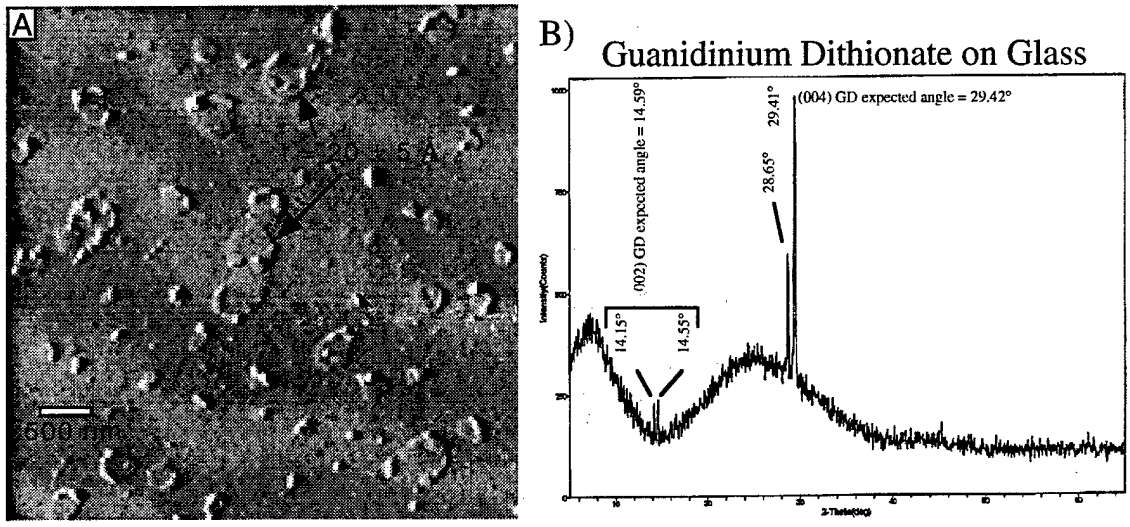

FIGURE 3.17. A) AFM image with dimensions of (5 μm)^2 indicating small islands of possibly GD on glass. These islands were located around the perimeter of a cluster of bulk crystals. B) X-ray diffraction pattern for this sample reveals the formation of the (002) and (004) planes of GD on glass with split peaks at 2θ = 14.15° and 14.55°, and 2θ = 28.65° and 29.41°.

The results obtained from the growth of GD and GMS on glass imply the 2-D growth of the H-bonded layers with an orientation of their surfaces parallel to the substrate. Thin islands were also observed by AFM and the lack of faceting of these features in the direct vicinity of the larger faceted crystals may indicate they are precursor thin films before continued growth into the bulk structure. Additionally, the additional peaks observed in the X-ray patterns for GD and GMS also suggest that there might be a modified structure for

the thin film. Further research would need to determine whether these peaks are due to an additional phase for the thin film, a polymorph induced by impurities, or another unknown reason.

3.3.2 CONFINED GROWTH of GD and GMS on GLASS and MICA

The growth of GD on glass was attempted with the solution confined within an o-ring. The rate of evaporation was decreased by covering the o-ring with PARAFILM. Initially the samples were viewed in acetonitrile under AFM, but the films were observed to dissolve into a cluster of spheres ($r \approx 25$ nm). Imaging of other samples in air suggested 2-D growth of thin crystalline films with thicknesses ranging from 50 nm to 1 μm. Two samples worth of note are listed in the following table.

Amt. of GD (g)	Solvent (mL)	Sol. Amt. (mL)	Film thickness (Å)
(1) 0.01	50 (H_2O)	0.03	215.0
(2) 0.004	100 (H_2O)	0.06	86.3

Table 3.2. List of samples for the attempted growth of GD on glass.

Sample (1) was prepared by adding enough solution as indicated in Table (3.2) to wet the entire surface of the substrate contained within the o-ring. Sample (2) was prepared by adding a smaller amount of solution as indicated in Table (3.2) so that it would not touch the o-ring, forming a droplet in the middle of the sample. Sample (1) formed flat hexagonal crystals on the area of the glass in contact with the o-ring and Sample (2) formed crystals in the shape of the meniscus as demonstrated in Figure (3.19A). Both of these samples evaporated within two days.

For Sample (1), amorphous shaped islands were observed in the outer perimeter of the sample near the large hexagonal crystals formed on the area of the glass in contact with the o-ring. The X-ray pattern for this sample contained a pair of peaks with angles of 29.48° (d = 3.03 Å) and 28.74° (d = 3.10 Å) (Figure 3.18A). The expected value for the (004) plane of GD is 29.42° (d = 3.03 Å). The small difference between the plane-spacing of the two peaks and the amorphous shaped islands may suggest the presence of an additional structure slightly different from the GD structure. Further research would need to determine if the additional peaks are due to a polymorph, a different phase for the thin film or an unknown reason.

The crystals in Sample (2) formed into a cluster mimicking the shape of the solution's meniscus with the substrate as viewed in Figure (3.19A and B). The AFM images in Figure (3.19) are of the outer edge of the cluster (C) and of crystals in the middle of the cluster (D). The thin material in Figure (3.19D) ranges from a thickness of 50 ± 10 nm in the middle of the image to 100 ± 20 nm in the upper left corner. The thicknesses of the crystals within the cluster ranged from 50 nm to 1 μm. The elongation of these crystals and the directional pattern of ridges found on the outer edge suggest preferentially growth at certain facets. Additionally, the long GD crystals appear to grow with influence from others as they had an evident tendency to align with each other. Notice the alignment of the smaller crystals into columns and the tendency of larger ones to curve in order to align with crystals in a new area. This sample will be discussed in Chapter 5. Nothing was noticeable outside this cluster when imaging with the AFM. The X-ray data of this sample contained strong peaks at 2θ = 29.31° and 44.36° (Figure 3.18B), which agree with the respective angles of 29.42° and 44.78° for the (004) and (006) planes.

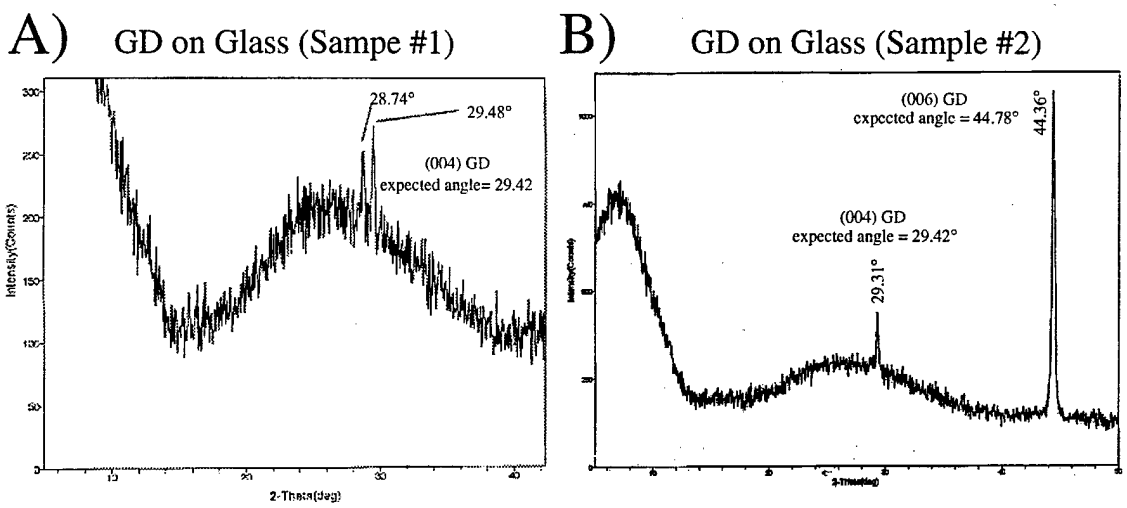

FIGURE 3.18. X-ray patterns for A) Sample (1) and B) Sample (2). The presence of doublet peaks for the (004) plane of GD in Sample (1) may represent a metastable thin film phase on the glass. The higher concentration of Sample (1) could have caused the molecules to be trapped by overgrowth before they were able to reposition to a lower energy.

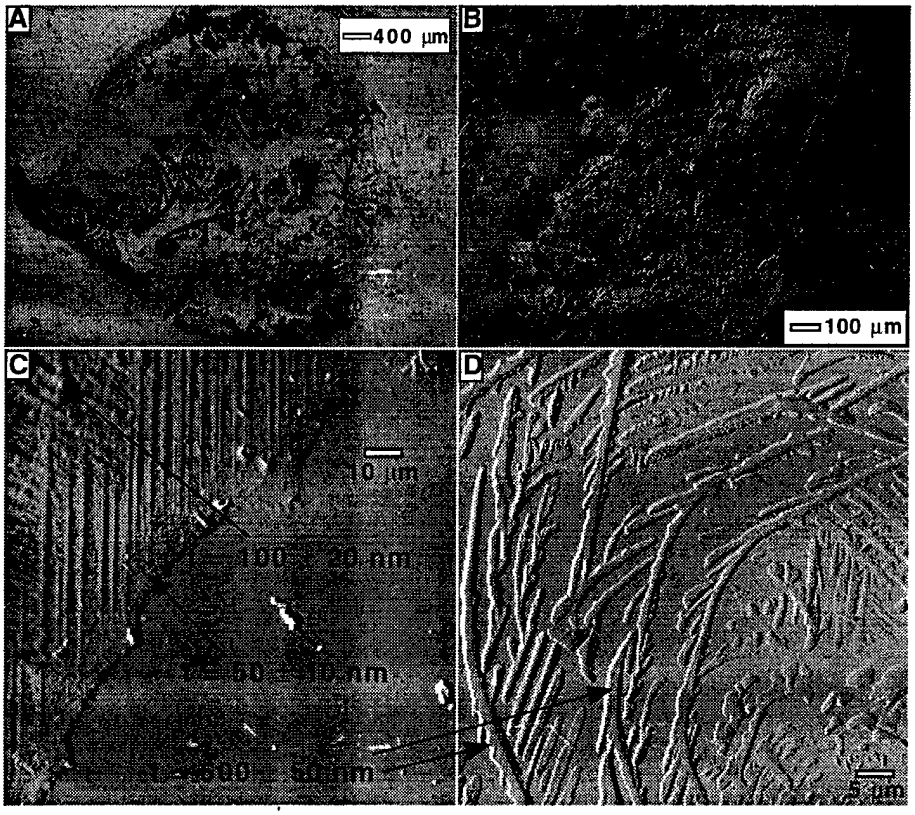

FIGURE 3.19. A) Optical microscope image at 2.5X magnification of GD crystals formed on glass (Sample 2). B) Image at 10X magnification of an area where the crystals had a tendency to simulate the shape of the solutions meniscus with the glass before complete evaporation. The AFM deflection images of the outer edge (C) and within the cluster (D) of crystals displayed in A. Notice their elongation and tendency to align with one another. The elongated shape suggests preferred growth at certain facets.

There was evidence for 2-D growth of GD on mica with two samples. The first sample was with a 0.1 mL of 8.92 x 10^{-5} M GD solution in H_2O, which took 2 1/2 days to evaporate from the surface of mica. The X-ray data of this sample contained a strong single peak at an angle of 29.06°, which agrees with the expected angle of 29.42° for the (004) plane of GD. Additional peaks were present, but could not be deciphered from peaks that were expected at similar angles for the (00l) planes of mica. Imaging through AFM found the formation of a layered material with thicknesses ranging from 18 - 53 Å. Figure (3.20A) depicts this layer, which suggests growth by the Volmer-Weber mode as islands appeared to have coalesced together. Chapter 5 will discuss more on the mode of growth of GS crystals on mica. This sample was imaged in a saturated solution of ethanol to minimize interactions, but the AFM tip etched away the material when attempting for lattice resolution.

The second sample involved evaporating a 7.14 x 10^{-4} M GD solution in 75 % MeOH and 25 % MeOH on mica. AFM images (3.20B) of the sample indicate 2-D growth of a material with a thickness of 75 ± 10 Å and a much larger surface area than the observed growth on the previous sample of GD on mica. Attempts were made to obtain lattices images on the island, but the tip etched away the material to obtain the lattice image of mica. No distinguishable peaks were observed in the X-ray diffraction pattern for this sample to verify growth of GD, but possible peaks for the H-bonded planes may have been hidden by the large peaks created by mica.

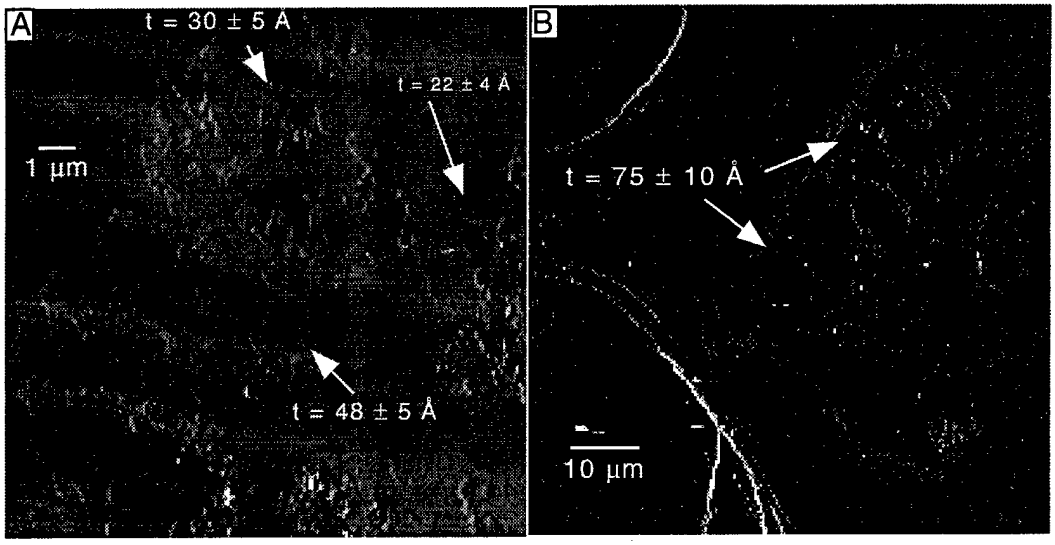

FIGURE 3.20. AFM deflection images indicating 2-D growth of GD on mica in A) the first sample and B) the second sample. The dimensions of the images are (13 μm)^2 for A and (71.8 μm)^2 for B.

The best results were obtained from the growth of GMS on mica. Lattice images were obtained in air on small islands with hexagonal facets. Figure (3.21A) is an AFM deflection image with dimension of (3.89 μm)^2 indicating hexagonally shaped crystals of GMS on mica grown by the evaporation of a 3.35 x 10^{-3} M GMS solution in MeOH. Lattice images were easily obtainable on these islands, but could not be obtained on the surrounding surface for an unknown reason. No etching was observed on the surrounding surface despite maximizing the force applied by the AFM tip. The step height of a single layer (8.22 Å) and the lattice constants (a_1 = 13.5 ± .5 Å, a_2 = 8.2 ± 0.3 Å, $\alpha = 90 \pm 1°$) of this thin material differed from the parameters of the bulk structure (a = 12.778 Å, b = 7.342 Å, $\gamma = 90°$). The limited 2-D growth of these islands and the discrepancy in the lattice parameters of the lattice image may be due to a strain induced by a lattice mismatch at the interface with the substrate. Figure (3.21B) is a deflection image of an area observed near the hexagonally shaped islands. This image indicates 2-D growth of a material with a thickness 90 ± 20 Å. This material suggests a second mode of growth for GMS as it lacks hexagonal facets. Thin films were scraped away by the tip when attempting to obtain lattice

images on their surface, implying a lower strength of adsorption to the substrate and/or a structure with less cohesion.

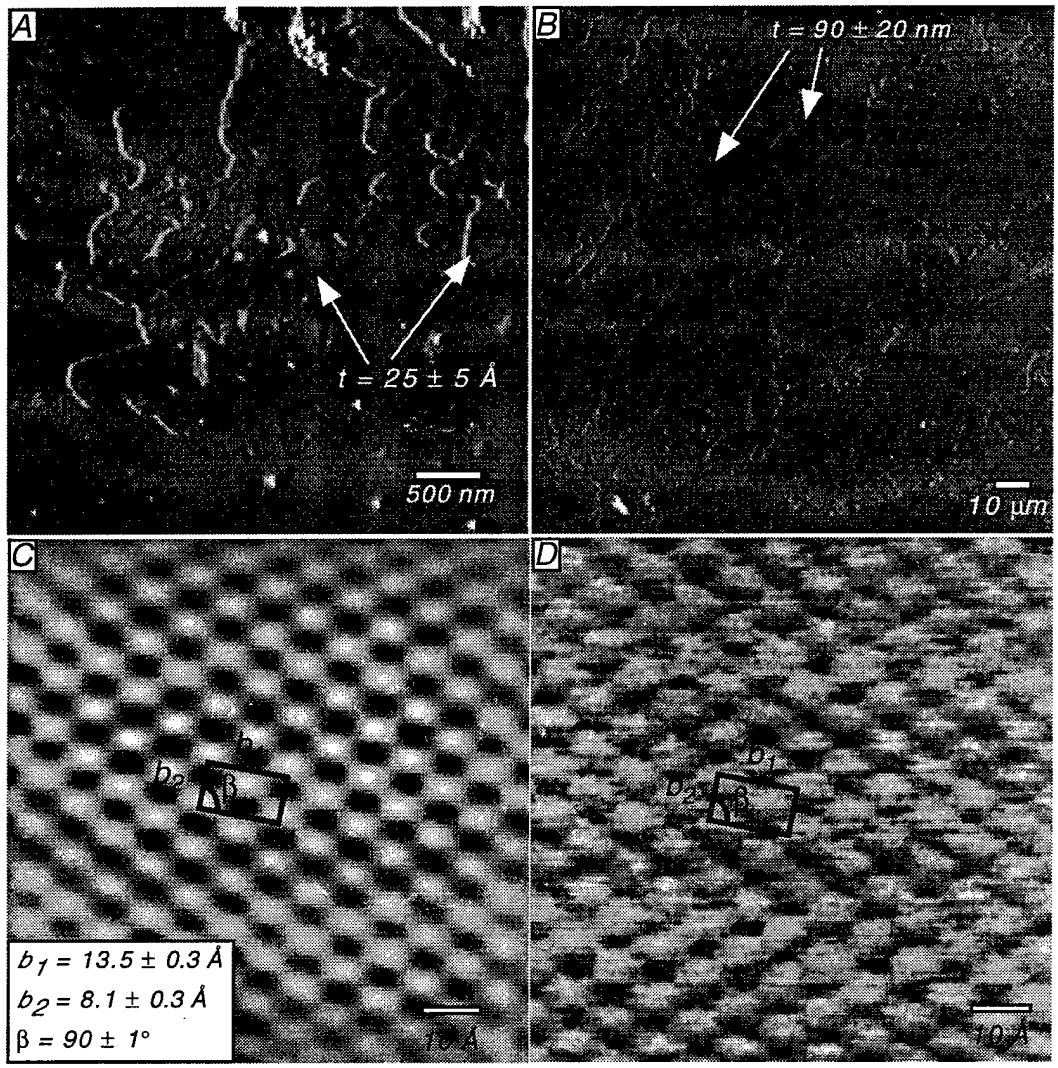

FIGURE 3.21. AFM deflection images implying 2-D growth of GMS on mica. Lattice resolution was obtained in air on the hexagonally shaped islands in Image A. Image B is of the less ordered material observed near the same area, but with more 2-D growth. The lower two images are the Fourier-filtered (C) and original deflection image (D) with lattice resolution obtained from the surfaces of the small islands.

A sample prepared by evaporation of a 2.68 x 10^{-3} M GMS solution in MeOH from mica displayed similar elongated growth to that observed for GD on glass in Figure (3.19D). Figure (3.22A) depicts the elongated GMS features that grew preferentially along

specific directions reflecting the 6-fold symmetry of mica. A larger image will be presented in Chapter 4 to display this growth over larger distances. Figure (3.22B) reveals the hexagonal facets of the GMS crystal, which had a thicknesses of 75 ± 10 Å. The lattice images obtained on the islands of GMS will be presented in Chapter 4 when discussing a possible epitaxial match with mica. Two possibilities for the directional growth of GMS could be crystal growth along the steps of mica or homoepitaxial growth if the bottom surface is GMS. The growth along the steps of mica would be improbable since mica was usually observed to be flat at the atomic level when viewed with scan sizes up to (175 mm)^2. When steps did occur, they were usually greater than 100 nm. The possibility of this growth occurring on GMS was also unlikely since lattice images of the surrounding surface matched that of mica. This sample will be discussed in detail later in Chapter 4.

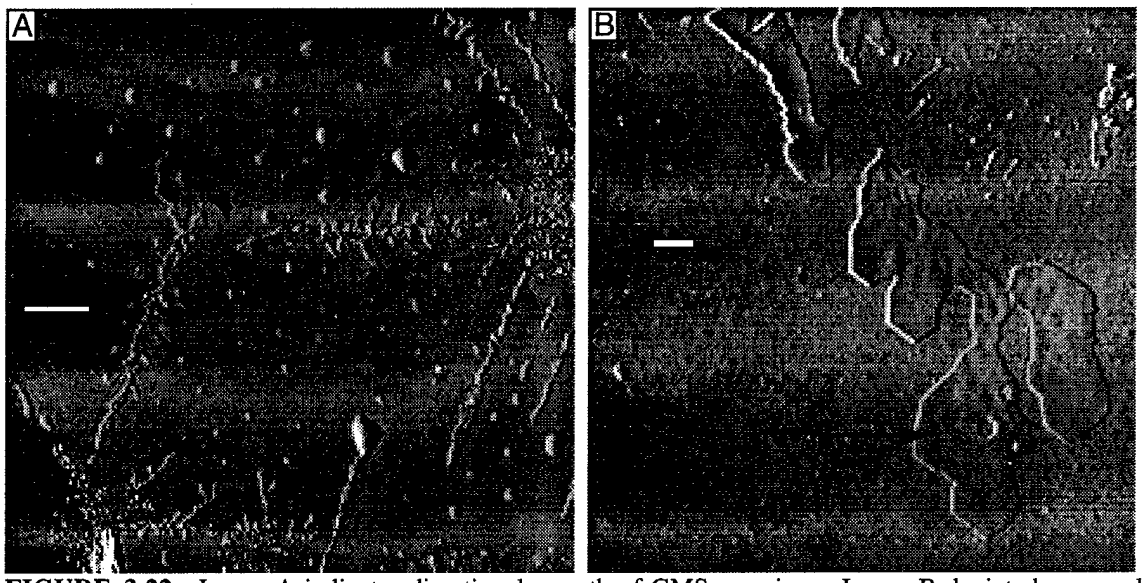

FIGURE 3.22. Image A indicates directional growth of GMS on mica . Image B depicts hexagonal facets of the thin crystal.

Crystal growth of GMS was observed on another sample to form with a circular shape on mica (Figure 3.23A and B). For this sample, only 0.015 mL of a 2.68 x 10^{-3} M GMS solution in MeOH was evenly disperse on mica. The deflection image in Figure (3.23A) displays a circular island with a thickness of 380 ± 50 nm. The formation of

circular islands were often observed with growth of GMS on mica. The formation of circular islands may be due to the attraction of molecules to crystal agglomerations to obtain a low surface energy. Figure (3.23B) depicts the surface of the island indicating the order of these crystals with aligned ridges in two directions rotated 60° from each other. The orientation of these ridges resemble the ribbon directions within H-bonded planes of GMS. The orientation of these ridges may be induced by H-bonding interactions.

Figure (3.23) exhibit a large (C) and a small (D) island of GMS located near the large circular island observed on the mica. The small island was a peninsula off the large island before the AFM tip etched away the part of the peninsula connecting the two islands. Lattice images were obtained on the small island (Figures 3.23E and F) with lattice parameters of $a_1 = 13.5 \pm 0.3$ Å, $a_2 = 8.1 \pm 0.3$ Å, and $\alpha = 90 \pm 1°$. The thickness of the small island was 30 ± 5 Å at the outer edges and 60 ± 5 Å in the middle. The resistance of these small hexagonal islands to mechanical damage by the AFM tip may be due to good adhesion to the mica and/or a large cohesion energy. The surface of the large island was level ($\Delta t = \pm 10$ Å) in some areas, but contained faceted islands like the small one in other areas. The level areas of the large island had a thickness of 85 ± 10 Å. The AFM tip etched away the small islands located on the large island when attempting to obtain lattice images of their surfaces. The lattice image of the large island displayed a periodicity that could only be filtered into rows with a spacing of 7.5 ± 0.2 Å. Continued attempts to obtain lattice images on the larger island resulted in etching. Lattice images could not be obtained on the surrounding area, but no etching was observed when maximum force was applied on the surface by the AFM tip. The X-ray data for this sample indicated growth of the (002) and (003) planes of GMS on the mica with a split peak at $2\theta = 22.22°$ and 22.59° and another small peak at 33.57°. The expected angles for these planes are 22.23° and 33.61°. The additional peak is due the shifting of the peak for the (005) plane of mica, which is also expected to occur at 22.23°.

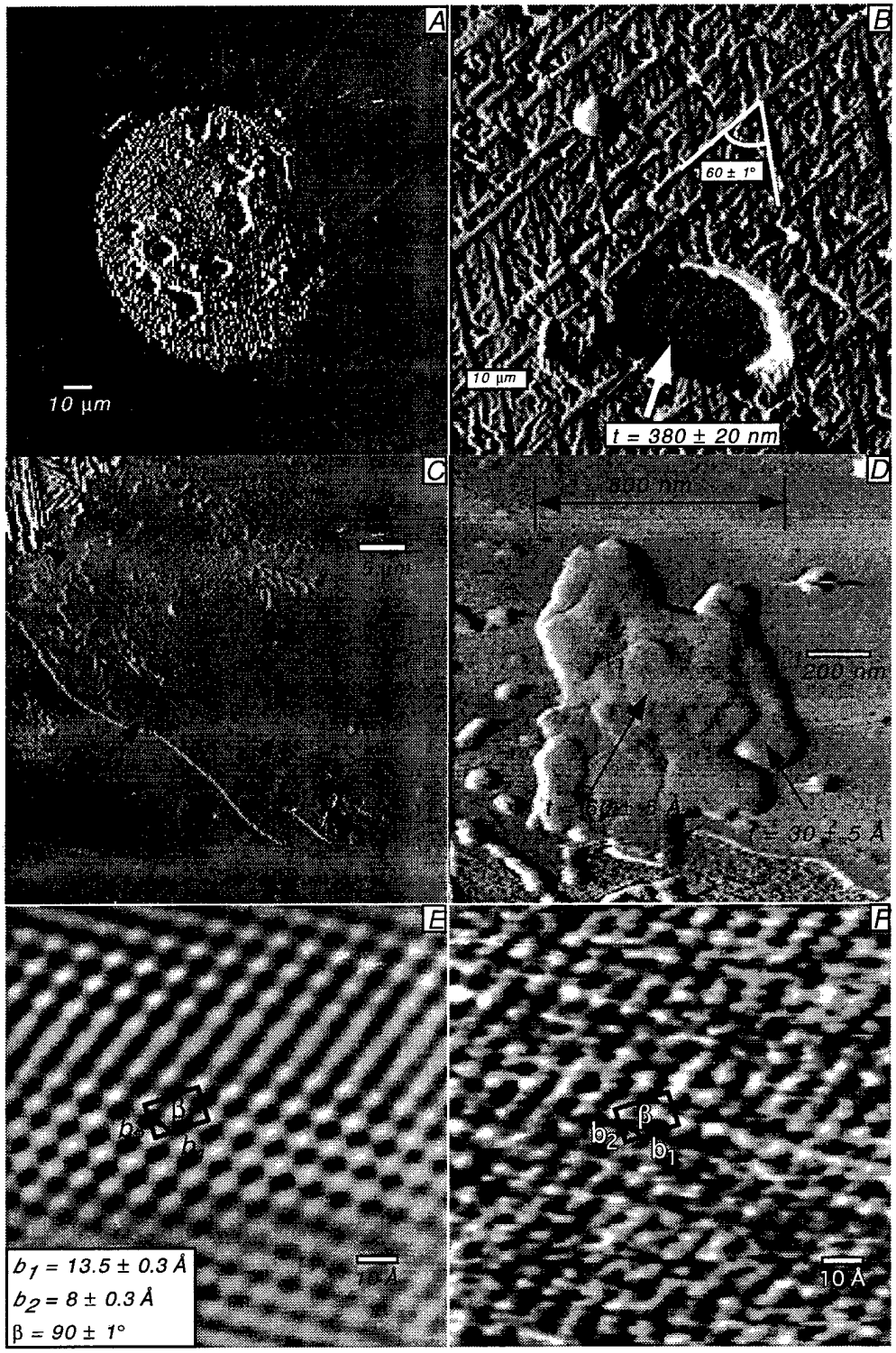

FIGURE 3.23. A sample viewed in air by AFM with features commonly observed for the growth of GMS on mica. A and B illustrate the formation a large circle containing ridges along two directions oriented 60° to each other. Image C depicts 2-D growth on a large scale. Image D is of a small island with a more defined shape. Images E and F are the Fourier-filtered and original deflection images indicating the 2-D lattice structure of the small island in Image D.

Only growth of GMS was observed on HOPG, which will be discussed later in Chapter 4 in terms of epitaxial growth. Other attempts of growth within the GS system included guanidinium biphenyldisulfonate•1,4-dichlorobenzene on glass and guanidinium ethanedisulfonate on mica. Lack of quality in X-ray and AFM results prevented adequate characterization, but images captured by AFM did imply 2-D growth of a material on the substrates (Figure 3.24).

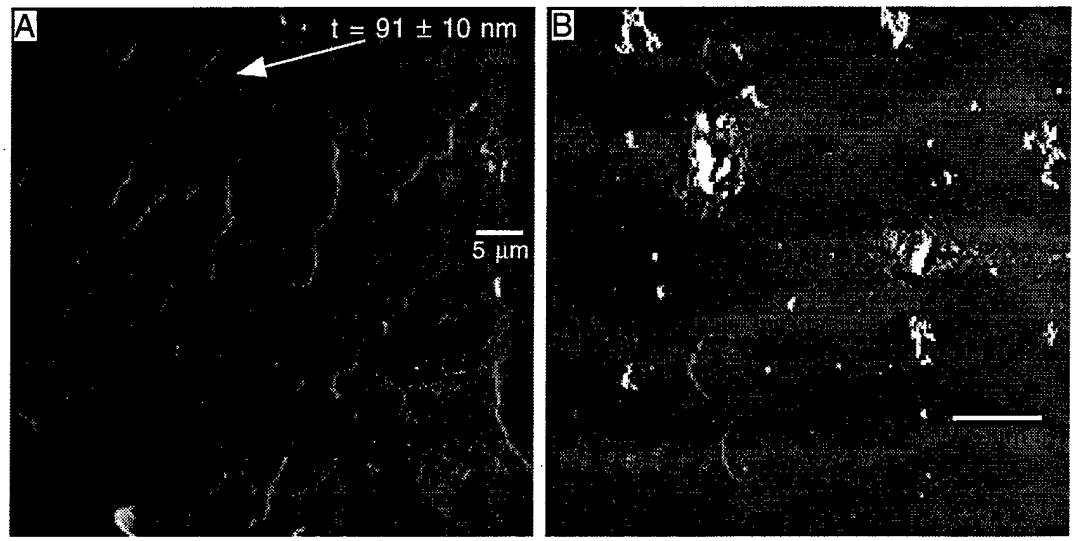

FIGURE 3.24. AFM images suggesting 2-D growth of guanidinium biphenyldisulfonate•1,4-dichlorobenzene on glass (A) and guanidinium ethanedisulfonate on mica (B). Both samples exhibit 2-D growth similar to that observed for 2-D growth of GMS and GD.

3.4 EFFECTS OF THE SOLUTION AND THE SUBSTRATE

Silicon wafers and silane treated mica were also used as substrates to determine how the 2-D crystal growth was affected by the degree of solution wetting on the substrate. The silane is suspected to form a chemisorbed monolayer on mica with siloxane bonds at the interface.[8] This monolayer is expected to create a hydrophilic surface by exposing the amino alkane tail. An additional layer of silane was suggested to grow on the chemisorbed

[8]Wang, D. and F. R. Jones. *Journal of Mat. Sci.* 28, (1993), 2481 - 2488.

layer because a large contact angle (100 ± 2°) was observed when a drop of H_2O was placed on the treated surface. The growth of additional layers have been observed to form a H-bonded cyclic structure, which arise from oligomeric or partially polymerized silane.[8] The cyclic structure results from the amino alkane tail forming a H-bond with an unpolymerized hydroxyl group on the silicon. The cyclic structure may expose the hydrocarbon chain on the surface, which could have induced the large contact angle observed when H_2O was placed on the treated surface. The observed contact angles of H_2O and MeOH on these and the other substrates are noted in Table (3.3).

Substrate	Angle of H_2O (°)	Angle of MeOH (°)
Glass	60 ± 2	23 ± 2
Muscovite(mica)	0	0
HOPG	58 ± 2	Initially a complete spread then formed islands - 45
Silicon wafer	60 ± 2	0
Silane treated mica	100 ± 2	26 ± 2

TABLE 3.3. A list of measured contact angles for H_2O and MeOH on the substrates used for the attempted growth of GMS and GD.

So far the extent of 2-D crystal growth versus growth in thickness was the best on mica, marginal on glass, and limited on HOPG. Several GS solutions were evaporated from within an o-ring on silane treated mica, but 2-D growth was not observed. The 2-D growth of GS crystals seems to depend on the solvents ability to wet the substrate. The growth of GMS on silicon wafer appeared to have this relationship as a larger extent of 2-D growth was observed from solvent that formed a smaller contact angle when placed on the substrate. The growth observed on silicon wafer was then compared to growth observed on other substrates, which had the same wettability with respect to the solvent.

The samples were prepared by evaporating a solution of 2.68 x 10^{-3} M GMS solution in H_2O, and another in MeOH, on separate silicon wafers. The GMS that grew on silicon wafer from H_2O formed as a cluster of thicker crystals at the outer edges by the o-ring, while growth was not observed in the middle of the sample. This result was similar to the growth of GD on glass. The 2-D growth of GS crystals appeared to be limited by the wettability of the substrate, as H_2O was observed to form a contact angle of 60 ± 2° when placed on glass and silicon wafer. The results obtained from the sample involving the growth of GMS on silicon wafer from MeOH also demonstrated this relationship as a larger extent of 2-D growth was observed on the surface, of which MeOH wets (0°). Growth features were observed on the substrate with smaller thickness and in more locations (Figure 3.25). The thicknesses of the islands depicted in the AFM images range from 12.5 Å to 100 nm. These results are were similar to the growth observed on the samples that involved evaporating GMS solutions in MeOH on mica (Figures 3.23). The 2-D growth of GMS also appeared to be enhanced by the ability of MeOH to completely wet mica (0°).

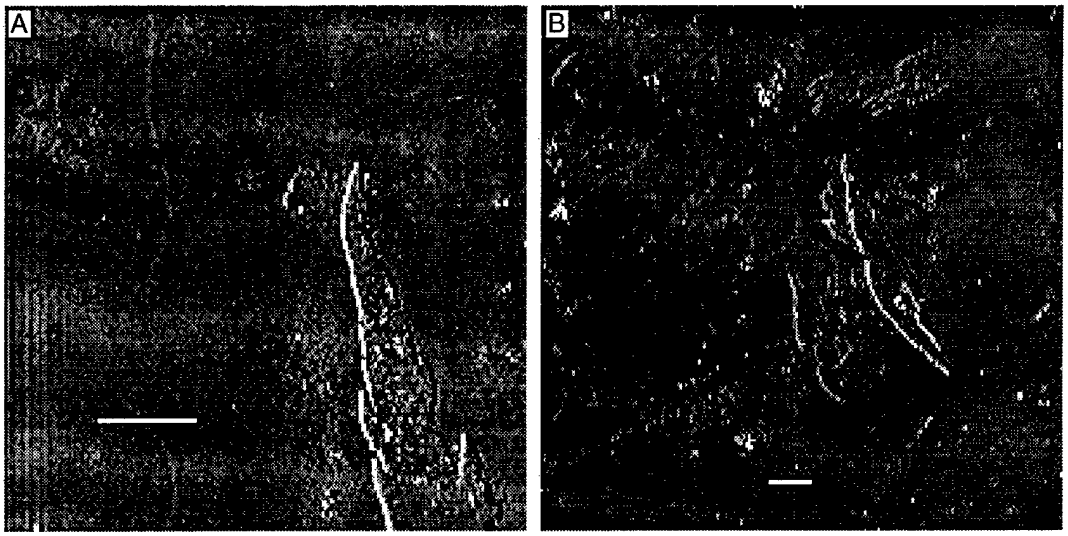

FIGURE 3.25. AFM images with 2-D growth of GMS from MeOH on silicon wafer. The material is assumed to be GMS because of the (001) peaks present in the X-ray diffraction data of this sample (Figure 3.27). This growth is also similar to growth of GMS found on mica.

The X-ray diffraction patterns obtained from the silicon wafer samples also suggest a difference in growth of GMS from H_2O than from MeOH. The X-ray pattern for the sample with growth from H_2O (Figure 3.26A) indicates a pair of peaks at angles of 2θ = 22.09° (d = 4.02 Å) and 22.45° (d = 3.96 Å), which are near the expected angle (22.23°) for the (002) (d = 3.99 Å) plane of GMS. This X-ray pattern also indicates a pair of peaks at angles of 2θ = 32.91° (d = 2.72 Å) and 33.46° (d = 2.67 Å), which are near the expected angle (33.61°) (d = 2.66 Å) for the (003) plane of GMS. The X-ray pattern for the sample with growth from MeOH (Figure 3.26B) indicates a pair of peaks at angles of 2θ = 22.10° (d = 4.02 Å) and 22.47° (d = 3.95 Å), which are near the expected angle (22.23°) for the (002) (d = 3.99 Å) plane of GMS. An additional peak is present at an angle of 2θ 34.11°, which is near the expected value of 2θ (33.61°) for the (003) (d = 2.66 Å) plane of GMS. The additional peaks may suggest crystal growth with a different orientation with respect to the substrate or it may indicate a slightly different structure for the thin film. These options may result because of preferred interactions at the crystal faces with the solvent. Preferred interactions with the solvent may be indicated since the left peak of each split was more intense for the samples grown from H_2O, while the right peak had more intensity for the samples grown from MeOH. The common occurrence of paired peaks observed in X-ray pattern for the samples presented in this chapter and their possible relationship to the solvents cannot be determined from current data. Further research would need to be conducted using different substrates of which the solvents wet equally upon. Similar wetting of the solutions would eliminate influences on the growth caused by the solution-substrate interactions. Also, using different solvents may help determine how the crystal growth is effected by the interactions between the crystal faces and the solution.

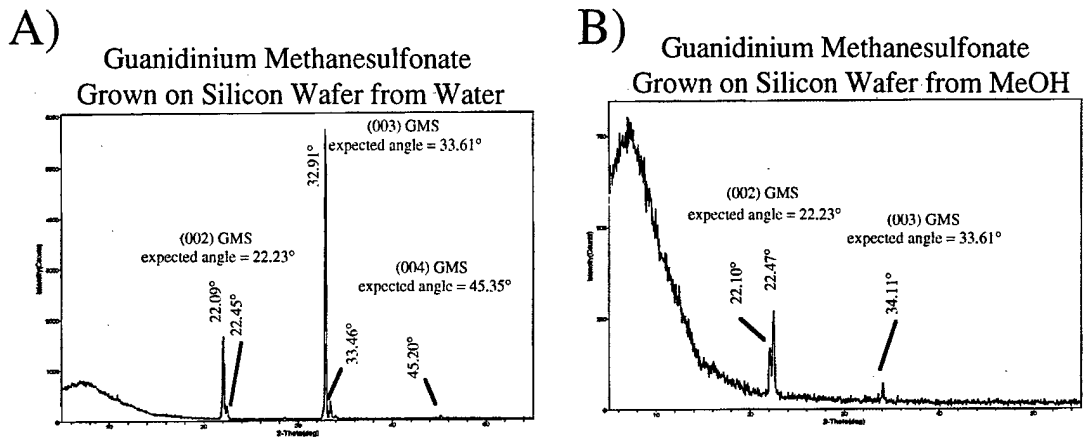

FIGURE 3.26. A) X-ray diagram for the sample of GMS grown on silicon wafer from H_2O. Peaks are indicated at angles of 22.09°, 22.45°, 32.91°, and 32.64°. B) X-ray diagram for the sample of GMS grown on silicon wafer from MeOH. Peaks are indicated at angles of , 22.47°, and 34.11°.

3.5 CONCLUSION

The data presented in this chapter suggests 2-D growth of GMS and GD on various substrates. Crystal growth was characterized by methods of AFM and wide angle X-ray diffraction. The crystals had a tendency to grow with an orientation of their (001) plane parallel to the substrate. This orientation agrees with the expected 2-D growth along the low energy growth mode of the H-bonded planes. Additionally, the observations of islands, with and without facets, on the substrate and paired peaks occurring at angles for the (00l) planes of the GS crystal may imply the presence of a material with a slightly different structure. The additional peaks may also indicate different crystal orientations, but could not be determined from the current data.

The 2-D growth of GS crystals tends to be enhanced by slow evaporation of the solution and by the ability of solution to spread on the substrate. Other interactions were suspected to influence growth, but could not be determined from current data. Chapter 4 will discuss possible epitaxial growth of GMS on mica and HOPG.

4

EPITAXIAL GROWTH OF GMS

HOPG and mica are good substrate candidates for the epitaxial growth of the GS system due to their layered structures, which expose a hexagonally ordered surfaces upon cleavage. An epitaxial match between the GS overlayer and the substrate would lower the interfacial energies to favor 2-D growth. This chapter describes possible epitaxial relationships of GMS to mica and HOPG, based on AFM images that indicate specific orientations to exist between the crystal and the substrate. These orientations are then compared with epitaxial matches found by simulation with EPICALC, in which the overlayers were rotated 60° with respect to the hexagonal substrates at steps of 0.2° to find coincident matches with a $V/V_o < 0.7$. The overlayer dimensions used were 25 $\mathbf{b_1}$ x 25 $\mathbf{b_2}$. Table (4.1) contains the 2-D lattice parameters (a, b, and γ) of each material's surface.

Material	a (Å)	b (Å)	γ(°)
GMS	12.778	7.342	90
GD	7.504	7.504	60
HOPG	2.46	2.46	60
Mica	5.2	5.2	60

Table 4.1. List of the 2-D lattice parameters for the crystals and the substrates.

4.1 EPITAXIAL GROWTH OF GMS ON MICA

The process of searching for epitaxial matches involved preparing numerous samples and then viewing them under AFM to find 2-D growth. The search by AFM was conducted by viewing random areas on the sample's surface. Although no lattice resolution was obtained for the 2-D growth of GD, it was obtained for three samples with growth of GMS on mica from MeOH. The three samples were already demonstrated in Chapter 3 to form small hexagonal islands. The lattice images found in two of the samples were obtained on the surfaces of small hexagonally faceted islands (Figures 3.21A and 3.23D). The lattice structure of these islands appeared to be strained as their lattice parameters were $b_1 = 13.5 \pm 0.3$ Å, $b_2 = 8.1 \pm 0.3$ Å, and $\beta = 90 \pm 1°$. The degree of strain in the lattice directions were 5.6 ± 2.3 % for b_1 and 10.3 ± 4.1 % for b_2. The islands had thicknesses of 20 - 60 Å and surface areas of 1 - 3.5 μm^2.

The third sample indicated a 2-D lattice structure similar to the bulk crystal, and suggested epitaxial growth when viewed at a larger scale A lattice image was obtained on the island depicted in Figure (4.1A). The periodicity is faint in the original image (Figure 4.1D), but evident after Fourier-filtering (Figure 4.1C). The lattice parameters determined from the lattice image were $b_1 = 12.8 \pm 0.3$ Å, $b_2 = 7.6 \pm 0.3$ Å and $\beta = 90 \pm 1°$, which agree with the structure of GMS. Additionally, the AFM images indicate the nearest neighbor directions to be parallel with the hexagonal facets of the island. Figure (4.1B) illustrates the facets occurring between H-bonded ribbons. The bottom two images of Figure (4.1) are the Fourier-filtered (E) and original deflection images (F), which display the lattice structure of mica. This data suggests the azimuthal angle between $\mathbf{b_1}$ and $\mathbf{a_1}$ to be 26-27°, but repeated calculations in EPICALC with iteration parameters and step sizes of $b_1 = 12.2$ - 13.2Å, at 0.01 Å steps, $b_2 = 7$ - 8 Å, at 0.01 Å steps, and 88.5 - 91.5°, at 0.01° steps, did not find any coincident matches on mica with $V/V_0 < 0.85$.

Despite the lack of a match, the sample was suspected to display epitaxy with observed 2-D crystal growth in specific directions. Figure (4.2) is an AFM image of the 2-D growth in six different directions from a central point, which are indicated to be 60° rotations. These star-like patterns of growth were oriented with respect to one another as are displayed in the image. The rotations of the outward growth suggest influence from the hexagonally structured surface of mica.

The noticeable differences between this sample and the two previous samples (Figures 3.21A and 3.23D) suggest the absence of a match with EPICALC to be a result of using lattice parameters of the crystal structure after it has relaxed upon growth. The smaller size and strained lattice parameters that were observed with the islands in the previous samples suggest a lattice mismatch occurs with the initial growth of GMS on mica. The GMS crystal in Figure (4.1A) has an area of approximately 9 μm^2, with a thickness of 75 ± 10 Å. The thickness of the island was relatively uniform as it only varied by a thickness of a GMS bilayer. The area of the 2-D growth is even larger than what it appears to be in Figure (4.1A) as the islands coalesced to form a continuous material over larger distances. Therefore, a comparison of both the lattice resolution and size of the 2-D growth found on this sample to the smaller islands found on the other two samples suggests relaxation of the lattice structure upon growth. Additionally, analysis with EPICALC using the strained lattice parameters of the smaller islands found a coincident match ($V/V_o = 0.5$) with lattice parameters: $b_1 = 13.5$ Å, $b_2 = 7.8$ Å and $\beta = 90.3°$. The coincident match occurs with an overlayer cell size of $2\mathbf{b_1} \times 2\mathbf{b_2}$ at an azimuthal angle of 30.1° on mica. This match agrees with the approximate angle of 25 - 28° found by AFM. Figure (4.3) illustrates the overlaying of the GMS on mica with the parameters and the orientation found with EPICALC. The corresponding strains for these lattice parameters are 5.7 % for b_1 and 6.2 % for b_2.

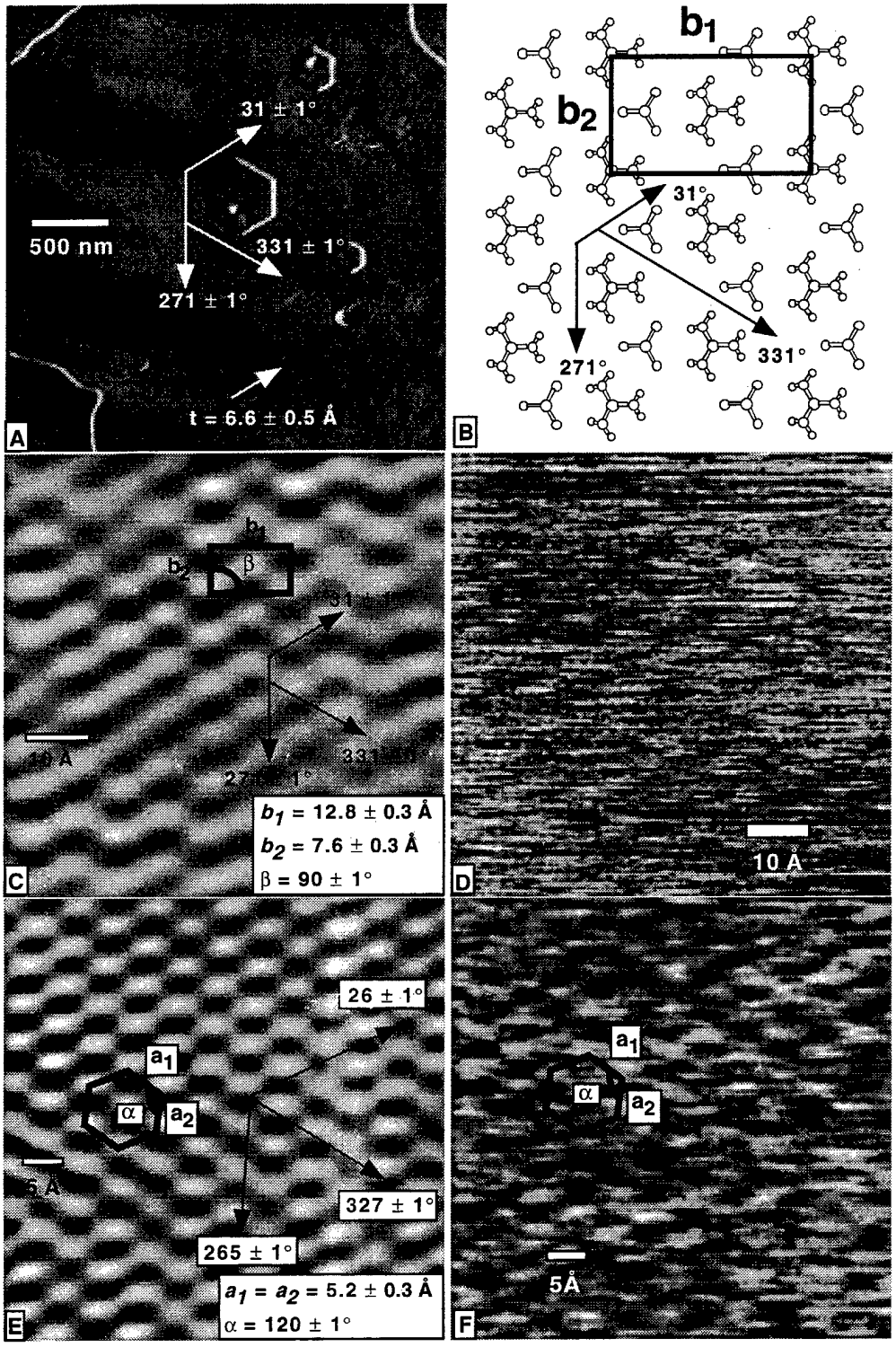

FIGURE 4.1. AFM images indicating epitaxial growth of GMS on mica A) Image of the island where the lattice image was obtained. B) Projection on the (001) plane of GMS. The lattice image of the island is depicted in Images C (Fourier-filtered) and D (original deflection image). The lattice image obtained from around this island indicated the 2-D lattice structure of mica. (Images E and F)

FIGURE 4.2. AFM image of the 2-D growth of GMS on mica at a large scale. The elongated crystal growth with six-fold symmetry indicates directional influence from the substrate.

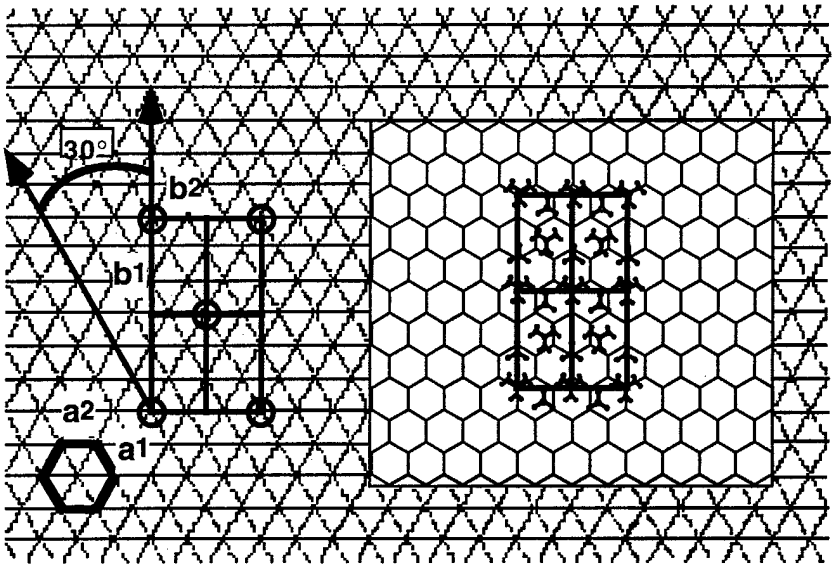

FIGURE 4.3. Illustrations of the lattice match between GMS on mica. The cell size of the overlayer is $2\mathbf{b_1}$ x $2\mathbf{b_2}$ with an orientation of 30° between $\mathbf{b_1}$ and $\mathbf{a_1}$.

The long range orientation between the separate crystal formations on the substrate suggests epitaxial growth. The six-fold symmetry of the growth may have been directed by the hexagonally structured surface of mica, the H-bonding interactions of the crystal, or their combined influence. The theoretical strains for the proposed lattice parameters are fairly similar. The strain perpendicular to the H-bonded ribbon axis may have limited the growth in that direction (b_1). The stronger H-bonds along the ribbon axis may have been able to overcome the strain induced in that direction (b_2) to commence growth, which may correlate with the three directions of growth observed on the substrate.

4.2 EPITAXIAL GROWTH OF GMS ON HOPG

A high degree of strain was suspected to occur at the interface between GMS and HOPG with a sample prepared by evaporating 0.1 mL of a 1.37 M GMS solution in MeOH from within an o-ring on HOPG. AFM revealed the growth of a few small GMS islands

on HOPG (Figure 4.4A), which indicated limited 2-D growth possibly due to unfavorable interactions with the substrate. Lattice images were obtained from the three islands depicted in Figures (4.4B, C and D). Comparing the thicknesses and lattice structures of these islands suggested limited growth due to lattice mismatches with HOPG.

The island in Figure (4.4B) had a thickness of 89.9 ± 9 nm with a lattice structure similar to the 2-D quasi-hexagonal lattice structure of GMS. The hexagonal structure is evident with the faceted features of this island. The lattice image of this island is depicted in Figure (4.5A) with lattice parameters: b_1 = 13.0 ± 0.3 Å, b_2 = 7.6 ± 0.3 Å, and β = 90 ± 1°. These parameters compare well to those of GMS, which are a = 12.778 Å, b = 7.342 Å, and γ = 90°. The lattice images obtained by AFM on the other two islands indicated different lattice structures than what was expected for the surface of GMS. The lattice image obtained on the island in Figure (4.4C) is displayed in Figure (4.5C) as a rectangular lattice with parameters: b_1 = 5.3 ± 0.2 Å, b_2 = 7.9 ± 0.3 Å, and β = 90 ± 1°, and the lattice image obtained on the island in Figure (4.4D) is displayed in Figure (4.5E) as a rectangular lattice with parameters: b_1 = 5.4 ± 0.2 Å, b_2 = 7.8 ± 0.3 Å, and β = 90 ± 1°. Additionally, these islands lacked the hexagonal facets observed for the island in Figure (4.4B). The thicknesses of the island in Figure (4.4C) was 187 ± 10 Å and the thickness for the island in Figure (4.4D) was 99.5 ± 5 Å. The structure of the islands appeared to relax upon growth in thickness as the lattice structure of the two thinner islands differed from both the lattice structure of the thicker island (Figure 4.4B) and what is expected for GMS.

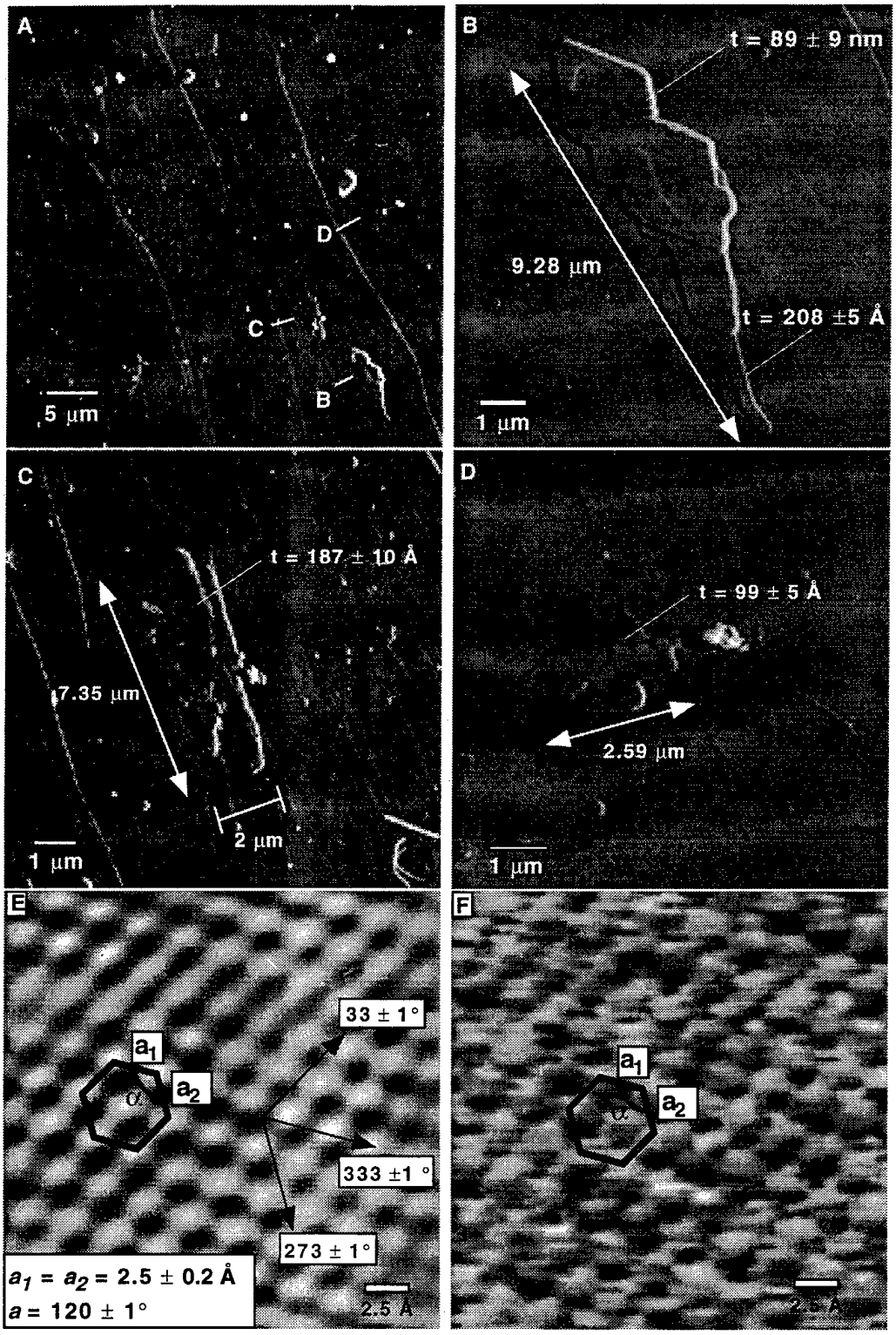

FIGURE 4.4. Images A-F for the growth of GMS on HOPG. Images B-D are the three islands where lattice images were obtained. Image E and F are the Fourier-filtered and original deflection image of the lattice structure for HOPG.

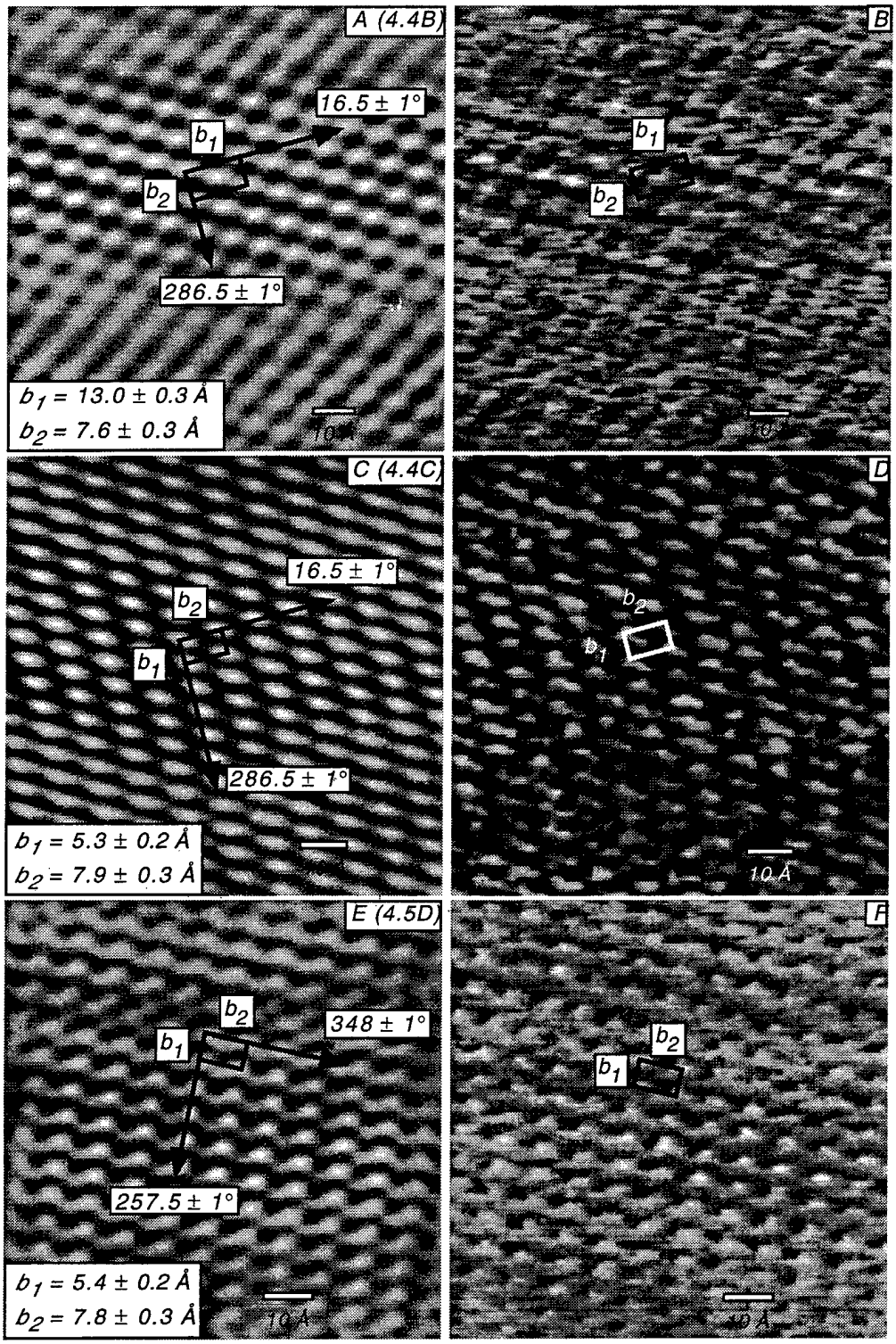

FIGURE 4.5. Images A-F are of the lattice images for the three islands of GMS on HOPG. The numbers in parenthesis indicate the island exhibited in Figure (4.4) from which the lattice image was obtained. The left column of images are the Fourier-filtered version of the original deflection images in the right column.

The lattice structures of the three islands (Figure 4.5) appeared to have similar b_2 and β lattice parameters. The b_2 lattice parameter observed in the lattice images for the thinner islands may correlate with H-bonded ribbon directions of GMS, which would indicate H-bonding interactions were able to tolerate strain occurring along these directions in the crystal. An integral rotation of approximately 30° is noticed between the b_2 lattice direction of each island, which suggests epitaxial growth. Additionally, the b_2 lattice directions for all the islands are rotated by an angle within the range of 13.5° - 16.5° from the closest lattice direction found in the lattice image of HOPG (Figure 4.4E and F). Lattice images of HOPG were obtained from underneath the two thinner islands and in another random location. The orientation of the substrate was assumed to be the same under all the islands since the three lattice images of HOPG were similar, and the thicker island was within only 4 μm from the island depicted in Figure (4.4C). The lattice directions of HOPG are labeled with angles from the horizontal in Figure (4.4E) and the lattice directions of the islands are labeled with angles from the horizontal in their respective lattice images (Figure 4.5). The rotations of the b_2 lattice parameter for each of the islands with respect to the closest lattice direction of HOPG were: 286.5° - 273° = **13.5 ± 2°**, 348° - 333° = **15 ± 2°**, and 33 - 16.5° = **16.5 ± 2°**.

b_1 (Å)	b_2 (Å)	β (°)	V/V_o	θ (°)	m_{11}	m_{12}	m_{21}	m_{22}	cell size
(1) 13.3	7.65	90.5	0.51	16.19	1.0	2.49	-6.0	4.5	$2b_1 \times 2b_2$
(2) 5.25	7.5	88.9	0.51	25.41	2.0	1.51	-2.0	2.25	$2b_1 \times 2b_2$

Table 4.2. Lattice matches found using EPICALC with lattices parameters near values observed for the thick film (1) and the thin film (2).

An analysis with EPICALC found two lattice matches (Table 4.2), each with similar parameters to those observed in the lattice images of the islands. Lattice match (1)

has lattice parameters similar to those of the thicker island and lattice match (2) has lattice parameters similar to those of the thinner islands (2). Match (1) appears to agree with the AFM results, since the azimuthal angle of 16.19° agrees with the azimuthal angles found for the three islands (13.5° 16.5°). Additionally, the azimuthal angle of 25.41° for Match (2) would not allow for the overlayers to be rotated 30° from each other, which is observed for this sample. This azimuthal angle would only allow the islands to be oriented 10°, 50°, or 60° with respect to one another. Since the AFM images are of the interaction between the tip and the surface, the periodicities observed for the thinner islands are probably different due to the overlayer being rotated with respect to the scan angle. The rotation of the crystal with respect to the substrate could be assumed with the rotation of the b_2 lattice parameter. The combination of this modified interaction and the strained lattice may have reduced the periodicity correlating to b_1 by a half. The simulation was repeated using the lattice parameters of the thinner islands except with $2 \bullet b_1$. The only matches found still had azimuthal angles within the ranges of 25 - 30°, which did not agree with the results obtained from the lattice images of the islands. Therefore, epitaxial growth of GMS on HOPG is suggested to occur with Match (1), which has an overlayer cell dimensions of $2\mathbf{b_1}$ x $2\mathbf{b_2}$ and an azimuthal angle of 16.19°.

The steps of HOPG may affect the orientation and growth of the GMS islands. The growth of one island along the steps of HOPG is evident in Figure (4.4D). The growth may even be suspected in Figures (4.4B) and (4.4C) as the crystals appear to be elongated in the same directions as the HOPG steps . Interactions with the steps may have affected the orientation of the islands or their lattice structure. Further experiments with different grades of HOPG would need to investigate the effect HOPG steps have on the growth of GMS.

4.3 CONCLUSION

The growth of GMS on mica and HOPG, presented in this chapter, indicate possible coincident epitaxial matches with overlayer cell dimensions of $2\mathbf{b}_1$ x $2\mathbf{b}_2$ at respective azimuthal angles of 30° and 16.19°. These relationships were determined by comparing coincident matches found with EPICALC to lattice orientations and parameters observed in AFM lattice images of the overlayer and substrate. The growth of GMS was suspected to be hindered by strain occurring within the crystal that was induced by lattice mismatches with HOPG and mica. Strain was observed in the lattice images of GMS, grown on both substrates, and was suspected to decrease upon growth in thickness as the structure observed in the lattice images of thicker islands had less strain than the structure observed in the lattice images of thinner islands. The epitaxial growth of GMS on mica and HOPG may indicate larger extent of 2-D growth of GS films to be possible when attempted under different experimental conditions or on a substrate with a similar structure. The experimental conditions could involve controlling the evaporation rate with humidity or slowly cooling the substrate.

5

GROWTH MODE OF GS THIN FILMS ON MICA

Determining the growth mode of GS crystals on mica was challenging because each sample produced different results. This chapter presents new data acquired from attempts at monitoring growth of GMS on mica with *in situ* AFM. These results will be discussed and compared with features observed on other samples to determine the mode of growth. The previously described observations of 2-D crystal growth were the alignment of long GD crystals on glass (Figures 3.19), and directional growth of GMS on mica (Figure 4.1). Observation of new samples will be discussed in the latter part of the chapter.

5.1 REVIEW OF OBSERVED 2-D CRYSTAL GROWTH

The directional growth of GD crystals on glass (Figure 3.19) forms as a result of H-bonding interactions directing the growth along directions corresponding to the H-bonded ribbon direction found in the bulk structure. The alignment of GD crystals on glass, and their limited growth in one direction is caused by crystals blocking the flux of surface diffusing clusters to the sides of growing crystals. The absence of blocking allows 2-D growth in directions 60° from each other, which indicate growth in directions with

similar orientations to the H-bonded ribbon axis. The observation of dendritic features of GD on glass demonstrates this mode of growth. Dendritic growth was observed with both an optical microscope and AFM (Figure 5.1).

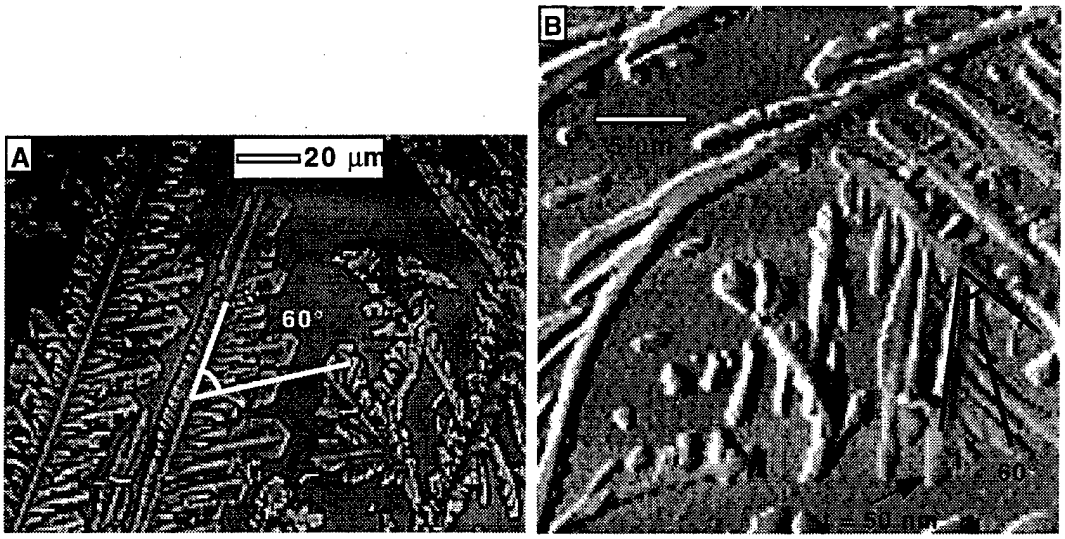

FIGURE 5.1. Images of the growth of GD on glass exhibiting directional growth induced by the H-bonding interactions along the ribbon directions. Image A was captured from an optical microscope at 100X magnification. Image (B) is zoomed in on an area of Figure (3.19B).

The star formations observed in Figure (4.2) also suggest H-bonding interactions control 2-D crystal growth on mica as long GMS crystals extend in directions 60° from each other. The same 2-D orientation of the star formations implied epitaxial growth on the substrate. This growth could be directed by the hexagonal structure of the mica, the H-bonding interactions, or a combined influence from both. Determining the growth mode of GMS on mica would help decipher the contributing influences.

5.2 MONITORING GROWTH OF GMS ON MICA BY *IN SITU* AFM

The first few attempts of monitoring the growth of GMS on mica with real-time *in situ* AFM involved filling a fluid cell with a 0.67 M GMS solution in MeOH, and then

allowing it to evaporate while scanning. The objective was to monitor the nucleation and growth of GMS on mica. This process was observed for a few days and the only observed event on the substrate was an immediate formation of spherical clusters with diameters ≈ 50 nm covering the whole area being imaged (Figure 5.2). This type of activity is not observed on mica when viewed in only MeOH. The formation of aggregates on the substrate may suggest an immediate adsorption of solute particles to the substrate due to convection caused by the rastering motion of the tip. Alternatively, the surface activity of mica may induce immediate adsorption of the solute.

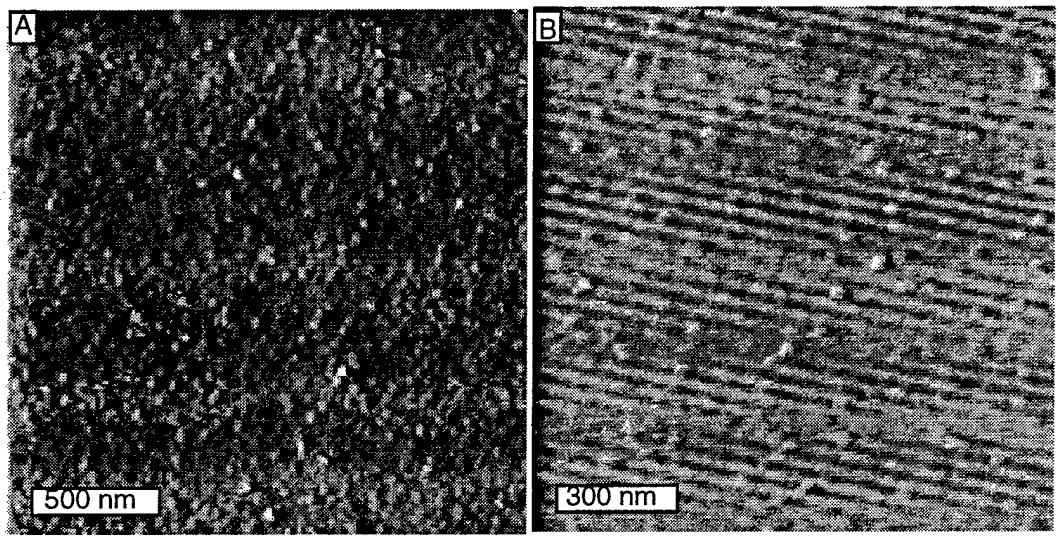

FIGURE 5.2. AFM images captured during attempts to monitor in-situ growth of GMS on mica by evaporation. The images indicate a cluster of spheres on the surface, which formed instantly. The radius of the spheres were approximately 50 nm. The scan sizes of Image A and Image B are (1.8 μm)2 and $(1.28\ \mu m)^2$. The lines in Image B are due to noise.

Other attempts at monitoring the growth of GMS on mica by *in situ* AFM involved using the Pico SPM model MS300 (version 1.0) obtained from the Molecular Imaging Corporation. This instrument differs from the previously mentioned AFM in that the scanner is positioned above the sample. An illustration of this set-up is displayed in Figure (5.3). The different positioning of the scanner allows for the substrate to be cooled by a temperature controller (model 321, Lake Shore Cryotronics, Westerville, OH). Cooling

the substrate would in theory initiate heterogeneous nucleation on its surface by lowering the solubility of the solution at the interface. Many attempts at scanning in solution with this instrument were unsuccessful. The Molecular Imaging (MI) microscope worked well when scanning in air (lattice images of mica were obtained), but consistent images could not be obtained when scanning in fluid.

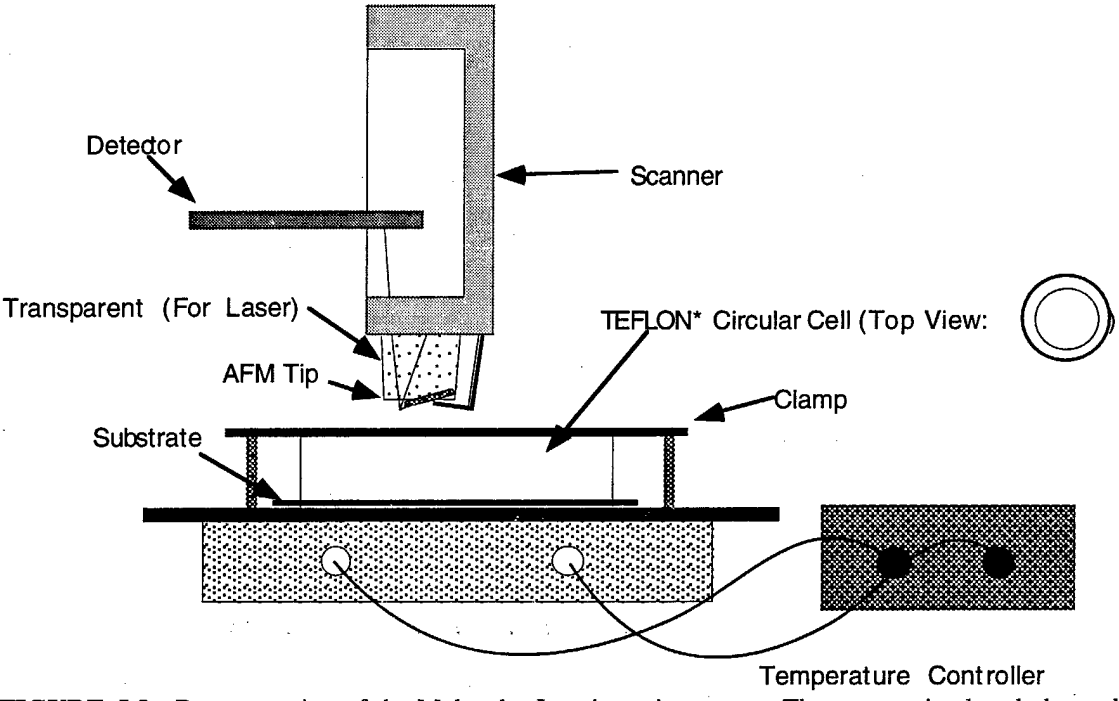

FIGURE 5.3. Demonstration of the Molecular Imaging microscope. The scanner is placed above the sample to allow the temperature controller to cool the substrate. The TEFLON* circular cell is hollow so it can be filled with solution. The tip is then submerged in the solution to scan the substrate.

The only successful attempt at monitoring the growth of GMS on mica with the MI microscope occurred when the surface of mica was scanned as it was wetted with a small amount of a 1.29 M GMS solution in MeOH. A lower solution level within the TEFLON* cell may have eliminated noise, caused by the tip stirring the solution, that was experienced in previous attempts when the cell was completely filled with solution. Figures (5.4A - F) display 2-D growth of a material on the mica, which is suspected to be GMS. Figure (5.4A) is an image of the freshly cleaved mica surface before it was wetted with solution,

and Figure (5.4B) indicates the initial formation of clusters on the surface observed after the mica was wetted with solution. The growth of the layer is initiated with the formation of an island (Figure 5.4C). The step growth continued until the whole area was covered within a one hour period (Figures 5.4D - F). The thickness of the layer was determined to be 25 ± 5 Å at the edge of the layer indicated in Figure (5.4 D).

The central location of the growth observed in Figures (5.4C - F) suggests it was enhanced by the AFM tip. The growth may be enhanced by a tip-induced defect formation, mixing of the boundary layer on the surface, or convective effects caused by the rastering motion of the tip. These influences have been observed with real time *in situ* crystal growth of soft organic and protein crystals. [1, 2, 3] A dislocation defect located in the middle of the island in Figure (5.4C) may have initiated the step growth on the surface. This defect is pointed out in Figures (5.4C - F). The increase in scan size from Figure (5.4C) to Figure (5.4D) revealed the enhanced growth to be within the scanned area. The localized growth appears to have been promoted by the tip mixing the boundary layer to enhance diffusion.

The next sequence of events occurred ten hours after the initial scanning. Upon scanning for the second time, an island (Figure 5.5A) was discovered to have formed on the surface of the material that was observed in Figure (5.4). An attempt was made to obtain a lattice image on the island's surface, but the material was etched by the AFM tip. The island continued to grow between periods of scanning to eventually double in size as

---

[1]Yip, C. M. and M. D. Ward. *Biophysical Journal.* 71, (1996), 1071 - 1078.
[2]Land, T. A.; Kuznetsov, Y. G.; McPherson, A; and J. J. De Yoreo. *Amer. Phys. Soc.* 75 (14), (1995), 2774-2777.
[3]Malkin, A. J.; Land, T. A.; Kuznetsov, Y. G.; McPherson, A; and J. J. De Yoreo. *Amer. Phys. Soc.* 75 (14), (1995), 2778-2781.

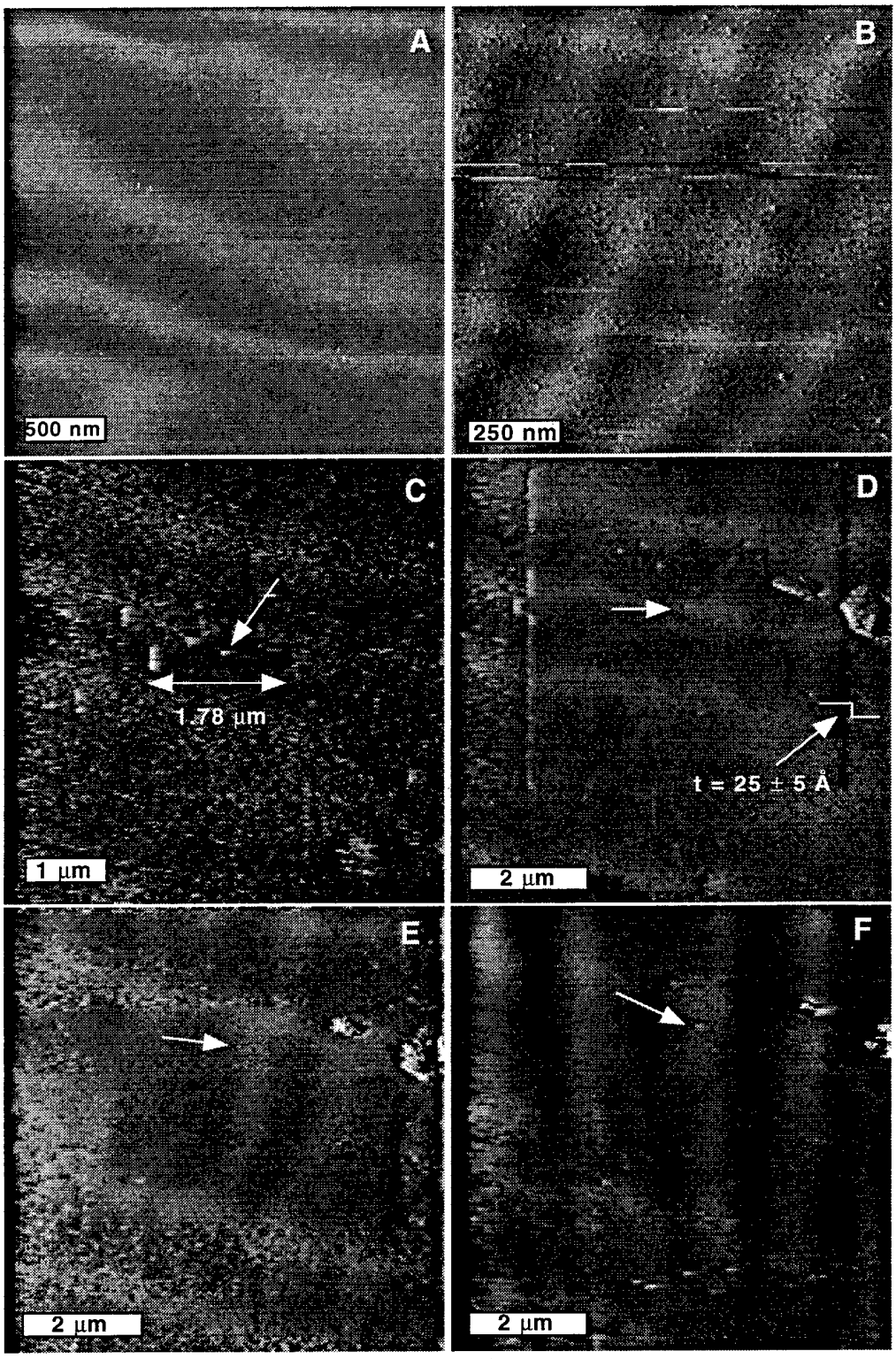

FIGURE 5.4. A Sequence of images captured while attempting to monitor growth of GMS on mica by real time *in situ* AFM. A) The surface of mica before adding solution. B) The initial formation of clusters on the surface after the GMS solution was introduced. Images C - F indicate the growth of a layer initiated by a dislocation source, which is indicated with the white arrow in all the images.

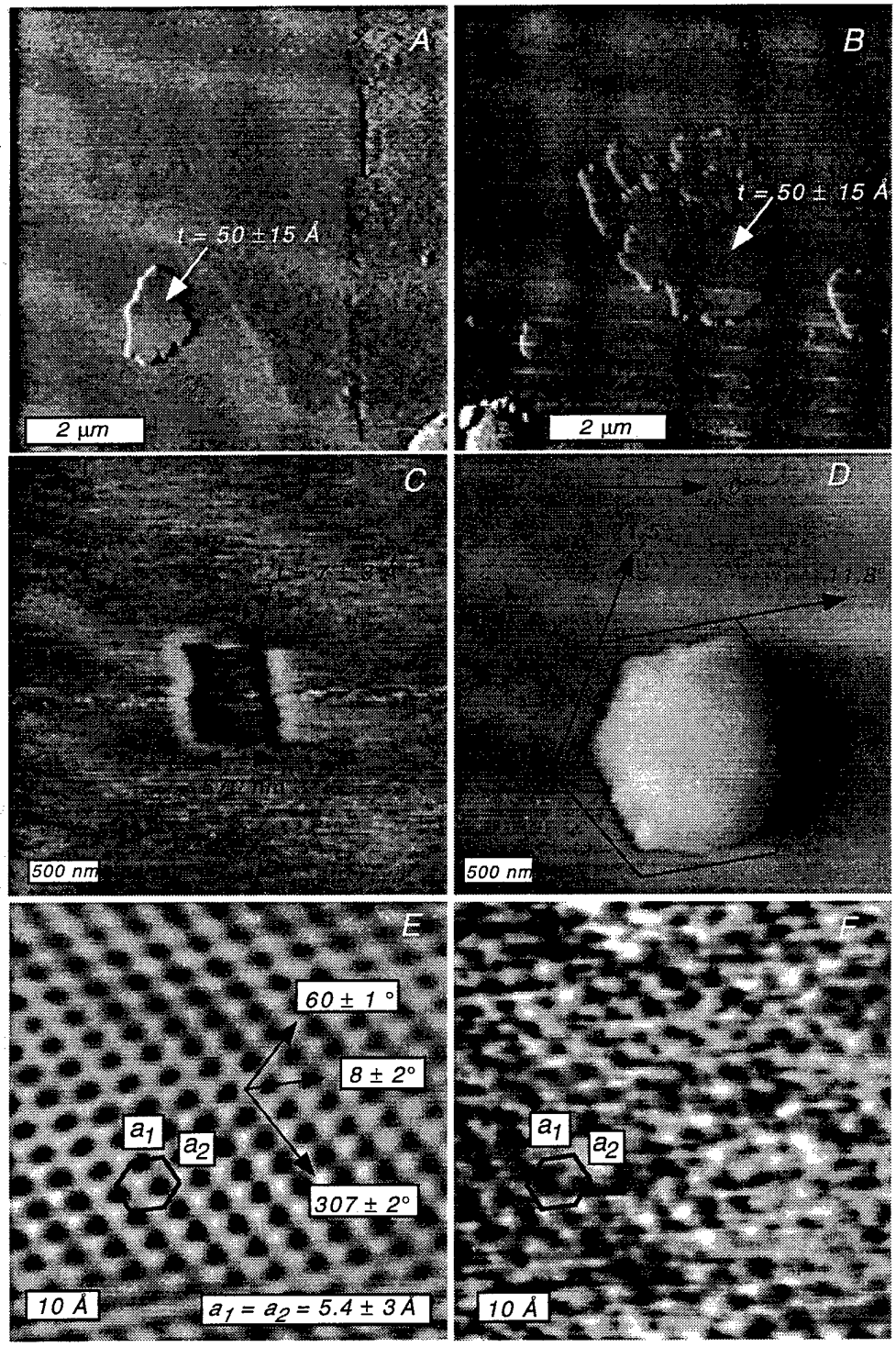

Figure 5.5. A) An island that formed after the growth displayed in Figure (5.4). B) The island after observing the growth for 50 hours. C) An area near the island in Image B where a layer was scraped away to reveal the surface of mica. D) Zoomed in on the island located in the lower left corner of Image B. This island appears to have some hexagonal shape, which is suspected to be oriented with the lattice image of mica (Image E and F).

demonstrated in Figure (5.5C). The time period between capturing the images in Figure (5.4C) and Figure (5.5B) was approximately fifty hours. The growth of the island over this extended period of time seems unusual since all the MeOH was expected to have evaporated. Remaining solution or H_2O from humidity may have been trapped within pores on the surface of the sample to allow continued growth. Further crystallization may have occurred from the remaining solution. Figure (5.5B) also reveals smaller islands in the near vicinity of the larger island. The thicknesses of the islands were 50 ± 15 Å. The formation of the islands suggests growth of GMS on mica to occur by the Volmer-Weber mode as they appear to grow by adsorbing material from the surface.

The AFM tip was observed to etch away a layer of material (Figure 5.5C) when attempting to obtain lattice images on the surface near the island in Figure (5.5B). The result was the same when repeated in different areas. The layer of material was suspected to be the growth that was observed in Figure (5.4). The thickness of the layer was 7 ± 3 Å, which agrees with the step height of GMS (7.99 Å).

The small island located in the lower left corner of Figure (5.5B) is observed at a larger in Figure (5.5D). This island appeared to possess some hexagonal shape with faces oriented with a $7 \pm 4.5°$ counter-clockwise rotation to lattice directions of the mica. The directions of the island's faces were assumed to represent the H-bonded ribbon directions. The orientation of these ribbon directions were 71.5°, 11.8° and 311.4°, with 0° as indicated (Figure 5.5D). The three directions for the periodicities found in the lattice image of mica were $60 \pm 1°$, $8 \pm 2°$, and $307 \pm 2°$. Figure (5.5E) is a Fourier-filtered version of the original deflection image on its right (5.5F), which is a lattice image of the mica surface. The lattice image mica is slightly distorted, but the range of orientations (2.5° - 11.5°) between the lattice directions of the two materials contains the expected orientation of $6 \pm 2°$. The expected orientation is based on the coincident match determined from the other samples of GMS on mica (Figure 4.1) discussed in Chapter 4.

5.3 GROWTH MODE OF GMS ON MICA

A possible transition from circular to faceted formations as observed in the previous section (Figure 5.5D) was also noticed on the surface of another sample. This sample involved evaporating 0.03 mL of a 1.37 x 10^{-3} M GMS solution in MeOH from within an o-ring on mica. AFM imaging of the sample discovered the formation of circular islands throughout its surface (Figure 5.6A). Images with smaller scan sizes revealed islands, which appeared to have some faceted edges. Figures (5.6C) and (5.7) both demonstrate the angles between some of the island's faces to be 135°, which suggests an octahedral shape. This shape is unusual considering the hexagonal (120°) surface structure of both mica and GMS. The octahedral shape may suggest an additional morphology for the GMS crystals before complete coalescence of the clusters into the expected crystal structure.

Other features were noticed from this sample upon further investigation. For instance, the diameter of the islands had a direct relationship to the thickness and the degree of spacing between the islands. The direct relationship of the island thickness to the diameter suggests island growth, which would indicate the Volmer-Weber mode. Four islands are labeled in either Figure (5.6A) or Figure (5.7) with numbers. Table (5.1) contains a list of the respective numbers for these islands along with their thickness and diameter.

Island Number	Diameter (μm)	Thickness (nm)
1	0.680	8.4
2	1.84	14.0
3	3.018	25.4
4	6.41	59.3

Table 5.1. A list of the respective numbers, diameters, and thicknesses for islands indicated in Figure 5.5A and Figure 5.6. The list indicates a linear relationship between the thickness and the diameter of the islands.

Ripening of the larger islands is suspected as they tend to possess a vacant zone boundary with small islands around the perimeter (Figure 5.7). These zones are probably due to the larger island absorbing smaller clusters in its near vicinity. Growth also appears to occur by islands coalescing, which are pointed out with circles in Figure (5.6c). Even the lower right region of the largest island appears to consist of smaller islands coalescing.

The facets forming on some of the islands may indicate the tendency of molecules to arrange into a structure with a lower free energy minima. A slower evaporation rate may allow molecules to diffuse to sites offering lower energy states, which promote 2-D growth. The 2-D structure would have a lower free energy due to the 2-D order induced by the H-bonding interactions in the GS plane.

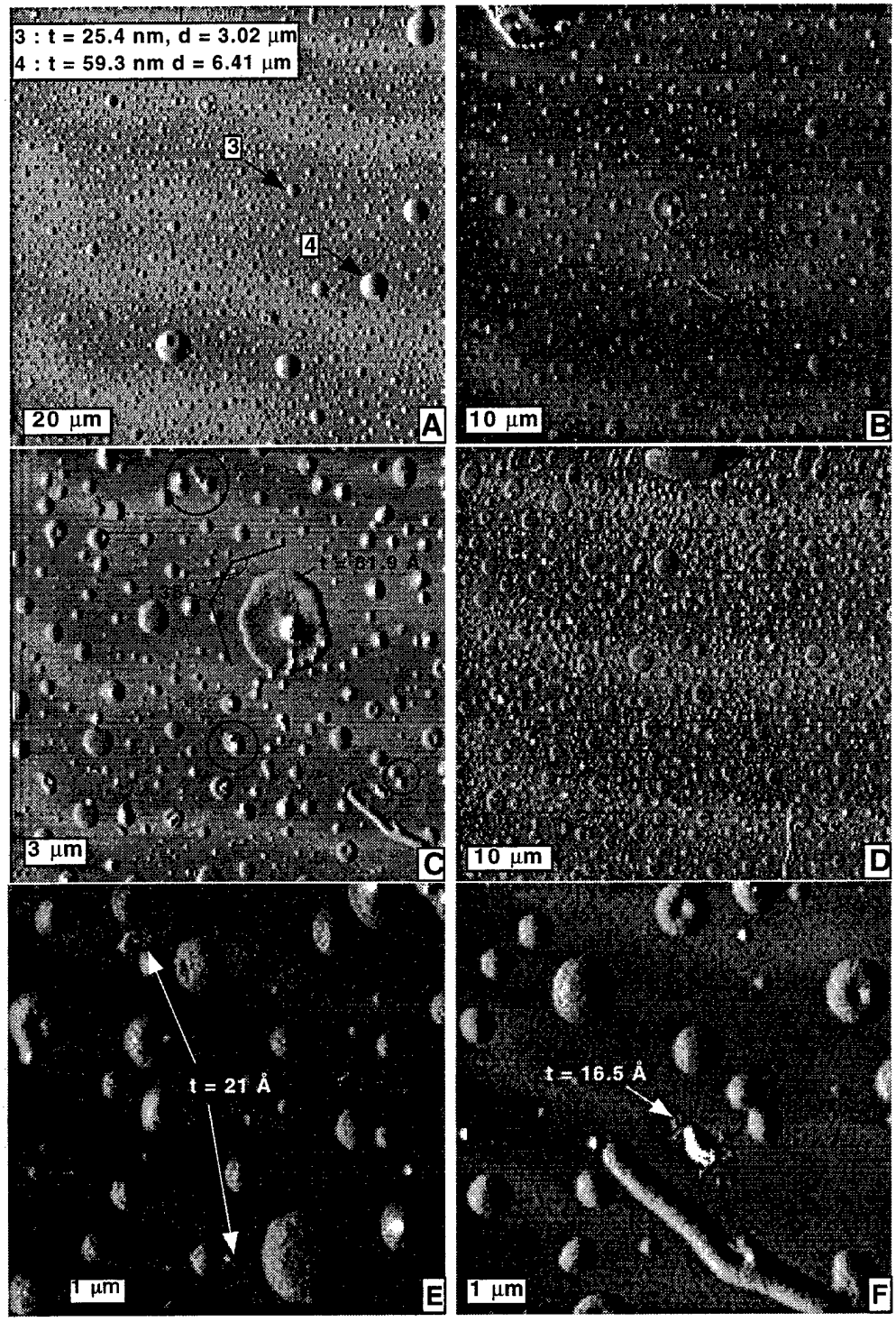

Figure 5.6. AFM images of circular islands suspected to be growth of GMS on mica. Image D is of the same sample viewed a month later after being exposed to the atmosphere. The higher degree of roughness may be due to growth promoted by humidity in the lab. C) Possible facets are indicated on the islands, which are at angles for an octahedral structure. E and F) Smaller islands are depicted with spherical caps and possible 2-D growth.

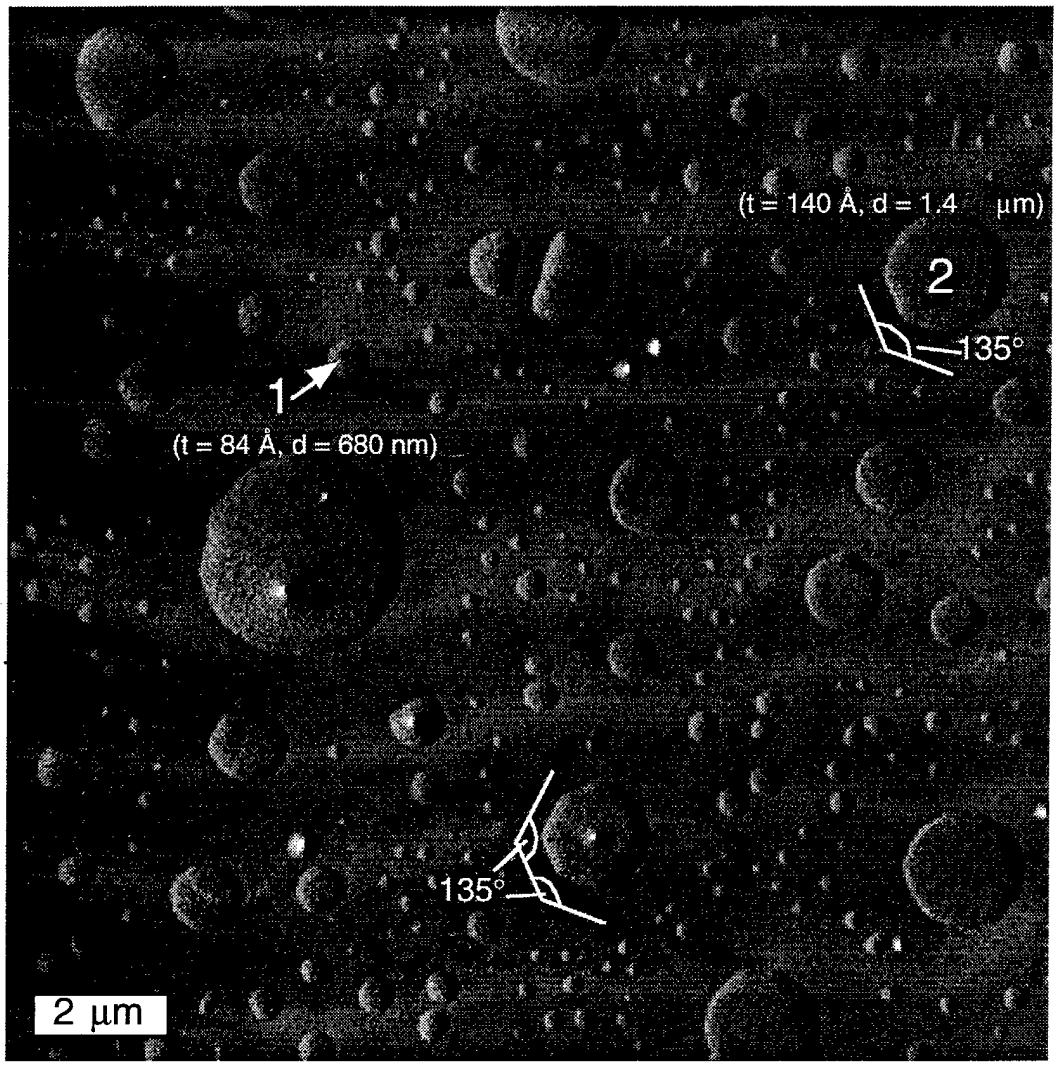

FIGURE 5.7. Large view of the surface to illustrate possible facets on some of the circular islands. Notice the pointed caps on some of the islands, which are suspected to form right before complete evaporation of the solvent. Again the facets of the islands are indicated to be at orientations of 135° to suggest an octahedral shape. Also note the tendency for the larger islands to posses a vacant zone boundary, which implies their ripening at the expense of smaller clusters.

Observing this sample by AFM a month later suggested continued growth over time despite complete evaporation of the solvent. This indication would agree with the growth observed *in situ* after 50 hours, which was enhanced by the AFM tip. The surface of the sample was observed to be a lot rougher, indicating further ripening of islands over time. This observation can be seen by comparing Image D (after a month) and Image B (initial)

of Figure (5.6), which have respective scan sizes of $(50.5\ \mu m)^2$ and $(55.2\ \mu m)^2$. These images may also be of different surface features observed at different areas on the sample. Further research would have to investigate whether the GS films continue growth when exposed to humidity. This observation may imply potential growth of GS crystals as thin films by controlling the humidity exposed to the surface of the sample.

Spherical caps were noticed on top of islands, which may indicate crystals that crashed out due to high solute concentrations at the top of the island just before complete evaporation of the solvent. The smaller islands depicted in Figures (5.6E and F) also have the spherical cap, but their lack of spherical shape suggests 2-D growth. The thickness of these islands were 16 ± 1 Å and 21 ± 1 Å, which agree with two (16 Å) or three (24 Å) bilayer thicknesses of GMS. The molecules may have been able arrange into a more favorable 2-D structure to form these smaller islands.

Depicted in Figure (5.9A) are islands observed on the surface of a sample, in which 0.1 mL of a 2.68×10^{-3} M GMS solution in MeOH was evaporated from within an o-ring on mica. These islands also had a spherical cap, and portray similar 2-D growth that was observed with the small islands in Figures (5.6E and F). The thicknesses of these islands were 38 ± 5 Å. The larger amount of solution may have allowed more time for molecules to diffuse to sites offering lower energy states before complete evaporation of the solvent. The 2-D growth may be a low energy growth mode due to strong H-bonding interactions in the GS plane.

The AFM image in Figure (5.9B) has a scan size of $(85.6\ mm)^2$ and is of the surface of a sample, in which 0.1 mL of a 1.37×10^{-3} M GMS solution in MeOH was evaporated from within an o-ring on mica. Again the larger amount of solution provided enough time for the molecules to diffuse to sites offering lower energy states, which resulted in 2-D growth. This growth is apparent with the circular island in Figure (5.9B), which has a relatively even thickness of 40 ± 10 Å and a large diameter of 55 μm.

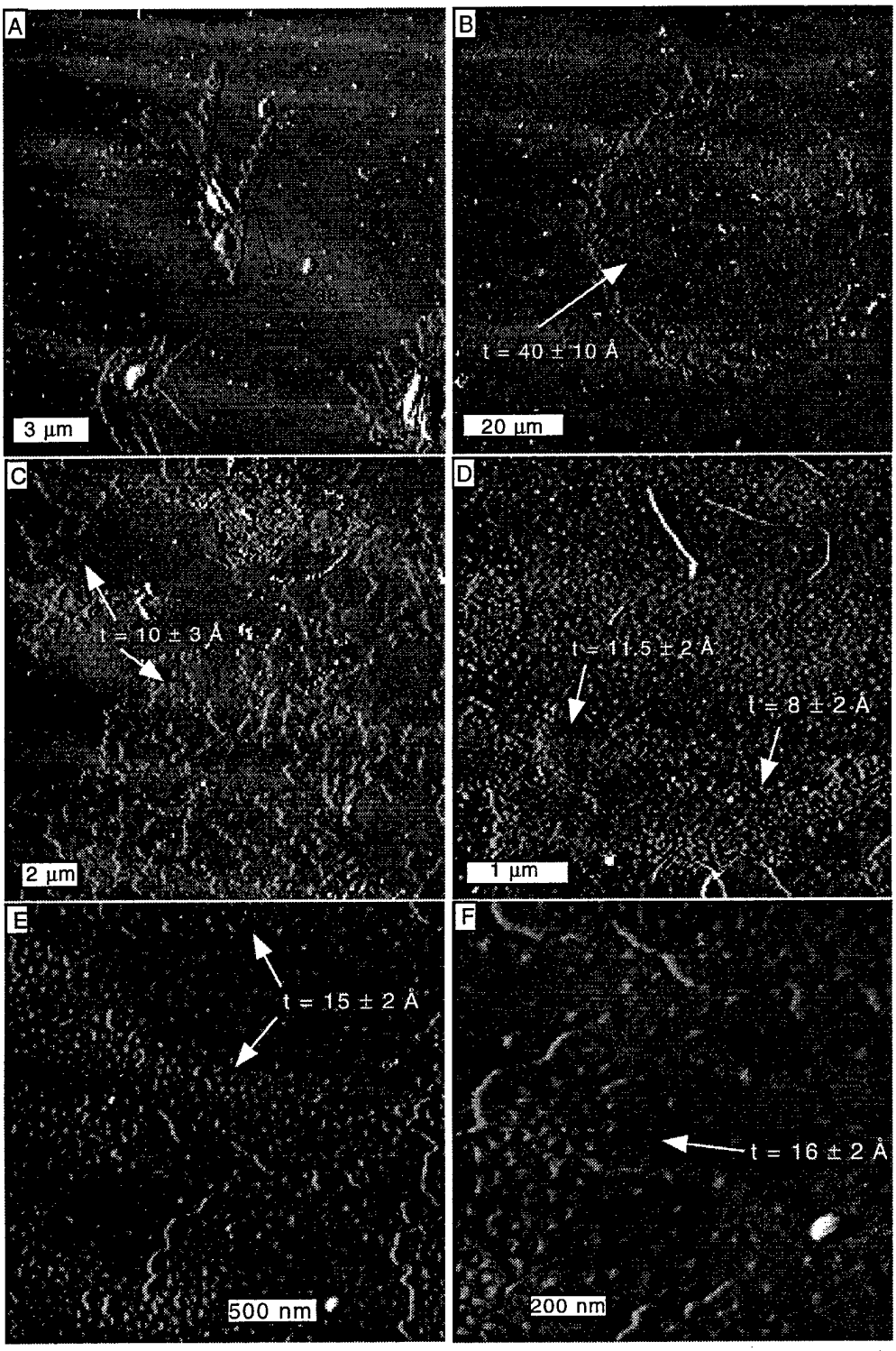

FIGURE 5.9. A) A sample viewed by AFM indicating 2-D growth of GMS on mica. The spherical caps are suspected to have formed right before complete evaporation. B) Circular island exhibiting growth of GMS on mica. C) 2-D growth located around the circular island. D) Zoomed in on the 2-D growth revealing them as cluster formations. E and F) Similar growth observed two days later, but with more cohesion and constant thicknesses.

2-D growth was observed outside the perimeter of this island as displayed in Figure (5.9C). The thickness of this 2-D growth was 10 ± 2 Å. Images of the surface at smaller scan sizes revealed the growth to be an agglomeration of circular aggregates with diameters around 50 nm (Figure 5.9D). This sample was viewed two days later to discover similar growth, but with a flat surface and more cohesion as indicated in Figures (5.9E and F). Although these images might be of different features at different areas on the sample, the lower degree of roughness suggests 2-D growth over time. The thickness of this growth was 16 ± 2 Å, which agrees to the thickness of two bilayers of GMS (16 Å).

5.4 CONCLUSION

The data presented in this section suggests growth of GMS on mica to occur by the Volmer-Weber mode. H-bonding interactions were pointed out in the beginning of the chapter to have a strong influence in directing the growth in directions correlating with the H-bonded ribbons. The results obtained from attempts at monitoring the growth of GMS on mica by *in situ* AFM implied the growth of these crystals to commence by forming clusters on the surface, which coalesced over time to form islands. The results obtained by analyzing growth features observed on other samples of GMS on mica also implied the growth to occur by the Volmer-Weber mode. This mode was indicated by the formation of the circular islands on the surface, which appeared to grow at the expense of smaller islands and by coalescence. The degree of 2-D growth was suspected to be dependent on the evaporation rate of solvent. The slower evaporation rate allowed the molecules to arrange into a 2-D structure induced by H-bonding interactions in the GS plane. Samples were also suspected to continue growth over time, which would provide reason to continue research in determining the effects of humidity on growth of GS.

CONCLUSION

The objective of this research was to investigate the possible growth of GS crystals as thin films on substrates. Two-dimensional growth of these crystals was expected to occur because of their tendency to self-assemble into two-dimensional layers with strong intralayer hydrogen-bonding. This research focused on the growth of crystalline guanidinium methanesulfonate and guanidinium dithionate as thin films on glass, mica, silicon wafer, HOPG, and silane treated mica substrates. The two GS materials used were chosen because they had the simplest structures and were easy to prepare.

AFM and wide angle X-ray diffraction indicated growth of the GS crystals on glass, mica, silicon wafer, and HOPG substrates. The crystals tended to grow with an orientation of (001) planes parallel to the substrate, which agrees with the expected low surface energies of the (001) H-bonded planes. The 2-D growth of the GS crystals appeared to be enhanced by slow evaporation of solution and the ability of the solvent to spread on the substrate. Other factors were suspected to have an influence on the 2-D growth, but no conclusions could be reached from the current experimental data. Further research is needed to study the 2-D growth of these crystals from different solvents. Interactions between the growing crystal and the solvent may promote growth at certain faces.

Adsorption interactions with the substrate may also influence the growth of GS crystals. The 2-D growth of GMS on mica and HOPG presented in this thesis indicate possible coincident epitaxial matches with an overlayer cell dimensions of $2\mathbf{b}_1$ x $2\mathbf{b}_2$ at

azimuthal angles of 30° and 16.19°, respectively. The extent of growth was limited on each substrate, possibly due to strain caused by lattice mismatches at the interface. The AFM lattice images obtained from the films also suggested the growing crystalline film structures may have relaxed upon growth in thickness.

The growth of the GS films on mica was believed to occur by the Volmer-Weber mode. The results of monitoring the growth of GMS on mica by *in situ* AFM implied that growth of these crystals commences by clusters forming on the surface, which coalesce over time to form islands. The Volmer-Weber mode was also apparent as island growth was observed on mica. The degree of 2-D growth was suspected to be dependent on the evaporation rate of solvent. A slower evaporation rate allowed the molecules to arrange into a state of lower energy induced by H-bonding interactions in the GS plane. Crystal growth was also suspected to continue over time, which would provide reason to continue research in determining the effects of humidity on growth.

Ideally, using GS crystals in thin film applications may prove to be advantageous, as their rapid self-assembled growth under ambient conditions will reduce the need for more expensive film growth methods. Furthermore, the wide selection of GS materials available for film preparation should allow tailoring of properties desired in applications such as chemical sensors, wave guides, electrical conductors, and optical applications.

APPENDIX A

Atomic force microscopy (AFM) was performed with a Digital Instruments Nanoscope III scanning probe microscope equipped with two different scan heads. An initial search for an area of interest on the sample was conducted by using scanner with a scan size of $(175\ \mu m)^2$. Imaging was then continued by using a scanner with a scan size of $(15\mu m)^2$ to observe smaller features on the surface. Scanning was attempted in contact mode by using Si_3N_4 Nanoprobe cantilevers with tips having spring constants of 0.06 N/m.

Imaging was attempted in fluid to minimize contact forces between the tip and the sample. Imaging in fluid involved using a silicone o-ring and a fluid cell purchased from Digital Instruments. The fluid was inserted within the o-ring, which was clamped between the sample and the fluid cell. Imaging was attempted in saturated and dilute solutions of ethanol and acetonitrile.

Imaging in fluid minimizes interactions between the tip and the sample to increase the mechanical stability of the observed material and obtain images with better resolution. The resolution scale of the AFM is dependent on the van der Waals forces between the tip and sample.[1] The following equation is used to describe how the resolution will improve

[1]Hutter, J. L., and J. J. Bechhoefer, *J. Appl. Phys.* 73, (1993), 4123.

with a larger Hamaker constant, thus weaker van der Waals attractions.

$$RS = \left(\frac{A_{132} R_o^2}{8KD_o^2} \right)$$

where R_o is the radius of the AFM tip, D_o is the minimum tip/surface separation allowed by repulsive contact forces, K is the combined elastic modulus of the tip and sample, and A_{132} is the Hamaker constant. According to the Lifshitz theory, a solvent media, with different dielectric and refractive indexes, can lower the van der Waals potential attraction between the tip and the sample as described.[2] This relationship has been described by the following equation.

$$A_{132} = \frac{3}{4} kT \left(\frac{\varepsilon_2 - \varepsilon_3}{\varepsilon_1 + \varepsilon_3} \right) + \frac{3h\nu}{8\sqrt{2}} \left(\frac{(n_1^2 - n_3^2)(n_2^2 - n_3^2)}{(n_1^2 + n_3^2)^{1/2}(n_2^2 + n_3^2)^{1/2}[(n_1^2 + n_3^2)^{1/2} + (n_2^2 + n_3^2)^{1/2}]} \right)$$

ε and n are the dielectric constants and refractive indices for the tip (1) and sample (2) and the solvent medium (3).

[2]Israelachvilli, J. N. Intermolecular and Surface Forces. 2nd Ed. , Academic Press: San Diego, CA, 1992.

APPENDIX B

Wide angle X-Ray diffraction was performed on the Siemens D-500 diffractometer with Cu as the source of radiation. The samples were mounted in the diffractometer under ambient conditions and scanned from 5° to 60° with step sizes of 0.25°. The following equations and parameters were used to determine the expected angles of diffraction from the planes of each material.[1] The tables contain a list of expected angles for the respective planes (hkl) of each material.

Hexagonal: $$\frac{1}{d^2} = \frac{4}{3}\left(\frac{h^2 + hk + k^2}{a^2}\right) + \frac{l^2}{c^2}$$

Monoclinic: $$\frac{1}{d^2} = \frac{1}{\sin^2\beta}\left(\frac{h^2}{a^2} + \frac{k^2\sin^2\beta}{b^2} + \frac{l^2}{c^2} - \frac{2hl\cos\beta}{ac}\right)$$

Bragg law: $\lambda = 2d\sin\theta$

$\lambda = 1.540562$ Å

d = plane spacing

[1]Cullity, B. D. Elements of X-Ray Diffraction. 2nd Ed. Addison-Wesley: London, 1978.

Guan. methanesulfonate (monoclinic, a = 12.78 Å, b = 7.34 Å, c = 10.00 Å, β = 126.96°)

h	k	l	d (Å)	2θ (deg)
0	0	1	7.99	11.06
0	0	2	3.99	22.23
0	0	3	2.66	33.61
0	0	4	2.00	45.35
0	0	5	1.60	57.62
0	0	6	1.33	70.66

Guan. dithionate (hexagonal, a = b = 7.50 Å, c = 12.13 Å)

h	k	l	d (Å)	2θ (deg)
0	0	1	12.13	7.28
0	0	2	6.06	14.59
0	0	3	4.04	21.96
0	0	4	3.03	29.42
0	0	5	2.43	37.01
0	0	6	2.02	44.78
0	0	7	1.73	52.77
0	0	8	1.52	61.04

Muscovite (monoclinic, a = 5.20 Å, b = 9.0 Å, c = 20.03 Å, β = 94.47°)

h	k	l	d (Å)	2θ (deg)
0	0	1	19.97	4.42
0	0	2	9.98	8.85
0	0	3	6.66	13.28
0	0	4	4.99	17.75
0	0	5	3.99	22.23
0	0	6	3.33	26.75
0	0	7	2.85	31.32
0	0	8	2.50	35.93
0	0	9	2.22	40.61